Metal Nanoparticles/Carbon Quantum Dots Based Electrochemical Sensors for Selected Biological Compounds

Thesis Submitted to AcSIR for the Award of the Degree of

DOCTOR OF PHILOSOPHY

In Chemical Sciences

By

Shereema R. M.

Registration No: 10CC12J39015

Under the guidance of

Dr. T. Prasada Rao

Chemical Sciences and Technology Division
National Institute for Interdisciplinary Science and Technology
Council of Scientific and Industrial Research
Trivandrum – 695 019
Kerala, India

2016

.....Dedicated to
My Family

DECLARATION

I hereby declare that, the work contained in this thesis entitled "**Metal Nanoparticles/Carbon Quantum Dots Based Electrochemical Sensors for Selected Biological Compounds**" is an independent work carried out by me at the Chemical Sciences and Technology Division, National Institute for Interdisciplinary Science and Technology (NIIST), CSIR, Trivandrum, under the supervision of Dr. T. Prasada Rao and Co-supervision of Dr. K. V. Radhakrishnan and has not been submitted to anywhere else for any other degree, diploma or title. To the best of my knowledge and belief, the thesis contains no materials previously published or written by another person except where due reference is made.

Shereema R. M.

Trivandrum

October, 2016

NATIONAL INSTITUTE FOR INTERDISCIPLINARY SCIENCE AND TECHNOLOGY (NIIST)

Council of Scientific & Industrial Research (CSIR)
Industrial Estate P O Trivandrum – 695 019, Kerala, INDIA.

Dr. T. Prasada Rao
Ex-Chief Scientist
Chemical Sciences and Technology Division

Tel: 91 471 2515 317
Fax: +91 471 2491 712
E-mail: tprasadarao@rediffmail.com

CERTIFICATE

This is to certify that the work incorporated in this Ph.D. thesis entitled **"Metal Nanoparticles/Carbon Quantum Dots Based Electrochemical Sensors for Selected Biological Compounds"** submitted by Ms. Shereema R. M. to Academy of Scientific and Innovative Research (AcSIR) in fulfillment of the requirements for the award of the Degree of Doctor of Philosophy in Chemical Sciences, embodies original research work under my guidance. I further certify that this work has not been submitted to any other University or Institution in part or full for the award of any degree or diploma. Research material obtained from other sources has been duly acknowledged in the thesis. Any text, illustration, table etc., used in the thesis from other sources, have been duly cited and acknowledged.

Shereema R. M.

Trivandrum

October, 2016

Dr. T. Prasada Rao

(Thesis Supervisor)

NATIONAL INSTITUTE FOR INTERDISCIPLINARY SCIENCE AND TECHNOLOGY (NIIST)

Council of Scientific & Industrial Research (CSIR)
Industrial Estate P O Trivandrum – 695 019, Kerala, INDIA.

Dr. K.V. Radhakrishnan
Principal Scientist
Chemical Sciences and Technology Division

Tel: 91 471 2515 420
Fax: +91 471 2491 712
E-mail: radhu2005@gmail.com

CERTIFICATE

This is to certify that the thesis entitled **"Metal Nanoparticles/ Carbon Quantum Dots Based Electrochemical Sensors for Selected Biological Compounds**" and which is being submitted to Academy of Scientific and Innovative Research (AcSIR), India, in partial fulfilment of the requirements for the award of Ph. D Degree in Chemical Sciences, was carried out by Ms. Shereema R. M., under my Co-guidance. To the best of my knowledge and belief the work embodied in this thesis has not formed early the basis for the award of any degree or diploma of any University or any other higher education institution.

Shereema R. M.

Dr. K. V. Radhakrishnan
(Co-Supervisor)

Trivandrum

October, 2016

Acknowledgement

I strongly believe that the completion of this thesis was possible because of God's Blessings. I thank God for giving me this opportunity and the strength to survive despite being far from the people that I love.

I apologize in advance for any omissions as they are purely unintentional. The folks mentioned here are primarily responsible for my successes but all the mistakes and shortcomings are completely my own.

This thesis would never have materialised without the contribution of many individuals to whom I have the pleasure of expressing my appreciation and gratitude.

I owe my deepest sense of gratitude to my esteemed mentor ***Dr. T. Prasada Rao****, Ex-Chief Scientist, Chemical Sciences and Technology division, National Institute for Interdisciplinary Science and Technology, Trivandrum, for accepting me as part of his research group and introducing me to this research field which made my Ph. D. work a memorable experience. Right from the time I started working on my thesis, he has been very helpful in organizing my ideas and putting together a very fine piece of work without him, I would never have reached this point! Dr. T. Prasada Rao is also worth special thanks for providing a research environment which promotes independent thoughts and creativity.*

I grateful acknowledge the persistent support and encouragement from, Dr. K. V. Radhakrishnan, Principal Scientist, Chemical Sciences and Technology division, National Institute for Interdisciplinary Science and Technology, Trivandrum, who is my co-guide. His passion for Chemistry and an enthusiastic vision of the world helped to shape my academic interests and positively influenced other aspects of my life as a Research Scholar. I am really indebted for his invaluable suggestions and advice throughout my Ph. D. work. Thanks a lot for making my dreams to come true!

I am highly grateful to Dr. A. Ajayaghosh, present Director and Dr. Suresh Das, former Director of NIIST, Trivandrum for giving me, an opportunity to pursue my dreams. Their encouragements and constant support especially for providing the necessary facilities helped me to make this thesis a better one. Thanks for them for the opportunity given to me to do research in this prestigious institute.

I would like to show my gratitude to Dr. Laxmi Varma and Dr. Mangalam S. Nair, present and former AcSIR Co-ordinator of NIIST, Trivandrum, for undertaking the unenviable task of serving on my thesis committee, I am indebted for their valuable contributions and suggestions when they were sorely needed, that shaped my AcSIR-800 project, course work and thesis, helped me to make it better.

I wish to express my sincere thanks to Dr. K. R. Gopidas and Dr. Ramaiah, present and former Head, CSTD and other scientists, staffs, and students of CSTD division for their help and cooperation during the course of this work.

I am very thankful to the Doctoral advisory committee members of the NIIST, Trivandrum, Dr. Ramaiah, Dr. Luxmi Varma and Dr. Prabakar Rao, with whom I had an opportunity to interact with during my research work. Their guidance and support helped me, to mature as a researcher and influenced the work I did in this thesis. Thanks a lot for your unconditional support and a never ending patience

I would like to express my sincere thanks to Dr. Sharath Shankar, CSIR- Nehru post doctoral fellow of my group for his valuable suggestions, fruitful criticisms and co-operation at various junctures of the work.

I am very much thankful to Dr. V. B. Sameer Kumar and Mrs. T. V. Sruthi of Department of Biochemistry and Molecular Biology, School of Biological Sciences, Central University, Kasargod, Kerala and Dr. K. G. Raghu and Dr. Vandana Shankar of Agroprocessing and Natural Products Division, NIIST, Trivandrum, for the successful collaboration.

I wish to express my sincere thanks to Mr. Kiran Mohan, Mr. Aswin, Mr. Chandran, Mrs. Lucy, Ms. Soumya and Ms. Varsha CSIR-NIIST, Trivandrum for providing TEM, AFM, SEM and Raman analysis. I convey my sincere thanks to Mr. Sharath, Amrita Center for Nanosciences and Molecular Medicine, Cochin, Kerala for XPS studies.

I would like to express my deep sense of gratitude to Dr. K. Karthiayini, Associate Professor, College of Veterinary & Animal Sciences, Mannuthy, for her suggestions and for providing the facilities to carry out my CSIR-800 project.

I also express my heartfelt thanks to Headmistress of GHS Pappanamcode, Trivandrum for allowing me to carry out the awareness class in the School as part of my 800 project.

I would like to express my sincere thanks to all my lab mates past and present in particular Dr. Sindhu R. Nambiar, Dr. Dhanya S., Dr. Milja T. Elias and Dr. Aneesh P. K. for the input they provided during numerous formal and informal discussions we had. Their continuous interest in my research, their jokes and occasional criticism provided a fresh perspective on my work, helped me to keep a positive outlook, and reinstated my confidence when it was needed.

I am extremely grateful to the Council of Scientific and Industrial Research (CSIR) for the financial support.

It is my pleasant duty to express my deep sense of gratitude to all my teachers who directly or indirectly moulded me as a good human being. I would also like to

thank all my roommates, who helped me in special ways that can never be tangibilized.

I am deeply grateful to my beloved parents, sister and brother for their constant love and care which have been a great source of inspiration. I would like to take the opportunity to express my feelings of gratitude to my loving husband, P. A. Sajeer and my naughty child Muhammad Ameen. It was their blessings, love and encouragement that gave me strength to carry out my work patiently.

Lastly, I offer my regards and blessings to all of those who supported me in any respect during the completion of my thesis.

Shereema R. M.

CONTENTS

Chapter 3: Bimetallic $Au_{90}Pt_{10}$ alloy nanoparticles on glassy carbon electrode for the nanomolar detection of phenol

List of Tables

List of Figures

List of Abbreviations

A549	Adenocarcinomic human alveolar basal epithelial cells
AldDH, AlDH	Aldehyde dehydrogenase
ASV	Anodic Stripping Voltammetry
AA	Ascorbic Acid
AFM	Atomic Force Microscopy
BCPE	Bare Carbon Paste Electrode
CNTs	Carbon Nanotubes
CPE	Carbon Paste Electrode
CQDs	Carbon Quantum Dots
CNS	Central Nervous System
CeO_2NPs	Cerium Oxide Nanoparticles
CMEs	Chemically Modified Electrodes
CAM	Chick Chorioallantoic Membrane
CA	Chronoamperometry
cDNA	Complementary Deoxyribo Nucleic Acid
$CuDipyCl_2$	Copper dipyridyl chloride complex
CE	Counter Electrode
CV	Cyclic Voltammetry
DNA	Deoxyribo Nucleic Acid
DPP	Differential Pulse Poralography
DPV	Differential Pulse Voltammetry
DMSO	Dimethyl sulfoxide
DA	Dopamine
DMEM	Dulbeccos Modified Eagle's Medium
DLS	Dynamic Light Scattering
FBS	Fetal Bovine Serum
FGF	Fibroblast Growth Factor
EIS	Electrochemical Impedance Spectroscopy
FRET	Fluorescence Resonance Energy Transfer

EDAX	Energy Dispersive X-ray Spectroscopy
FTIR	Fourier Transform Infrared spectroscopy
FWHM	Full Width at Half Maximum
GCE	Glassy Carbon Electrode
AuNPs	Gold nanoparticles
AuPtNPs	Gold Platinum alloy Nanoparticles
HBSS	Hanks Balanced Salt Solution
He La	Henrietta Lacks
HPLC	High Performance Liquid Chromatography
HRTEM	High Resolution Transmission Electron Microscopy
HOPG	Highly Oriented Pyrolytic Graphite
HEK	Human Embryonic Kidney
HIV	Human Immunodeficiency Virus
IPE	Ideally Polarisable Electrode
IR	Infrared Spectroscopy
LSV	Linear Seep Voltammetry
mRNA	Messenger Ribonucleic Acid
MTT	Methyl Thiazolyl Tetrazolium
MWCNTs	Multi-walled Carbon Nanotubes
NIR	Near-Infrared
NADH, NADs	Nicotinamide Adenine Dinucleotide
NPP	Normal Pulse Polarography
PdNPs	Palladium Nanoparticles
PSD	Particle Size Distribution
Ppb	Parts per billion
PMS	Phenazine methosulfate
PBS	Phosphate Buffer Solution
PL	Photoluminescence
PCS	Photon Correlation Spectroscopy
PtNPs	Platinum Nanoparticles
PDMA-PSA	Poly 2, 5-dimethoxyaniline phenanthrene sulphonic acid

PCR	Polymerase Chain Reaction
PNR	Poly Neutral Red
PPy-FeCN	Polypyrrole doped with ferricyanide
PVA-SbQ	Polyvinyl alcohol bearing styrylpyridinium
PPF	Pyrolysed Photoresist Film
QDs	Quantum Dots
QYs	Quantum Yields
ROS	Reactive Oxygen Species
RE	Reference Electrode
RSD	Relative Standard Deviation
RNA	Ribonucleic Acic
SCE	Saturated Calomel Electrode
SEM	Scanning Electron Microscopy
AgNPs	Silver Nanoparticles
SWCNTs	Single Walled Carbon Nanotubes
SWV	Square Wave Voltammetry
SHE	Standard Hydrogen Electrode
SEGA	Subependymal Giant cell Astrocytoma
SERS	Surface Enhanced Raman Scattering
TEA	Tetra-ethyl ammonium
TBA	Tetra-n-butyl ammonium
UV-Vis	Ultraviolet and Visible Spectroscopy
UA	Uric Acid
VEGF	Vascular Endothelial Growth Factor
VEGFR2	Vascular Endothelial Growth Factor Receptor 2
WE	Working electrode
XRD	X-ray Diffraction Spectroscopy
XPS	X-ray Photoelectron Spectroscopy

PREFACE

The focus of the work covered in this thesis was to controllably alter the properties of carbon surfaces, so that the surfaces are useful for desired sensor applications. Carbon was the chosen surface, as it is highly conducting with a wide potential window, structurally stable, relatively inexpensive and stable layers of modifiers can attach to the surface in a controllable manner. Here we made an attempt to synthesis some nano materials like cerium oxide nano particles, hybrid of gold platinum nanoparticles and carbon quantum dots. All the synthesized materials are well characterized with different techniques such as XRD, DLS, TEM, SEM, FTIR, XPS, UV- Visible spectroscopy and Raman spectroscopy etc. The electrochemical techniques were also employed for the characterization. In this research work the compounds like acetaldehyde, phenol, and dopamine were investigated at modified electrode surface by using voltammetric techniques. The following aspects like, number of electrons involved in the electrochemical reaction, rate constants, nature of intermediates in the electrode reaction and nature of electrode process were observed. Moreover the biological aspects of carbon quantum dots such as cytotoxicity, cell labelling, and angiogenesis were also demonstrated.

The work carried out in this thesis is divided and described into five chapters.

Chapter – I: Introduction and Overview of Electrochemical sensors and Nano particles

This chapter covers the introduction, fundamentals of electrochemical process. Basic and fundamental principles, theoretical aspects and application of voltammetry, solvents, supporting electrolytes and electrode interaction can be seen in this section. A brief introduction on nanoparticles, nanoscience, and quantum dots has also been presented. Introduction towards angiogenesis and various characterization techniques is also included in this chapter.

Chapter – 2: CeO_2-MWCNTs nanocomposite based electrochemical sensor for acetaldehyde

In this chapter, a highly sensitive and selective electrochemical sensor for acetaldehyde was described. A CeO_2-MWCNTs nanocomposite film was fabricated

on the glassy carbon electrode as follows: chemically synthesized CeO_2 nanoparticles (CeO2NPs) were subjected to adsorb on MWCNTs by sonication and this was further drop casted on the electrode surface. The prepared nanocomposite was characterized by XRD, UV-Visible absorption spectroscopy, SEM and electrochemical impedance spectroscopy (EIS). Under optimal conditions, the developed sensor detected acetaldehyde in the concentration range of 10^{-8} to 10^{-5} M with a detection limit of 7.4×10^{-9} M, accompanied with a good precision of 1.6 % at 10^{-6} M of acetaldehyde. The fabricated sensor exhibits reasonably good selectivity towards acetaldehyde in conjunction with different co-existing organic species and was successfully applied to synthetic fruit juice samples.

Chapter – 3: Galvanostatic Synthesis of Bimetallic AuPtAlloy Nanoparticles on Glassy Carbon Electrode

This part furnishes the details of the synthesis of bimetallic AuPt alloy nanoparticles (AuPtNPs) on glassy carbon electrode (GCE) by galvanostatic method. SEM and AFM techniques were employed for the evaluation of their surface morphology. The formation of AuPtNPs on GCE was characterized by XRD, UV-Visible absorption spectroscopy and XPS analysis. Further, AuPtNPs modified GCE (AuPtNPs/GCE) was employed for the nanomolar detection of phenol in 0.1 M CH_3COONa+0.05 M KCl electrolyte of pH 6.4. This chapter also explains about the effect of concentration of Au and Pt on the formation of AuPtNPs on GCE, deposition time, deposition potential and solution pH. Different parameter such as diffusion coefficient, rate constant and electron transfer coefficient were calculated by electrochemical methods. Here we observed that the modified electrode could detect phenol from 6.5 nM onwards. The possible interference from various compounds was also verified on the designed electrode.

Chapter – 4: One step green synthesis of carbon quantum dots and its application towards the bioelectroanalytical and biolabelling studies

This chapter describes the preparation of green luminescent carbon quantum dots (CQDs) from maltose by Microwave assisted method. The size of the prepared particle was found to be 2 nm. XPS, FTIR and Raman spectroscopy was employed for the surface characterization. These studies revealed the presence of functional groups such as C=O, C-OH on the surface of sp^2 hybridized carbon. Further the prepared carbon quantum dots were used for the modification of

carbon paste electrode. Electrochemical characterization studies on modified carbon paste electrode revealed that the synthesized carbon quantum dots showed higher electrocatalytic property, conductivity and surface area. Therefore, the modified electrode was introduced for the electrochemical determination of dopamine individually and simultaneously from its ternary mixture, which contains ascorbic acid and uric acid. The developed sensor was effectively applied for the real sample analysis with satisfactory results. Moreover, biological studies in He La cell lines was studied and proclaimed that the cell viability was unaffected (100 % viability) on incubation with the carbon dots. Being green luminescent its applicability towards the cell labelling studies was also carried out with the carbon quantum dots.

Chapter – 5: Angiogenic profiling of synthesized carbon quantum dots

Synthesis, characterization and biological applications of green luminescent carbon quantum dots (CQDs) from styrene soot were presented in this portion. The toxicity studies were performed with various cell lines and observed that they are highly cell viable. Due to its non toxicity and green luminescence they can acts as a suitable candidate for labelling cells. The angiogenic activity of carbon quantum dots on ChorioAllantoic Membrane were performed and found significant reduction in density of branched vessels after the treatment with CQDs. It was observed that CQDs significantly down regulate the expression levels of pro-angiogenic growth factors like VEGF and FGF. Expression of VEGFR2 and levels of hemoglobin were also significantly lower in CAMs treated with CQDs, indicating that the CQDs inhibit angiogenesis. Based on the studies we came to a conclusion that CQDs can selectively target cancer cells and have potential in the field of cancer therapy.

Chapter 1

An Overview of Electrochemical Sensors and nanomaterials

1.1 Introduction

It is beneficial to fabricate functionalized membranes on the surface of a carbon based electrode for several reasons. First of all, such a configuration allows for precise control or measurement of the potential across model membrane. The second reason is that additional surface analytical techniques can be applied to study the interactions of analytes with such fabricated films with molecular resolution. Finally, the knowledge, gained during such research, can be directly applied for the design of novel biosensors and other molecular devices.

Traditional electrodes such as gold electrodes, platinum electrodes and conducting carbon materials including glassy carbon (GC), highly oriented pyrolytic graphite (HOPG), pyrolysed photoresist film,(PPF), carbon paste electrode have widely been used as the working electrode for the electrochemical analysis.[1-3] These electrodes are having serious disadvantages like, low detection limit, mechanical damage, poor reproducibility and repeatability. This can be overcome by means of chemical or physical modification of the electrodes. There has been an increasing interest in the creation of modified electrode surfaces that differ from the corresponding bare surface and produce an electrode surface that generates reproducible results, which has a vast application in electro catalysis, electronics, [4] biological and chemical sensing. New class of carbon based materials like fullerenes, single walled and multiwalled carbon nano tubes, boron-doped diamond, carbon quatum dots, vapor deposited carbon films have been developed by various scientists. The significant properties of these materials like high conductivity, large surface area, higher chemical stability etc., forced the electrochemist to tune them for various applications including surface modification of the working electrode. Due to more sensible sites the nano sized materials have also been used as an electrode modifier for the electro active compounds.[5] Moreover these materials show structural polymorphism, chemical stability, rich surface chemistry, and strong carbon-carbon

bonds present both internally and often between the carbon material and this surface modifier, make them suitable candidates as the modifier. In the present study we used the carbon based material electrodes such as glassy carbon and carbon paste electrode as the base electrode for the modification purpose. This is because of the advantages of carbon electrodes over other solid electrodes include low cost, wide potential window, relatively inert electrochemistry, and electrocatalytic activity for a variety of redox reactions of organic and biological molecules in both aqueous and non-aqueous media.[6, 7]

Hence, the scope of the thesis work is limited to physical and analytical electrochemistry of some selective electrochemically active compounds like acetaldehyde, phenol and some neurotransmitters like dopamine, ascorbic acid and uric acid using carbon based modified electrodes with various modifiers. As much as possible, here we also attempt to synthesize another type of carbon material ie; carbon quantum dots and its applicability in the field of bioimaging and angiogenesis.

1.2 Fundamentals of electrochemical process

The fundamental process in electrochemical reactions is the transfer of electrons between the molecules and electrode in the interfacial region either in solution or immobilized at the electrode surface. A species capable of undergoing electron transfer process is called an electroactive species. In order to carry out electron transfer process with the electrode, the electroactive species has to come from the bulk solution and approaches the electrode surface. Hence the electron transfer plays a fundamental role in governi+ng the pathways of chemical reactions.

Measurement of the rate of the electron transfer process and the number of electrons involved in a chemical reaction are easily measurable by the electrochemical techniques where as it is difficult in traditional experimental methods like spectroscopy. [8] Electrochemical methods recommend the potential to investigate the process directly by the determination of number of electrons involved; this will aid to predict the driving

force for many reactions. Electrochemical studies of biologically active compounds serve to elucidate biological processes and their inter-relationship that are involved in living organisms.[9, 10] For any series of interrelated processes within a system, it is normally necessary to study the component part of the system.

Electrochemical techniques provide easy surface modifications of the electrodes. During this process a species from solution can either be physically adsorb, electropolymerised, or covalently attached onto the electrode surface at certain controlled potential.[11] The surface modifications could be influenced by the microstructure and roughness of the electrode surface, the blocking of active sites on the electrode surface by adsorbed materials, and the nature of the functional groups present on the electrode surface.[12] Recently many researchers have been seriously involved in the chemical modification of the working electrodes. The chemically modified electrodes (CMEs) find use in analytical chemistry including the relationship of heterogeneous electron transfer and chemical reactivity of electrode surface chemistry, electron as well as ionic transport phenomena in polymers, energy conversion and storage, electrostatic phenomena at electrode surface, the design of electrochemical devices and systems for applications in chemical sensing, electrochromic displays, electro-organic synthesis and molecular electronics.[13-15] The applicability of these CMEs is wide-ranging, but one important application is analyte sensing.

1.3 Electrode Process

The reaction taking place between the electrode surface and species within the solution can proceed through a series of steps that causes the conversion of the dissolved oxidised species (O) to reduced species (R) in solution (Figure 1.1). The electrode reaction rate is governed by the process such as

i. Mass transfer

ii. Electron transfer of non-adsorbing species.

iii. Chemical reactions preceding or following the electron transfer which could be homogeneous such as protonation or dimerization or heterogeneous ones like catalytic decompositions on the electrode surfaces.

iv. Other surface reactions such as adsorption, desorption, crystallisation etc.

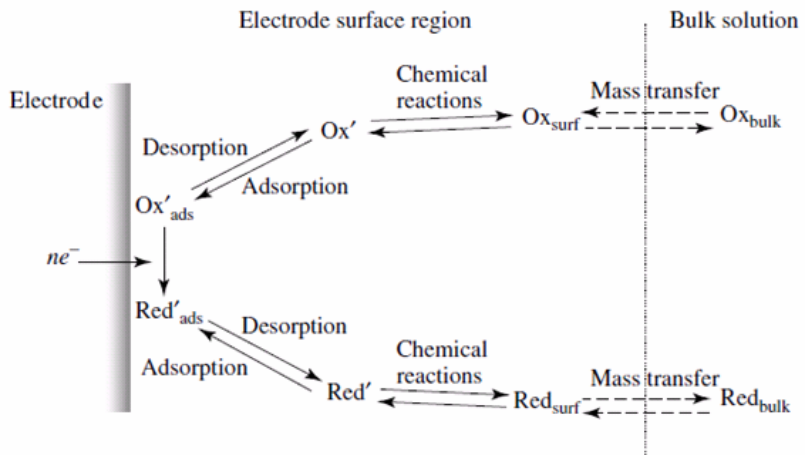

Figure 1.1: *Typical steps involved in an electrode reaction*

The simplest reaction involves only mass transfer of reactant to the electrode, heterogenous electron transfer involving non adsorbed species and the mass transfer of the product to the bulk solution. More complex reaction sequence involving a series of electron transfer, protonations, branching mechanisms, parallel paths or modifications of the electrode surfaces are quite common. When a steady state current is obtained, the rates of all reactions steps are the same. The magnitude of this current is often limited by the inherent sluggishness of one or more reactions called rate determining steps. The more facile reactions are then held back from maximum rates by the slowness with which such steps disposes of their products or create their participants.

1.3.1 Mass Transfer Process

Whenever an electrochemical charge transfer process takes place at the electrode surface, the electroactive material gets depleted and a concentration gradient is set up. Under such conditions the reactant diffuses towards the electrode surface and the

corresponding product of the electrode reaction diffuses away from the electrode surface. Mass transfer in electrochemistry illustrates the movement of electroactive species from one location in solution to another arising from differences in electrical or chemical potential at the two locations. There are three forms of mass transport which can influence an electrolysis reaction (Figure 1.2):

i Diffusion

ii Migration

iii Convection.

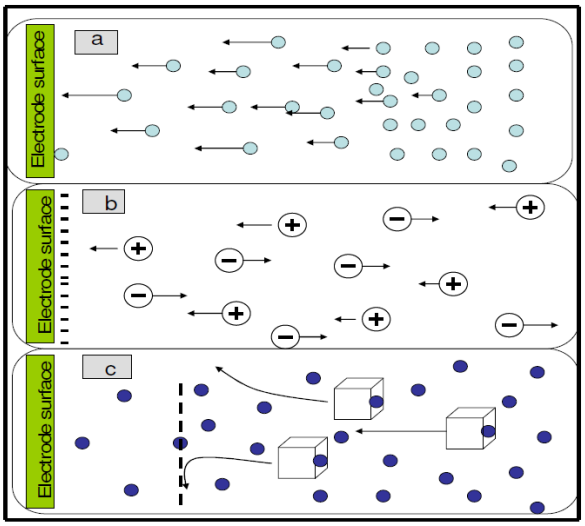

Figure 1.2: *The three modes of mass transfer process: (a) Diffusion, (b) Migration and (c) Convection*

1.3.1.1 Diffusion

Diffusion is the movement of a species down a concentration gradient and it must occur whenever there is a chemical change at a surface. It arises due to the depletion of the electroactive ion near the electrode surface; this depletion is only due to the charge transfer occurring at the electrode surface. The diffusion processes are named after the detailed study of geometry of the electrodes viz, planar diffusion (to a plane electrode), spherical diffusion (to a spherical electrode i.e. mercury electrode) and cylindrical

diffusion (to a wire electrode). The diffusion is characterized and governed by Fick's laws of diffusion.[16]

Consider a stationary planar electrode-electrolyte interface. If a species O is reduced to R at the interface, its concentration C_0 at the surface is lowered when compared with its bulk concentration. Hence O from the bulk will move towards the electrode. After a long interval of time, a steady rate of flow of O towards the surface (called the flux, J) would be established. This rate is given by Fick's first law [16]

$$J = - D_{ox} \delta C_{ox}(x,t) / \delta x$$

where, D_{ox} is the diffusion coefficient at the electroactive ion (in $cm^2 s^{-1}$).

The rate of change of concentration with time is given by Fick's second law of diffusion

$$\delta C_{ox}(x,t) / \delta x = D_{ox} \delta^2 C_{ox}(x,t) / \delta x^2$$

in this equations, the concentration is written as $C_{ox}(x,t)$ which specifically indicate that its value depends on both distance (x) from the planar interface and time (t). Similar equations may also be written for C_{Red}. These two equations will take different forms depending upon geometry of the electrode. The value of D varies from system to system.

1.3.1.2 Migration

Migration involves the movement of charged ions under the influence of electric field. Since migration is nonspecific in nature, migration due to the electroactive ion cannot be distinguished from the migration of other charged species present in the solution. Therefore, it becomes necessary to add a large excess of inert electrolyte to the cell solution, in order to eliminate the migration of the electroactive ions of interest. The inert electrolyte, which is generally called the supporting electrolyte, neutralizes the electrostatic forces of attraction acting between the working electrode and electroactive ion by suppressing the transport number of the reactants.

1.3.1.3 Convection

Convection is the movement of ions due to mechanical forces. Natural convection arises due to the difference in density and temperature at different parts of the solution and it cannot be duplicated or reproduced. Sometimes it is forced by stirring the solution in a known fashion. The forced convection can be reproduced and treated mathematically. The natural convection because of its non-reproducible nature complicates the electrode process. It is imperative to eliminate it. This can be achieved by carrying out the electrolysis in a thermostat in the absence of stirring or vibrations. Care should be taken to restrict the electrolysis time to a few minutes otherwise the natural convection sets in and reproducible results may not be achieved.

1.4 Voltammetry

Voltammetry is a collection of electroanalytical techniques in which information about the analyte is derived from the measurement of current as a function of applied potential. It is widely used by chemists for non-analytical purposes including fundamental studies on redox processes, adsorption processes on surfaces, electron transfer mechanisms and electrode kinetics.

Historically, the branch of electrochemistry we now call voltammetry developed from the discovery of polarography in 1922 by the Czech chemist Jaroslav Heyrovsky, for which he received the Nobel Prize in 1959 in chemistry.[17] Unlike potentiometric measurements, which employ only two electrodes, voltammetric measurements utilise a three electrode electrochemical cell. The use of three electrodes (working, auxillary and reference) along with the potentiostat instrument allows accurate application of potential functions and measurement of the resultant current.

Analytical chemists were largely depending on the voltammetric techniques for the quantitative determination of a variety of dissolved inorganic and organic substances.[17-19] Chemists from Inorganic, Physical, and Biological field routinely use

voltammetric techniques for the fundamental studies of redox process in various media, surface adsorption processes, for predicting reaction mechanism, thermodynamic properties of solvated species and for its electron transfer calculation.[20] Voltammetric methods coupled with HPLC are applied to the determination of compounds of pharmaceutical interest and for the analysis of complex mixtures.[21]

1.5 Voltammetric Techniques

The different voltammetric techniques such as Linear Seep Voltammetry (LSV), Square Wave Voltammetry (SWV), Anodic Stripping Voltammetry (ASV), Normal Pulse Polarography (NPP), Differential Pulse Poralography/Voltammetry (DPP/ DPV), Chrono Amperommetry (CA) Cyclic Voltammetry (CV) and Fast Scan Cyclic Voltammetry (FSCV) are distinguished from each other primarily by the potential function that is applied to the working electrode to drive the reaction, and by the material used as the working electrode. In this work we mainly used CV, DPV and CA. A detailed description of the same is given below.

1.5.1 Cyclic Voltammetry (CV)

Cyclic voltammetry is a method for investigating the electrochemical behaviour of a system. It was first reported and theoretically described by Randles in 1938.[22] It is the first experimental and most widely used technique for acquiring qualitative information and rapid location of redox potentials of the electroactive species. It also provides considerable information on the thermodynamics of redox processes, on the kinetics of heterogeneous electron-transfer reactions, and on coupled chemical reactions or adsorption processes.

1.5.1.1 Basic principles of cyclic voltammetry

Cyclic voltammetry is a potential sweep technique. A cyclic voltammogram is obtained by applying a linear potential sweep (that is, a potential that increases or decreases linearly with time) to the working electrode. As the potential is swept back and

forth the formal potential of an analyte, a current flows through the electrode that either oxidizes or reduces the analyte. The magnitude of this current is proportional to the concentration of the analyte in solution, which allows CV to be used in an analytical determination of concentration. A typical cyclic voltammogram is shown in below (Figure 1.3). From the CV an electrode potential is sweeping between the potential limits E_1 and E_2 at a known sweep rate (also called scan rate). On reaching the limit E_2, the sweep is reversed to E_1 to obtain a cyclic scan. The CV scan is a plot of current verses potential and indicates the potential at which redox process occur.

The important parameters of a cyclic voltammogram are the magnitudes of anodic peak current (i_{pa}), the cathodic peak current (i_{pc}), the anodic peak potential (E_{pa}) and the cathodic peak potential (E_{pc}). At the start of the experiment, the bulk solution contains only the reduced form of the redox couple (R) so that at potentials lower than the redox potential, i.e. the initial potential, there is no net conversion of R into O, the oxidised form (point A).

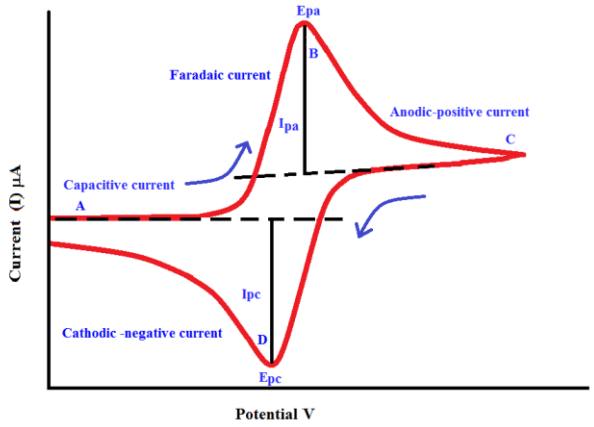

Figure 1.3: *Typical cyclic voltammogram for a reversible process*

As the redox potential is approached, there is a net anodic current which increases exponentially with potential. As R is converted into O, concentration gradients are set up for both R and O, and diffusion occurs down these concentration gradients. At the anodic peak (point B), the redox potential is sufficiently positive that any R that reaches the electrode surface is instantaneously oxidised to O. Therefore, the current now

depends upon the rate of mass transfer of R to the electrode surface and so the time dependence is quite resulting in an asymmetric peak shape. Upon reversal of the scan (point C), the current continues to decay with a quantity until the potential nears the redox potential. At this point, a net reduction of O to R occurs which causes a cathodic current which eventually produces a peak shaped response (point D).

If a redox system remains in equilibrium throughout the potential scan, the electrochemical reaction is said to be reversible. In an electrochemically reversible process the electron transfer is not rate limiting. For a chemically reversible process, both forms of redox couple (O for oxidized form and R for reduced form) are stable in the time scale of measurement. The rate of electron transfer is fast compared to the rate of mass transport and does not control the overall rate. In this process the rate of reaction is fast enough to maintain equal concentration of the oxidized and reduced species at the surface of electrode. The concentration C_{ox} and C_{red} of oxidized and reduced forms of the redox couple respectively follow the Nernst equation

$$E = E^{o} + RT/ nF \ln C_{ox} / C_{red}$$

where, n is the number of electrons transferred, F is the Faraday constant, R is the Gas constant and T is the temperature. If the system is diffusion controlled then the Fick's law of diffusion holds for both oxidation and reduction. Under these conditions, peak current is given by Randles Sevcik equation;

$$i_p = (2.69 \times 10^5)\, n^{3/2} A D^{1/2} C_0 \nu^{½}$$

where n is the stoichiometric number of electrons involved in the electrode reaction, A is the area of electrode in cm^2, D_o is the diffusion coefficient of the species O in $cm^2 s^{-1}$, C_o is the concentration of the species O in mol cm^{-3} and υ is the scan rate in V s^{-1}. From the slope of the plot of i_p Vs $\nu^{½}$ the diffusion coefficient of the analyte on the electrode can be calculated. In order to obtain the value of the electron-transfer coefficient for the reaction, the Tafel plot (b) was drawn. For a diffusion controlled process,

$$Ep = (RT/n\alpha F) \ln \nu + \text{constant}$$

where α is the electron transfer co-efficient, R is the universal gas constant, T is the absolute temperature, ν is the sweep rate and n is the number of electrons involved in the rate determining step. Thus using the dependency of peak potential on the logarithm of sweep rate, based on the above equation electron-transfer coefficient can be determined. Significances of such reversible cyclic voltammogram is given below

i. $\Delta E_p = E_{pa} - E_{pc} = 59/n$ mV, where n is number of electrons change

ii. $i_{pa}/i_{pc} = 1$

iii. $i_p \ \alpha \ \nu^{1/2}$

iv. E_p is independent of ν

The situation is different in case of irreversible electrode process. For an irreversible process, only an oxidation or reduction peak is observed (Figure 1.4a**)**. This process is usually due to slow electron exchange or slow chemical reactions at the electrode surface.[23] In an irreversible electrode process, the mass transfer step is very fast as compared to the charge transfer step.

For an Irreversible reaction, the peak current is given by

$$i_p = 2.99 \times 10^5 \ n \ (\alpha n)^{1/2} \ A \ D_0^{1/2} \ \nu^{1/2} \ C_o$$

$$(\alpha n_a) = 47.7/E_p - E_{p/2}$$

Following are the significances of an irreversible cyclic voltammogram

i. no reverse peak

ii. $i_p \ \alpha \ \nu^{1/2}$

iii. E_p shifts $= 30/\alpha n_a$ mV, where α is charge transfer coefficient

iv. $[E_p - E_{p/2}] = 47.7/\alpha n_a$ mV

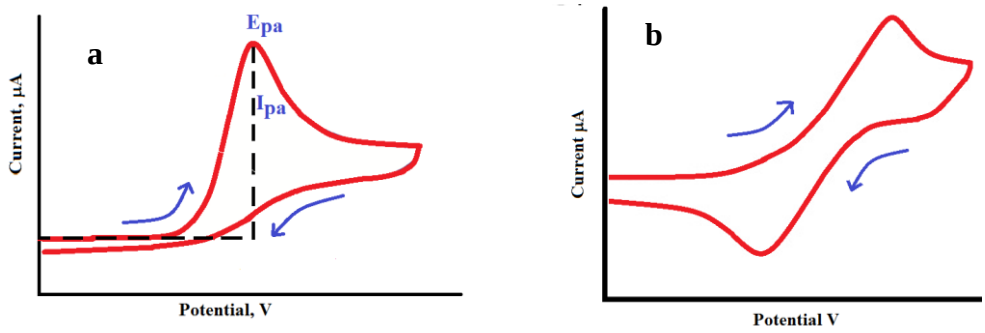

Figure 1.4: *Typical cyclic voltammogram for (a) irreversible process and (b) quasi-reversible process*

There is another class of electron process called quasi-reversible process (Figure 1.4b). This is a class of electrode reactions in which the rates of charge transfer and mass transfer are comparable or competitive. Quasi-reversible process is an intermediate between reversible and irreversible systems. The process occurs when the relative rate of electron transfer with respect to that of mass transport is insufficient to maintain Nernst equilibrium at the electrode surface. In the quasi-reversible region both forward and backward reactions make a contribution to the observed current. Following are the significances of a quasireversible cyclic voltammogram.

i. i_p increases with scan rate, but is not proportional to scan rate

ii. $i_{pc}/i_{pa} = 1$, provided $\alpha_c=\alpha_a = 0.5$

iii. ΔE_p is greater than 59/n mV and its increases with increasing scan rate

iv. E_{pc} shifts negatively with increasing ν

1.5.2 Differential pulse voltammetry (DPV)

DPV is a technique that is designed to minimize background charging currents and was proposed by Barker and Gardner.[24] Comparing with CV, DPV provides greater sensitivity and more efficient resolution and differentiation of various species. In this technique each potential pulse is fixed, of small amplitude and the current is measured between two points from each pulse, just before the application of the pulse and at the end of the pulse. The difference between the current measurements at these points for

each pulse is determined and plotted against the base potential. At potentials around the redox potential, the difference in current reaches a maximum and decreases to zero as the current becomes diffusion controlled. The current response is therefore a symmetric peak.

1.5.2.1 Basic principles of DPV

The waveform in DPV is a sequence of pulses, where a baseline potential is held for a specified period of time prior to the application of a potential pulse. Current is sampled, at time τ', just prior to the application of the potential pulse. The potential is then stepped by a small amount (typically < 100 mV) and current is sampled again, at time τ at the end of the pulse. The potential of the working electrode is then stepped back by a lesser value than during the forward pulse such that baseline potential of each pulse is incremented throughout the sequence.

Consider a reaction O + e → R, where O is reduced in a one electron step to R. At values sufficiently more positive than formal potential ($E^{0'}$) no faradaic current flows before the potential step (to more negative values). The application of the potential step does not produce an appreciable increase in current. Thus, the differential is very small. At values significantly negative of $E^{0'}$ the baseline potential is reducing O at a maximum rate. The application of a small potential step (towards more negative values) is unlikely to increase the rate of reduction and hence the differential current is again small. Only at potentials around $E^{0'}$ will the differential current be significant. The period during the application of the baseline potential has O being reduced at some rate. The potential step (to more negative values) increases the rate of reduction and hence the differential current will be significant. Under normal conditions (pulse height < 100 mV) the maximum peak current is given by the equation

$$(\delta i)_{\max} = \frac{nFAD_0^{1/2}C_0}{\pi^{1/2}(\tau - \tau^1)} \frac{(1-\sigma)}{(1+\sigma)}$$

where n is the number of electrons, F is Faraday's Constant (96485 C mol^{-1}), A is the electrode area (cm^2), D is the diffusion coefficient (cm^2 s^{-1}), C_O is the concentration of electroactive species (mol cm^{-3}) and σ is given by

$$\sigma = \left[\frac{nF\Delta E}{2RT} \right]$$

where ΔE is the pulse height, T is the temperature (K) and R is the Universal Gas constant (8.314 J K^{-1} mol).

1.5.3 Chronoamperometry (CA)

Chronoamperometry is an electrochemical technique in which the potential of the working electrode is stepped and the resulting current from faradaic processes occurring at the electrode (caused by the potential step) is monitored as a function of time. Limited information about the identity of the electrolyzed species can be obtained from the ratio of the peak oxidation current versus the peak reduction current. However, as with all pulsed techniques, CA generates high charging currents, which decay exponentially with time as any RC circuit. In most electrochemical cells this decay is much slower than the charging decay--cells with no supporting electrolyte are notable exceptions.

Chronoamperometry experiments are most commonly either single potential step, in which only the current resulting from the forward step is recorded, or double potential step, in which the potential is returned to a final value (E_f) following a time period, usually designated as τ, at the step potential (Es).

The most useful equation in chronoamperometry is the Cottrell equation, which describes the observed current at any time following a large forward potential step in a reversible redox reaction (or to large overpotential) as a function of $t^{-1/2}$

$$i = \frac{nFAC_j^{\,0}\sqrt{D_j}}{\sqrt{\pi t}}$$

where n is the stoichiometric number of electrons involved in the reaction; F is the Faraday's constant, A is the electrode area (cm^2), C_0 is the concentration of electroactive species (mol^{-1} cm^3), and D_0 is the diffusion constant for electroactive species (cm^2 s^{-1}). With the above equation it is also possible to calculate the diffusion coefficient from the slope of the plot of i vs $t^{-1/2}$.

The rate constants of the reactions can be derived from the chronoamperograms according to the equation:

$$I_C/I_L = \lambda^{1/2} [\pi^{1/2} \text{ erf } (\lambda^{1/2}) + \exp (-\lambda)/\lambda^{1/2}]$$

where I_C is the catalytic current in the presence of analyte, I_L is the limiting current in the absence analyte, $\lambda = kCt$ (k , C and t are the catalytic rate constant, bulk concentration and the elapsed time, respectively) is the argument of the error function. For $\lambda > 1.5$, erf $(\lambda^{1/2})$ almost equals unity and the equation becomes,

$$I_C/I_L=\pi^{1/2}(kCt)^{1/2}$$

From the slope of the plot of I_C/I_L Vs $t^{1/2}$ the rate constant can be obtained.

1.6 Faradaic and non Faradaic current

In voltammetric analysis the current will be arising from either faradaic process or from non faradaic process (background current). If the current arises due to the electron transfer process across the metal or electrolyte interface termed as faradaic process. The redox reaction of solution species that takes place is controlled by Faraday's laws, [25] that is, the amount of electricity which is passed (charge) is proportional to the number of moles of reactant converted. Electrode process where Faradaic process takes place are classified as charge transfer electrodes, since the extent of reaction depends on the measured charge passing through the electrode surface.

It is also possible to generate current due to charging of double layer or adsorption and desorption of ions from the electrode surface, such currents are termed as non faradaic current. The interface between the electrolyte and the working electrode acts

like a capacitor. Therefore, a current is required to change the potential applied to the working electrode and this is referred to as non faradaic current. Since the potential in a CV experiment is constantly changing, there is an approximately constant charging current, which makes a major contribution to the background current and is not governed by faraday's laws. In non faradaic current, the charging current is directly proportional to the sweep rate whereas the faradaic current is directly proportional to the square root of the scan rate.[26]

1.7 Polarisable and non polarisable interfaces

When a metal is dipped in its on solution (Cu in $CuSO_4$ solution) the metal of the electrode undergoes association or dissociation. When a constant current is passed through it, there will not be any change in its potential but the same current will utilize for undergoing chemical reaction. Such electrode whose potential is not changing with the supply of direct current through it is known as non polarisable electrodes.

Another kind of electrode interface is also there which is known as polarisable interface. In case of such electrode interface the externally applied potential will induce a substantial build-up of excess charges at the interface, hence, the electrode is termed polarisable. When a potential is applied externally to the electrode, the transfer of electrons through the interface is negligible. Here a small change in current flow results a considerable change in the electrode potential. An ideally polarisable interface is one which can allow the passage of current without causing a change in the potential difference across it. In addition, when the current associated with charging the electrode-electrolyte interface arises purely from capacitive effects; such an interface is termed an ideally polarisable electrode (IPE).[27] In fact no real electrode behaves ideally over the entire potential range but some electrode-solution systems over limited potential ranges acts as ideal. For example a mercury electrode in contact with a de-aerated potassium chloride solution which behaves as an IPE at potentials in excess of 1.5 V.

1.8 Electrochemical cell

All the electrochemical experiment is performed in a conventional three-electrode potentiostat connected to three electrodes immersed in a test solution. The three electrodes are:

- Working electrode (WE)
- Reference electrode (RE)
- Counter electrode (CE) or auxiliary electrode

The potentiostat applies and maintains the potential between the working and reference electrode while at the same time measuring the current flowing between the counter electrode and the working electrode.

1.8.1 Working electrode

The working electrode is very clean metal surface with a well-defined geometry on which the chemical reaction of interest molecule is occurring. Working electrodes should be stable and inert over a wide range of potential. Platinum, gold and silver are the most commonly used working electrodes. In spite of this various forms of carbon materials have also been using as working electrode.[28] Solid metals are typically fashioned into disks surrounded by a chemically inert shroud made from Teflon, glass, or epoxy. Mercury, being a liquid, tends to be used as a spherical droplet in contact with the solution.

The size and shape of the electrode surface also has an effect on the voltammetric response of the electrode.[29] The overall current observed at an electrode is directly related to its surface area, and disk shaped electrodes with diameters greater than 100 μm, or macroelectrodes, generally produce easily measured currents in the microamp to milliamp range. Electrodes with dimensions less than 100 μm are generally referred to as microelectrodes, and these typically produce currents in the picoamp to nanoamp range.[30]

Although the overall currents observed at microelectrodes are small enough to require specialized electrochemical equipment, these electrodes enjoy a greater signal to-background ratio and, being small, find uses in applications where the availability of sample limited.

1.8.1.1 Carbon based electrodes

Now a day's carbon based materials are commonly used as working electrode.[31, 32] The main advantage of carbon electrodes over other working electrodes is the ability to work at more negative potentials in aqueous solutions. More over this carbon based electrode could be useful over a fairly wide potential window in both the positive and negative directions. Most of the carbon based electrodes are less expensive than that of the platinum and gold electrode. Glassy carbon electrode, in which a carbon material is sealed by a glassy material, has been widely used as the working electrode for the study of metal detection, biological studies, electro catalytic studies etc. The main disadvantage of this working electrode is that it needs to be polished quite frequently, and the surface sometimes has to be activated by various empirical methods in order to obtain maximal performance from the electrode.

The demerit of the GCE can be avoided by using another kind of carbon based working electrode that is carbon paste electrode.[33] Carbon paste electrode is prepared as follows: A known amount of graphite powder is grinding with some binding agents like silicon oil, nafion etc, for 30 minutes and then filled in to the cavity of a homemade cylindrical recess made up of teflon. The paste is carefully polished to a smooth disk shaped surface. Electrical contact of the electrode is possible through the conductive metal placed in the back of the recess (Figure 1.5). The main advantage of this electrode is that they are very cheap and easy to construct. Moreover in each time a fresh surface is exposed to the sample solution. Working with a carbon paste electrode is technically more demanding because the paste can be gouged inadvertently after being polished.

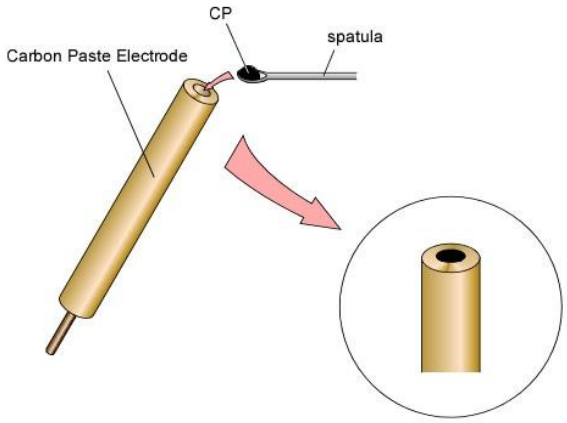

Figure 1.5: *Schematic representation of preparation of carbon paste electrode*

1.8.2 Reference electrode

The potential of a working electrode in a voltammetric experiment is always controlled with respect to some standard, and that standard is the reference electrode. While the thermodynamic scale of half reaction potentials found was measures electrode potentials against the standard hydrogen reference electrode (SHE), in actual practice the SHE is much too cumbersome to use. For this reason, a number of other reference electrodes have been developed. Experimental measurements of potential are made against these alternate reference electrodes, and then the potentials are corrected by simple addition or subtraction and reported against the SHE.

The calomel electrode or saturated calomel electrode (SCE) is the most important reference electrode and was used exclusively for many decades as the reference electrode. The half reaction that occurs inside of an SCE reference is given below.

$$Hg_2Cl_2(s) + 2e^- \Longleftrightarrow 2\ Hg\ (l) + 2\ Cl^-(aq)$$

At 25°C, the formal potential for the SCE half reaction lies 0.2415 volts which is more positive than the SHE. A potential measured against using an SCE can be reported versus the SHE simply by adding 0.2415 volts to it.

The SCE must be constructed in an appropriate piece of glassware that can keep a small amount of mercury in direct contact with solid calomel (Hg_2Cl_2) paste while at the

same time keeping the paste in contact with a saturated aqueous solution of potassium chloride. The short hand notation for the SCE half cell is as follows:

$$Hg(l) / Hg_2Cl_2(s) / KCl\ (aq,\ sat'd)\ //$$

Other useful reference electrodes are based on half reactions involving a silver electrode. For work in aqueous systems, the silver-silver chloride (Ag/AgCl) reference is quite popular. The half reaction for this reference electrode is as follows:

$$AgCl(s) + e^- <\text{-----}> Ag(s) + Cl^-(aq)$$

The actual potential assumed by an Ag/AgCl reference electrode depends only on the activity of the chloride anion. (The other two species appearing in the half reaction are solids which always have unit activity). To serve as a reference, the chloride activity needs to be held constant. To accomplish this, a silver wire (coated with a layer of silver chloride) is immersed in an internal solution saturated with potassium chloride. The chloride ion concentration remains fixed at the saturation limit. The short hand notation for this reference electrode half cell is given below:

$$Ag(s) / AgCl(s) / KCl\ (aq,\ sat'd)\ //$$

1.8.3 Counter electrode

A traditional two electrode cells consist of one working electrode and a reference electrode. During the measurement of current, it is necessarily forced to flow through the reference electrode. At this point there will be a chance to alter the internal chemical composition of the electrode. This will cause a drift in potential from the expected standard value. Hence it is desirable to make electrochemical measurements without current flowing through the reference electrode. In order to avoids this drift in potential an additional counter electrode be introduced into the electrochemical cell. This counter (auxiliary or) electrode provides an alternate route for the current to follow, so that only a very small current flows through the reference electrode.

The counter electrode material should have desired electrode geometry and large surface area. Besides this the material should be chemically inert in the particular test solution being studied. If the electrochemical cell is made up of metal, then the cell itself might be used as the counter. In most cases, a coil of platinum wire is used as the counter electrode. Stainless steel, copper or aluminium wire may also be used as the counter electrode in non-corrosive solutions where metal cation interference is not a concern.

Because current flows at the counter electrode, electrochemical processes will also occur there. If the working electrode is reducing something, then the counter electrode must oxidize something, and vice versa. The products generated at the counter electrode, if allowed to diffuse to the working electrode, may interfere with the experimental measurement. When this is a problem, the counter electrode is placed in a separate compartment containing an electrolyte solution that is in ionic contact with the main test solution via a glass frit. In most cases, however, the auxiliary can be placed right in the test solution along with the reference and working electrodes.

1.9 Supporting electrolytes

The electrochemical processes are taking place on the electrode surface/ liquid interface. In most of the experiments the anlytes are in lower concentration range, mostly lesser than the micromolar level. Hence a carrier has to carry the analytes from the solution to the electrode surface. In some cases the analyte may have poor conductivity which will affect the overall performance. Here comes the important of the supporting electrolyte, they will carry the analytes to the electrode surface and in some circumstances electrolytes impart conductivity to the solvent and hence enable continuous current flow in solution. All ionic salts or ionisable compounds may act as supporting electrolytes.[33] A good supporting electrolyte must have the following features. They must remain electroactive in the potential region of interest, the concentration of the supporting electrolyte should be very high, in order that they do not form space

charges near the surface and hence the space charge potential do not influence the charge transfer kinetics. They should not get adsorbed on the surface, in which case they can catalyse or inhibit other reactions. They should neither form ion pairs with anion radicals formed in the electrode process nor form complexes with the reactants or products.

H_2SO_4, $HClO_4$ and HCl are normaly employed for studies in acidic aqueous solutions and NaOH or KOH are employed for alkaline media. In neutral region, if buffering is important, acetate, citrate, pyrophosphate and phosphate buffers are usually employed. Britton-Robinson (B-R) buffer is used over a wide pH range. If the redox process does not involve acid-base reactions, no buffer is needed and any electrolyte may be used. Solubility is the main consideration in selecting supporting electrolyte for aprotic solvent. A number of tetra-ethyl ammonium (TEA) salts show good solubility in an aprotic media. TEA salts and more recently tetra-n-butyl ammonium (TBA) salts are widely employed for this purpose. TEA salts are frequently available in the form of halides.

1.10 Nanoscience and nanoparticles

In nanotechnology, a particle is defined as a small object that behaves as a whole unit in terms of its transport and properties. It is further classified according to size: particles with size ranges between 100 and 2500 nanometers are termed as fine particles. On the other hand ultrafine particles are having a particle size ranges from 1 to 100 nanometers. Similarly size of the nanoparticles is also lying between 1 and 100 nanometers. Size-related properties of the nanoparticles are totally different from that of the fine particle or bulk materials.[34, 35] Even though individual molecules may have the particles size with the same range are not considered as nanoparticles. Nanoclusters have at least one dimension between 1 and 10 nanometers and a narrow size distribution. Similarly agglomerates of ultrafine particles, nanoparticles, or nanoclusters are termed as

nanopowders.[36] Nanometer-sized single crystals, or single-domain ultrafine particles, are often referred to as nanocrystals.

Nano sized material is a star material in all the branch of science due its application in the area of biomedical, catalytic, optical and electronic fields. Reason for its specific attraction is its size related properties. Nano particles, which in general terms are defined as engineered structures with, are devices and systems produced by chemical or physical processes having specific properties.[37] The particles diameter < 100 nm possess unique features due to their surface to mass ratio, which will allow to adsorb or carry other compounds to the reaction site. Due to this specific property they have the capacity to promote chemical reaction. More over most of the nano sized material shows fluorescent property, and such materials are having wide application in the fields of solar cells and bioimaging. Depending on the presence of reactants and adsorbing compounds the nano particles may have surface modification. Hence the reactivity and quantum phenomena of the nanoparticles are unpredictable. This surface modification can attain simply by changing the compound or by changing the thermodynamic conditions. Thus the nano particles will provide large or functional surface area which is able to bind, adsorb and carry other compounds such as drugs, probes and proteins. As result of this, nanoparticles have reactive surface site that might be chemically more reactive compared to their fine analogues.[38]

1.11 Classification of nanomaterials

Based on different criteria nanometerials are classified in to different categories, such as,

1.11.1 Synthetic and natural nanomaterials:

Based on origin nanomaterials are classified into synthetic and natural. Natural nanomaterials are those materials which are having natural origin. For example virus, mineral such as clays, natural colloids, such as milk and blood, fog (aerosol type),

gelatine (gel type), mineralised natural materials, such as shells, corals and bones, Insect wings and opals, Spider silk, Lotus leaf.[39, 40]

Synthetic nanomaterials are those nanomaterials which are manmade and are prepared deliberately through a well-defined mechanical and fabrication process.[41] The examples of such materials are carbon nanotubes, semiconductor nanoparticles like quantum dots etc.

1.11.2 One, two, three and zero dimensional nanoparticles:

Based on dimensions nanoparticles are classified as one dimensional, two dimensional, three dimensional and zero dimensional nanoparticles.

1.11.2.1 One dimensional nanoparticles (1D)

One dimensional system, such as thin film or manufactured surfaces, has been used for decades in electronics, chemistry and engineering. Production of thin films (1-100 nm) or monolayer is now common place in the field of solar cells or catalysis.[42-44] These thin films are used in different technological applications, including information storage systems, chemical and biological sensors, fiber-optic systems, magneto-optic and optical device.

1.11.2.2 Two dimensional nanoparticles (2D)

Two dimensional nanoparticles are ultrathin nanomaterials with a high degree of anisotropy and chemical functionality. These two dimensional materials are well known for their mechanical, chemical, and optical properties due to its size, shape, biocompatibility, and degradability. Carbon nanotubes, with hexagonal network belong to this category. Here the layers of graphite are rolled up into cylinder of carbon atoms with 1 nm in diameter and 100 nm in length. Further they are classified into single walled carbon nanotubes (SWCNTs) and multi-walled carbon nanotubes (MWCNTs). These materials possess small dimensions of carbon nanotubes, combined with their remarkable physical, mechanical and electrical properties, which make them unique materials for

various applications.[45, 46] Based on how the carbon leaf is wound on itself they exhibit metallic or semi conductive properties. It can be used as a superconductor because the carbon nanotubes can carry extremely high current density up to one billion amperes per square meter. It is also reported that these particles are having high mechanical strength which is sixty times greater than the best steels. Carbon nanotubes are chemically inert and have a greater capacity for molecular adsorption.

1.11.2.3 Three dimensional nanoparticles (3D)

Three dimensional nanoparticles include bulk materials composed of the individual blocks which are in the nanometer scale (1-100 nm). Fullerenes are the best example for this category. They are spherical cage like molecules composed of 60 carbon atoms (C_{60}) joined together by single and double bonds with 12 pentagonal and 20 hexagonal faces, similar to a football.[47, 48] Due to its unique physical properties, this material has been used widely as a lubricant because they don't want to combine with each other. Likewise rubber, when an extreme pressure is applied to the fullerenes its structure will get elaborated, when the pressure is released it will regain their original shape. They have interesting electrical properties and find potential in the electronic field, ranging from data storage to production of solar cells. Fullerenes are offering potential application in the rich area of nanoelectronics. Since fullerenes are empty structures with dimensions similar to several biological active molecules, they can be filled with different substances and it has been suggested to use them in the medical field.[49, 50]

1.11.2.4 Zero dimensional nanoparticles (0D)

These nanomaterials have Nano-dimensions in all the three directions. Metallic nanoparticles including gold and silver nanoparticles and semiconductor such as quantam dots are the perfect example of this kind of nanoparticles. Most of these nanoparticles are

spherical in size and the diameter of these particles will be in the1-50 nm range. Cubes and polygons shapes are also found for this kind of nanomaterials.

1.11.3 Carbon based nanomaterials, metal based nanoparticles, dendrimers and nanocomposites:

On the basis of structural configuration nanomaterials can be classified into four types:

1.11.3.1 Carbon based nanomaterials

These nanomaterials are composed mostly of carbon, and are found in the form of a hollow spheres, ellipsoids, or tubes. Spherical and ellipsoidal carbon nanomaterials are referred to as fullerenes, while cylindrical ones are called nanotubes. These particles have many potential applications, including improved films and coatings, stronger and lighter materials, and applications in electronics.[51, 52]

1.11.3.2 Metal based nanoparticles

Metal based nanoparticles are another kind of nano materials mainly consist of nanosized metal such as nanoplatinum , nanogold, nanosilver, nanoiron, nanopalladium and metal oxides, such as cerium oxide etc. Similar to the other kind of nano materials, metallic nanoparticles are also have different physical and chemical properties from the corresponding bulk metals. These properties include lower melting points, higher specific surface areas, specific optical properties, mechanical strengths, and specific magnetizations. Due to all this improved properties they become precious candidate in various industrial applications.[53-56] Nanoscale features are often incorporated into bulk materials and large surfaces.

The search for new functional materials is one of the defining characteristics of modern science and technology. Chemical and physical properties of metal nanoparticles especially platinum nanoparticles (PtNPs) are widely used in various fields of science like catalysis [57] and photonics.[58] Platinum-containing films are found to be useful for the

enzyme immobilization.[59] It is widely used as a catalyst in the field of automobiles for the reduction of pollutant gases.[60] The stability of PtNPs is of great importance to the development of efficient and durable proton exchange membrane fuel cells and the coalescence of PtNPs is responsible for a reduction in the electrochemically active surface area that reduces cell performance. Furthermore, because of its high conductivity and stability, PtNPs is used widely for the manufacture of conductive thick film circuits and internal electrodes of multilayer ceramic capacitors.[61]

Gold nanoparticles have advantages over other metal nanoparticles due to their biocompatibility and non-cytotoxicity. Gold is used internally in human from last 50 years due to their chemical inertness. The size of gold can be controlled during their synthesis and can be functionalized with different groups. Gold nanoparticles (AuNPs) possess distinct physical and chemical attributes that make them excellent scaffolds for the fabrication of novel chemical and biological sensors.[62-64] AuNPs can be synthesized in a straightforward manner and can be made highly stable. Hence, they possess unique optoelectronic properties and high surface-to-volume ratio with excellent biocompatibility using appropriate ligands.[65] These properties of AuNPs can be readily tuned by varying their size, shape, and the surrounding chemical environment. Due to the color change during AuNPs aggregation (or redispersion of an aggregate) provides a practical platform for absorption-based colorimetric sensing of any target analyte. It can also serve as an excellent fluorescence quenchers for FRET-based assays due to their extraordinary high molar extinction coefficients and broad energy bandwidth.[66, 67] Another attractive feature of this particle is their excellent conductivity, high surface area and catalytic properties that make them excellent materials for the electrochemical detection of a wide range of analytes.[68-70] Surface Enhanced Raman Scattering (SERS)-based sensors, surface plasmon resonance sensors, quartz crystal microbalance-based sensors have also been fabricated with this outstanding material.[71-73] AuNPs-based

biobarcode assay to detect DNA has also been reported by various groups.[74, 75] AuNPs are being utilized in imaging, with colloidal AuNPs used in the immunogold labelling of samples to be viewed using transmission electron microscopy (TEM).[76]

Like AuNPs, silver nanoparticles (AgNPs) are also well known and are initially used for the manufacture of yellow stained glass. Presently they have been received much more attraction due to its applications in the medicinal field. Scientists have introduced AgNPs for the improvement of medical devices including bone cement, surgical instruments, surgical masks, etc. In early years silver sulfadiazine was used in treating wounds which are now replaced with right quantities of AgNPs.[77] Various aspects of respiration can be inhibited by AgNPs, because of its ability to combat infection. AgNPs are also acting as an effective anti-microbial agent owing to its larger surface areas, increasing the area available for interactions.[78, 79] Samsung introduced a material called Silver Nano, which can be used to build surfaces of household appliances. Like other nano particles, silver also exhibits attractive physiochemical properties and are received considerable attentions in biomedical imaging using SERS. In fact, the surface plasmon resonance and large effective scattering cross-section of individual AgNPs make them ideal candidates for molecular labeling.[80] Thus, many targeted silver oxide nanoprobes are currently being developed. Recently scientists have reported that, AgNPs undergo a size-dependent interaction with HIV-1 with particles exclusively in the range of 1–10 nm attached to the virus.[81] They further suggested that silver nanoparticles interact with the HIV-1 virus via preferential binding to the gp120 glycoprotein knobs.

Feridex, iron-based magnetic nanoparticles have mostly been used in vitro or in vivo experiments, for example in tracking the movement of stem cells implanted into a wound site.[82] Similarly palladium nanoparticles (PdNPs) are also being synthesized by various groups. Eychmuller [83] reported on a seed-mediated growth route to the synthesis of PdNPs in solution and on the surfaces. It is also demonstrated that this route can also

be effectively utilized to grow PdNPs onto gold-sputtered substrates, which subsequently show good electrocatalytic ability for O_2 reduction. They also reported that PdNPs could enhance the SERS signals.

Most of the metals are highly active towards oxygen and form corresponding metal oxides. Such metal oxides play crucial role in many areas of chemistry, physics and materials science.[84-86] The metal elements are able to form a large diversity of oxide compounds.[87] These can adopt a vast number of structural geometries with an electronic structure that can exhibit metallic, semiconductor or insulator character. Due to their limited size and a high density of corner or edge surface sites metal oxide nanoparticles can exhibit unique physical and chemical properties. Such kind of metal oxides are used in the fabrication of microelectronic circuits, sensors, piezoelectric devices, fuel cells, coatings for the passivation of surfaces against corrosion, and as catalysts. In order to display mechanical or structural stability, a nanoparticle must have a low surface free energy.[88] As a consequence of this requirement, phases that have a low stability in bulk materials can become very stable in nanostructures. As the particle size decreases, the increasing number of surface and interface atoms generates stress/strain and concomitant structural perturbations. In any material, the nanostruture produces the so-called quantum size or confinement effects which essentially arise from the presence of discrete, atom-like electronic states. Significance of the nanostructured oxide surface is absence or limited Madelung field, mean while this field is wider in range for the bulk oxide surface.[89-91] Most of the bulk oxides have wide band gaps and a low reactivity, [92] this band gap can be reduced by converting them into nano metal oxides. Hence nano metal oxides are having high conductivity and chemical reactivity than that of the bulk. Surface properties are a somewhat particular group included in this subject due to their importance in chemistry.[93, 94] In the case of nanostructured oxides, surface properties are strongly modified with respect to 2D-infinite surfaces, producing solids with unprecedent

sorption or acid/base characteristics.[95] Furthermore, the presence of under coordinated atoms (like corners or edges) or O vacancies in an oxide nanoparticles should produce specific geometrical arrangements as well as occupied electronic states located above the valence band of the corresponding bulk material, which will enhance the chemical activity of the system.[96, 97] CeO_2 nano particle is an example for such metal oxide nano system.

Like other nano metal oxide ceria or cerium oxide nanoparticles (CeO_2NPs) is also act as a semiconducting material with a wide band gap.[98] This material exhibits excellent catalytic properties and are using as a catalytic converter, solid oxide fuel cells and oxygen buffers.[99] Cerium, one of the elements in lanthanide series exhibit both oxidation states +3 and +4 and has the capacity to switch over these oxidation states very easily. These CeO_2NPs are used as UV absorbents and filters.[100] Various group proved the applicability of CeO_2NPs towards the design and fabrication of electrochemical sensors and gas sensors.[101] It is found that the modification of electrochemical sensors by CeO_2NPs could improve the response time, sensitivity, selectivity, and linear response. In fact during the modification, it forms a nano interface between the electrode and the biological element. CeO_2NPs have wide range of biological and biomedical applications.[102, 103] For example the reactive oxygen species (ROS) is responsible for a number of diseases like vision loss. The specific redox properties of CeO_2NPs make it interact with a large number of ROS and minimize their harmful effects.[104] The introduction of the CeO_2NPs into the in-vitro cell culture increases the life span of the cells and decreases the cell damage caused by H_2O_2 (ROS). A recent study revealed CeO_2NPs plays an effective role in spinal cord damage and some diseases related to the Central Nervous System (CNS) due to oxidative stress.[105]

1.11.3.3 Dendrimers

Dendrimers are manmade, spherical polymeric material with nanometer-scale dimensions. They are highly branched, star shaped macromolecules with a central core, an interior dendritic structure (the branches) and an exterior surface with functional surface groups. We can improve the properties of these dendrimers by varying any one of these three parts. The varied combination of these components yields products of different shapes and sizes with shielded interior cores. By varying the cores of the dendrimers we can control the cavity size, absorption capacity, and capture release characteristics which make them ideal candidates for applications in both biological and materials sciences. The possibility of changing surface groups of the dendrimers provides surface modifications which will helps to improve properties like solubility and chelation ability. Due to a large number of modification options and sites they are having wide applications in the field of drug delivery, gene transfection, catalysis, energy harvesting, photo activity, molecular weight and size determination.[106] The pharmaceutical applications of dendrimers include nonsteroidal anti-inflammatory formulations, antimicrobial and antiviral drugs, anticancer agents, pro-drugs, and screening agents for high through put drug discovery.[107] They are compatible with organic structure such as DNA and can also be fabricated to metallic nanostructure and nanotubes or to possess an encapsulation capacity.[108] In some occasion dendrimers may be toxic because it carries a positive charge on their surface which will disrupt the cell membranes.[109]

1.11.3.4 Metal nanocomposites

Nanocomposites are made up of two or more material in which at least one of the phases shows dimensions in the nanometre range.[110] Generally they are of two types, polymer based nano composites and non polymer based nano composites. Mechanically the term nanocomposites are differ from conventional composites due to the exceptionally high surface to volume ratio of the reinforcing phase. Hence the

nanocomposites are considered as materials of 21st century.[111] After the discovery of carbon nanotubes (CNTs) variety of nanocomposites have been prepared with the incorporation of CNTs with other materials. The unique mechanical, thermal and electrical properties of CNTs have been largely utilized for the fabrication of electrical and thermal conducting composites which added a new and interesting dimension to this area. [112, 113] The possibility of spinning CNTs into composite products and textiles [114] made further inroads for the processing and applications of CNT-containing nanomaterials. Being environmentally friendly, nanocomposites offer new technology and business opportunities for all sectors of industry.[115] A flexible battery is constructed by soaking a conductive paper, which is made up of nanocomposite of cellulous materials and nanotubes, to the electrolyte. This advanced material has been successfully utilized for the preparation of anti-corrosion barrier coatings, UV protection gels, lubricants and scratch free paints. With the help of nanocomposites scientists have prepared fire retardant materials, scratch/abrasion resistant materials and fibres/films with superior strength.[116]

1.12 Quantum Dots (QDs)

QDs are colloidal semiconductor nanocrystals ranging from 2 to 10 nm in diameter and are discovered in 1980s by Alexie Ekimov and Louis E Brus.[117] Quantum dots can have anything from a single electron to a collection of several thousands. The size, shape and number of electrons can be precisely controlled. They have been developed in a form of semiconductors, insulators, metals, magnetic materials or metallic oxides.[118] Generally they are composed of atoms from groups II and VI (that is CdSe, CdS, and CdTe) or III and V (such as In P) at their core. The most commonly used QDs are cadmium selenide (CdSe), cadmium telluride (CdTe) and indium phosphide (InP).

The electronic structure of materials is strongly related to the nature of the material. When the electronic motion is confined in one direction creates two-

dimensional (2D) structures that have been termed quantum wells or quantum films. Carrier confinement in two directions produces one-dimensional (1D) quantum wires and confinement in three dimensions produces mentioned quantum dots or quantum boxes, where the electrons are mostly localized; these structures are zero-dimensional (0D).[119]

The size-dependent optical and electronic properties of this material make them star in all fields of science. Size of the quantum dots are smaller than that of the Bohr excitation diameter then more energy is required to promote the electron from the valence band to the conduction band. In other words, smaller the nanocrystal larger will be the band gap of the material, so higher energy/shorter wavelength will be needed for the excitation of electrons from the nanocrystals. Due to the above fact and quantum confinement these quantum dots are showing unique size tunable properties like fluorescence. Another factor which affects the fluorescence property of the QDs is surface defect. A large number of atoms are located at or near the surface of the NPs, leading to a preponderance of dangling bonds and defects, besides adsorbed impurities. That results in surface states, which can act as traps or recombination sites generating quite complex light-emission profiles. With different-sized QDs with similar surface passivation, the smallest were found to be highly luminescent. The presence of surface defect states near the Fermi level may explain the usually observed dependence of the maximum-emission wavelength and emission-line shape on the excitation wavelength.[120] This makes them very appealing for a variety of applications and new technologies.

Due to all these advantage the QDs have application in all the field of science. It has been widely used in catalysis, [121] electronics, [122] sensing, [123] photonics and optoelectronics devices.[124] Color coded quantum dots are used for fast DNA Testing.[125] QDs also provide enough surface area to attach therapeutic agents for simultaneous drug delivery [126] and in vivo imaging, [127] as well as for tissue engineering.[128]

1.12.1 Carbon quantum dots (CQDs)

CQDs are a new class of carbon nanomaterials with sizes below 10 nm, which were first obtained during purification of single-walled carbon nanotubes through preparative electrophoresis in 2004.[129] To date, a variety of techniques have been developed to prepare CQDs. In general, the established techniques can be classified into two main types, top-down strategy and bottom up strategy. Top-down strategy consists of arc discharge, [129] laser ablation, [130] combustion/ thermal/ hydrothermal acid oxidation [131-133] and electrochemical oxidation.[134] Bottom up strategy consists of hydrothermal treatment, [135] ultrasonic method, [136] microwave method [137] and supported method.[138] In the present work we have adopted the microwave and combustion method for the synthesis of CQDs.

CQDs emerge as a superior and universal fluorophores because of its unique combination of a number of key merits, including excellent photostability, small size, biocompatibility, highly tunable photoluminescence (PL) property, exceptional multi-photon excitation (up-conversion) property, electrochemiluminescence, ease to be functionalized with biomolecules, and chemical inertness.[139-143] These glowing carbon nanocrystals provide unprecedented opportunities for bioimaging and optical sensing.[144] Because of their small size and biocompatibility, they may also serve as effective carriers for drug delivery while allowing simultaneous visual monitoring of releasing kinetics.[145] Furthermore, their unique catalytic and physicochemical properties promise various biomedical applications.[146] Additionally, CQDs can exhibit PL emission in the nearinfrared (NIR) spectral region under NIR light excitation, which is particularly significant and useful for in vivo bionanotechnology because of the low autofluorescence and high tissue transparency in the NIR region.[147] Except strong fluorescence, CQDs also own other properties such as electrochemical luminescence, photoinduced electron

transfer property, photocatalysis and optoelectronics [148] which all extend their applications in various areas.

1.13 Chemical sensors, biosensors and electrochemical biosensors

A sensor is a device that measures a physical quantity (mass, amount of substance, length, time, temperature, electric current, light intensity, force, velocity and density) and converts it into a 'signal' which can be read by an observer or by an instrument. Broadly, sensors can be classified into chemical sensors and biosensors. A chemical sensor is a device that provides information about a specific chemical species. Further chemical sensors are classified into mechanical, optical, thermal and electrochemical sensors based on the physical phenomena. Because of the ease of detectability, experimental simplicity and low cost, electrochemical sensors are getting much more attraction in all the fields of analytical chemistry.[149]

Based on the technique employed for sensing, electrochemical sensors are generally classifies into potentiometric, amperometric, voltammetric, and conductometric sensors. In case of potentiometric sensors, without applying any potential the potential difference between the working and the reference electrode is measured and this potential is directly proportional to the concentration of the analyte in the gas or solution phase. Hence potentiometric sensors have been widely used for determining various inorganic and organic ions in medical, environmental and industrial analyses. Amperometric sensors are considered as a subclass of voltammetric sensors. Here a constant potential is applied for the oxidation and reduction of the analyte, further the current generated by the redox process is recorded as a function of time. Whereas in voltammetric sensors current is being measured as a function of voltage. In coductometric sensors conductivity of the electrolyte is measured as a function of frequencies.[150]

A biosensor is a device which can detect biological compounds by using any of the above mentioned techniques and the process of gathering information about the living

system by using biosensors are termed as biosensing. Like other sensors, biosensors transducer translate one kind of energy into another and must be placed into a chain of components that detect, translate and modify an original sign of life into a useful signal.[151] They are also subject to the same performance criteria as electric sensors (sensitivity, selectivity, accuracy, precision, repeatability, noise tolerance etc.). Biosensors consist of two important components such as transduction platform or transducer and a bio-recognition element or receptor. Both transducer and receptor play an important role in the construction of a sensitive and specific device for the target analyte. Normally, electrochemical, optical, piezoelectric, and thermal transducers are employed for the construction of biosensors. [152]

An electrochemical biosensor is a self-contained integrated device, which is capable of providing specific quantitative or semi-quantitative analytical information using a biochemical receptor which is retained in direct spatial contact with an electrochemical transduction element.

1.14 Angiogenesis

Angiogenesis is a process of origination and development of new capillary blood vessels in normal or malignant tissue. It is an important natural process in the body used for the healing and reproduction. Angiogenesis is necessary so that a growing or enlarging tissue with its increasing metabolic needs, obtains an adequate blood supply providing oxygen, nutrients and waste drainage. The body controls angiogenesis by producing a precise balance of growth and inhibitory factors in healthy tissues. When this balance is disturbed, the result is either too much or too little angiogenesis.[153] Various angiogenetic factors are secreted by blood deprived cells and these operate on the inner lining of existing blood vessels to cause the budding out of new blood capillaries. Abnormal blood vessel growth, either excessive or insufficient, is now recognized as a common denominator underlying many deadly and debilitating conditions, including

cancer, skin diseases, age-related blindness, diabetic ulcers, cardiovascular disease, stroke, and many others. Angiogenesis can be exploited in two ways in medicine. It can be inhibited in the treatment of cancer, diabetic retinopathy, obesity, endometriosis and atherosclerosis; or it can be encouraged to treat heart attack, ununited fractures, neurodegenerative disease, peripheral blood circulation deficiencies and baldness.[154] All cancerous tumors, for example, release angiogenic growth factor proteins that stimulate blood vessels to grow into the tumor, providing it with oxygen and nutrients. Antiangiogenic therapies literally starve the tumor of its blood supply by interfering with this process. New classes of cancer treatments that block angiogenesis are now approved and available to treat cancers of the colon, kidney, lung, breast, liver, brain, and thyroid, as well as multiple myeloma, bone gastrointestinal stromal tumors, and SEGA tumors. Some older drugs have been rediscovered to block angiogenesis, as well. These are being used to treat angiogenesis-dependent conditions, such as hemangiomas, colon polyps, and precancerous skin lesions.[155]

Therapeutic angiogenesis, in contrast, stimulates angiogenesis where it is required but lacking. This technique is used to replenish the blood supply to chronic wounds to speed healing, and it prevents unnecessary amputations. New research suggests this approach can also be used to save limbs afflicted with poor circulation, and even oxygen-starved hearts. Therapeutic angiogenesis may even help to regenerate damaged or lost tissues in ways that were previously considered impossible, such as with nerves and brain tissue.[156]

1.15 Characterization techniques

The following are the important characterization techniques used in this work

1.15.1 Dynamic light scattering (DLS)

Currently, the fastest and most popular method of determining particle size is photon-correlation spectroscopy (PCS) or dynamic light scattering (DLS). DLS is widely

used to determine the size of Brownian nanoparticles in colloidal suspensions in the nano and submicron ranges. Shining monochromatic light (laser) onto a solution of spherical particles in Brownian motion causes a Doppler shift when the light hits the moving particle, changing the wavelength of the incoming light. This change is related to the size of the particle. It is possible to extract the size distribution and give a description of the particle's motion in the medium, measuring the diffusion coefficient of the particle and using the autocorrelation function. The photon correlation spectroscopy (PCS) represent the most frequently used technique for accurate estimation of the particle size and size distribution based on DLS.[157]

1.15.2 Scanning electron microscopy

Scanning electron microscopy (SEM) is giving morphological examination with direct visualization. The techniques based on electron microscopy offer several advantages in morphological and sizing analysis; however, they provide limited information about the size distribution and true population average. For SEM characterization, nanoparticles solution should be first converted into a dry powder, which is then mounted on a sample holder followed by coating with a conductive metal, such as gold, using a sputter coater. The sample is then scanned with a focused fine beam of electrons. The surface characteristics of the sample are obtained from the secondary electrons emitted from the sample surface. The nanoparticles must be able to withstand vacuum, and the electron beam can damage the polymer. The mean size obtained by SEM is comparable with results obtained by dynamic light scattering. Moreover, these techniques are time consuming, costly and frequently need complementary information about sizing distribution.[158]

1.15.3 Transmission electron microscope

TEM operates on different principle than SEM, yet it often brings same type of data. The sample preparation for TEM is complex and time consuming because of its

requirement to be ultra thin for the electron transmittance. The nanoparticles dispersion is deposited onto support grids or films. To make nanoparticles withstand the instrument vacuum and facilitate handling, they are fixed using either a negative staining material, such as phosphotungstic acid or derivatives, uranyl acetate, etc, or by plastic embedding. Alternate method is to expose the sample to liquid nitrogen temperatures after embedding in vitreous ice. The surface characteristics of the sample are obtained when a beam of electrons is transmitted through an ultra thin sample, interacting with the sample as it passes through.[158]

1.15.4 Atomic force microscopy

Atomic force microscopy (AFM) offers ultra-high resolution in particle size measurement and is based on a physical scanning of samples at sub-micron level using a probe tip of atomic scale. Instrument provides a topographical map of sample based on forces between the tip and the sample surface. Samples are usually scanned in contact or noncontact mode depending on their properties. In contact mode, the topographical map is generated by tapping the probe on to the surface across the sample and probe hovers over the conducting surface in non-contact mode. The prime advantage of AFM is its ability to image non-conducting samples without any specific treatment, thus allowing imaging of delicate biological and polymeric nano and microstructures. AFM provides the most accurate description of size and size distribution and requires no mathematical treatment. Moreover, particle size obtained by AFM technique provides real picture which helps understand the effect of various biological conditions.[159]

1.15.5 Raman spectroscopy

Raman spectroscopy is the most powerful, analytical technique, which can be used for the characterization of the chemical composition and structure of a material that helps us to understand more about the materials we analyze. This technique is very easy to handle and can be used for the identification of a specific materials or unknown materials

(species) present in the sample. It is also useful for the identification variation in a parameter of a material such as stress state. The material distribution, size, relative amounts of species and the thickness or composition of layered materials can be calculated by Rama spectroscopy. Here a sample is illuminated using a single colour of light and the light will interacts with the sample. Each materials has their own Raman spectral finger prints therefore we can identify unknown materials, typically using databases of known spectra. Ideally one can use a Rama instrument with high spectral resolution across the whole Raman range.

1.15.6 X-ray photoelectron spectroscopy (XPS)

The principle of the XPS technique is the emission of electrons from atoms by absorption of photons. The sample is often irradiated with monoenergetic x-rays, and usually Mg Ka (1253.6 eV) or Al Ka (1486.6 eV) is used. Photoelectron emission occurs when a photon transfers its energy to an electron, and a photoelectron can be emitted only when the photon energy is larger than the binding energy of the electron. The emitted photoelectrons have kinetic energies, E_{kin}, given by:

$$E_{kin} = h\nu - E_b - F,$$

where $h\nu$ is the energy of the photon, E_b is the binding energy of the atomic orbital from which the electron originates and F is the work function of the spectrometer (assuming conductive samples). As the energy of the photons and the spectrometer work function are known quantities, the measurement of the electron binding energies can be obtained by measuring the kinetic energies of the photoelectrons. Here the relaxation energy can dissipate either as an x-ray photon or it can be given to a second electron, an Auger electron. Since the emission of x-ray photons is low in the energy range used in XPS, photoionisation normally leads to two emitted electrons: a photoelectron and an Auger electron

XPS is a very surface sensitive analyzing method. This is due to the relatively short inelastic mean free path for the photoelectrons and the Auger electrons, i.e. the transportation of emitted electrons, generated in the solid, to the surface can only occur from a certain depth. Using XPS it is possible to detect all elements except for H and He. An XPS spectrum shows the number of photoelectrons as a function of binding energy. The spectrum will be a superposition of photoelectron and Auger lines with accompanying satellites and loss peaks and a background due to inelastic scattering in the substrate. However, the main advantage of using the XPS-technique lies in the fact that the binding energy of a photoelectron is sensitive to the chemical surrounding of the atom, i.e. there is a chemical shift in the binding energy. These shifts are very important since they provide a tool to identify individual chemical states of an element. Unfortunately, it is not always straightforward to interpret these chemical shifts because they depend both on initial and final state effects.

1.15.7 X-ray powder diffraction (XRD)

X-ray powder diffraction (XRD) analysis is the most powerful and widely used technique for the identification and quantification of crystal phases with known structure. In XRD, the scattered signal contains the same information as the single-crystal experiment, but the three-dimensional pattern is compressed into one dimension. The diffraction pattern from a powder consists of rings of diffracted intensity with cone angles corresponding to the Bragg 2θ angles of each plane. Consequently, there is usually considerable overlap of peaks in the powder diffraction pattern, leading to severe ambiguities in extracting the intensities I(hkl) of individual diffraction maxima. As a result, XRD is rarely used for structure determination, except for inorganic compounds with relatively small cells and highly symmetric structures.

When an X-ray beam hits a sample and is diffracted, we can measure the distances between the planes of the atoms that constitute the sample by applying Bragg's

Law, $n\lambda = 2d \sin\theta$, where the integer n is the order of the diffracted beam, λ is the wavelength of the incident X-ray beam, d is the distance between adjacent planes of atoms (the d-spacings), and θ is the angle of incidence of the X-ray beam. From this equation we can measure the d-spacings. The geometry of an XRD unit is designed to accommodate this measurement. The characteristic set of d-spacings generated in a typical X-ray scan provides a unique "fingerprint" of the metal or metals present in the sample. When properly interpreted, by comparison with standard reference patterns and measurements, this "fingerprint" allows for identification of the material.

1.16 Scope of the work

In view of the above discussion on the various electrochemical sensors and its application, it has shown great future for the design and development of new kind of sensors. It is beneficial to detect the biologically important compounds such as acetaldehyde and dopamine due to their crucial role in many of the biological activities. Phenols are environmentally pollutant compound and therefore their detection is very crucial. Most of the methods like spectroscopy, used for the determination of such compounds are having limitation such as high detection limit, poor reproducibility and reusability. Therefore there is a large scope for the fabrication of novel electrochemical sensors for such compounds. Hence as much as possible we tried to synthesize some metal based nanoparticles on the surface of the GCE. Further the applicability of these synthesized materials towards the detection of phenol and acetaldehyde has been evaluated. This thesis also deals with the design and development of CQDs based bio-electrochemical sensors for compounds such as dopamine. Detailed studies of the prepared compounds, optimized condition for the preparation etc and sensing parameters like sensitivity, selectivity, stability and reproducibility of the developed sensors has been also demonstrated. Moreover the thesis envisages studies on the application of CQDs for the cell imaging studies and angiogenic studies.

1.17 References

1) McCreery, R. L. Advanced Carbon Electrode Materials for Molecular Electrochemistry. *Chem. Rev.* **2008**, *108*, 2646–2687.
2) Zhang, W.; Zhu, S.; Luque, R.; Han, S.; Hu, L.; Xu, G. Recent Development of Carbon Electrode Materials and Their Bioanalytical and Environmental Applications. *Chem. Soc. Rev*. **2016,** *45*, 715-752.
3) Awad, M. I.; Saleh, M. M.; Ohsaka, T. Recent Progress in the Electrochemistry of Planar and Reticulated Vitreous Carbon: Fundamentals and Applications. *Current topics in electrochemistry* **2012**, *17*, 15-40.
4) Kaushik, A.; Kumar, R.; Jayant, R. D.; Nair, M. Nanostructured Gas Sensors for Health Care: An Overview. *J. Pers. Nanomed.* **2015**, *1*, 10–23.
5) Wang, J. Carbon-Nanotube Based Electrochemical Biosensors: A Review. *Electroanalysis* **2005**, *17*, 7-14.
6) Goyal, R. N.; Bishnoi, S. Surface Modification in Electroanalysis: Past, Present and Future. *Indian J. Chem. Sect. A* **2012**, *51A*, 205-225.
7) Sharma, V. K.; Jelen, F.; Trnkova, L. Functionalized Solid Electrodes for Electrochemical Biosensing of Purine Nucleobases and Their Analogues: A Review. *Sensors* **2015,** *15*, 1564–1600.
8) Christopher, M. A. B. Electroanalytical Techniques for the Future: The Challenges of Miniaturization and of Real-Time Measurements. *Electroanalysis* **1999**, *11*, 1014–1016.
9) Kalvoda, R.; Parsons, R. *Electrochemistry in Research and Development;* Plenum Press: NewYork, 1985; p 181.
10) Paula, F. S. D.; Cioletti, A. G.; Filho, J. F. D. S.; Santana, A. E. G.; Santos, A. F. D.; Goulart, M. O. F.; Fruttero, M. V. R. Electrochemical Studies of Biologically

Active Arylazoxy Compounds. The Relationship between Redox Potentials and Molluscicidal Activities. *J. Electroanal. Chem.* **2003,** *544*, 25-34.

11) Bard, A. J.; Chemical Modification of Electrodes. *J. Chem. Educ.* **1983**, *60*, 302-304.
12) AlNashef, I. M.; Hayyan, M. Kinetics of Homogeneous Reactions in Ionic Liquids. *Int. J. Electrochem. Sci.* **2012,** *7*, 8236 – 8254.
13) Murray, R. W.; Ewing, A. G.; Durst, R. A. Chemically Modified Electrodes. Molecular Design for Electroanalysis. *Anal. Chem.* **1987**, *59*, 379A–390A.
14) Zen, J. M.; Kumar, A. S.; Tsai, D. M. Recent Updates of Chemically Modified Electrodes in Analytical Chemistry. *Electroanalysis* **2003**, *15*, 1073–1087.
15) Ciucu, A. A. Chemically Modified Electrodes in Biosensing. *J. Biosens. Bioelectron.* **2014**, *5*, 154-164.
16) Scholz, F. *Electroanalytical Methods;* Springer: New York, 2010; p 11.
17) Farghaly, O. A.; Hameed, R. S. A.; Alhakeem, A.; Nawwas, H. A. Analytical Application Using Modern Electrochemical Techniques. *Int. J. Electrochem. Sci.* **2014**, *9*, 3287 – 3318.
18) Smyth, M. R.; Smyth, W. F. Voltammetric Methods for the Determination of Foreign Organic Compounds of Biological Significance. A Review. *Analyst* **1978**,*103*, 529-567.
19) Gupta, V. K.; Jain, R.; Radhapyari, K.; Jadon, N.; Agarwal, S. Voltammetric Techniques for the Assay of Pharmaceuticals—A Review. *Anal. Biochem.* **2011,** *408*, 179–196.
20) Nicholson, R. S. Theory and Application of Cyclic Voltammetry for Measurement of Electrode Reaction Kinetics. *Anal. Chem.* **1965**, *37*, 1351–1355.
21) Long, Y.; Zhang, W.; Wang, F.; Chen, Z. Simultaneous Determination of Three Curcuminoids in Curcuma Longa L. By High Performance Liquid Chromatography Coupled with Electrochemical Detection. *J. Pharm. Anal.* **2014**, *4*, 325–330.

22) Randles, J. E. B. A Cathode Ray Polarograph. Part II.—The Current-Voltage Curves. *Trans. Far. Soc.* **1948,** *44*, 327-338.

23) Kissinger, P. T.; Heineman, W. R. Cyclic Voltammetry. *J. Chem. Educ.* **1983**, *60*, 702-706.

24) Hibbert, D. B. *Introduction to Electrochemistry*; Macmillan: London, 1993; p 350

25) M. Faraday, Experimental Researches in Electricity. Seventh Series. *Phil Trans. Roy. Soc.* A **1834,** *124*, 77-122.

26) Alberts, G. S.; Shain, I. Electrochemical Study of Kinetics of a Chemical Reaction Coupled Between Two Charge Transfer Reactions. Potentiostatic Reduction of P-Nitrosophenol. *Anal. Chem.* **1963**, *35*, 1859–1866.

27) Appleby, A. J. *Comprehensive Treatise of Electrochemistry;* Plenum Press: New York, 1983; p 173.

28) Li, G.; Miao, P. *Electrochemical Analysis of Proteins and Cell;* Springer-Verlag Berlin Heidelberg: New York, 2013; p 5.

29) Amatore, C.A. *Physical Electrochemistry: Principles, Methods and Applications;* Marcel Dekker: New York, 1995; p 131.

30) Montenegro, I. Queirós, M. A. Daschbach, J. L. *Microelectrodes: Theory and Applications;* Springer: New York, 1991; p 3.

31) Randin, J. P. *Encyclopedia of Electrochemistry of the Elements*; Marcel Dekker: New York, 1976; p 1.

32) Panzer R. E.; Elving, P. J. Nature of the Surface Compounds and Reactions Observed on Graphite Electrodes. *Electrochim. Acta*, **1975,** *20*, 635-647.

33) Adams, R. N. *Electrochemistry at Solid Electrodes;* Marcel Dekker: New York, 1996; p 13.

34) Buzea, C.; Pacheco, I.; Robbie K. Nanomaterials and Nanoparticles: Sources and Toxicity. *Biointerphases* **2007**, *2*, MR17– MR71.

35) Kestell A. E.; DeLorey, G. T. *Nanoparticles: Properties, Classification, Characterization, and Fabrication*; Nova Science Publishers: New York, 2010; p 353.

36) B. D. Fahlman, *Materials Chemistry*; Springer: New York, 2007; p 282–283.

37) Gwinn, M. R.; Vallyathan. V. Nanoparticles: Health Effects—Pros and Cons. *Environ. Health Perspect.* **2006,** *114*, 1818- 1825.

38) Borm P. J. A.; Kreyling. W. Toxicological Hazards of Inhaled Nanoparticles Potential Implications for Drug Delivery. *J. Nanosci. Nanotechnol.* **2004,** *4*, 1-11.

39) Taylor, D. A. Dust in the Wind. *Environ. Health Perspect*. **2002,** *110*, A80-A87.

40) Houghton, J. Global Warming. *Rep. Prog. Phys.* **2005,** *68*, 1343–1403.

41) Buzea, C.; Blandino, I. I. P.; Robbie, K. Nanomaterials and Nanoparticles: Sources and Toxicity. *Biointerphases* **2007,** *2*, MR17 - MR172.

42) Gandham, A P. D.; Sweeya, P. S. R.; Karra, G.; Chidrawar, V. R.; Rao, V. U. M. The Current Big Thing is Really Small – A Review on Nanomaterials in Medicine with an Overview of Metal Oxide Nanomaterial Toxicity. *Asian Journal of Pharmaceutical Research and Development* 2013, *1*, 123-136.

43) Tiwari, J. N.; Tiwari, R. N.; Kim, K. S. Zero-Dimensional, One-Dimensional, Two-Dimensional and Three-Dimensional Nanostructured Materials for Advanced Electrochemical Energy Devices. *Prog. Mater. Sci.* **2012,** *57*, 724–803.

44) Dresselhaus, M. S.; Dresselhaus, G. Ph. Avouris, *Carbon Nanotubes: Synthesis, Structure, Properties, and Applications;* Springer Berlin Heidelberg: New York, 2001; p 448.

45) Harris, P. F. *Carbon Nanotubes and Related Structures: New Materials for the Twenty-first Century;* Cambridge University Press: United Kingdom, 1999; p 1.

46) Williams, H. A. *The Most Beautiful Molecule: The Discovery of the Buckyball;* Aurum Press: United Kingdom, 1995; p 340.

47) Fowler, P.W.; Manolopoulos, D. E. *An Atlas of Fullerenes.* Dover Publications: United State of America, 2007; p 416.

48) Yadav, B. C.; Kumar, R. Structure, Properties and Applications of Fullerenes. *Int. J. Nanotechnol. Appl.* **2008,** *2*, 15–24.

49) Anton, W. J.; Stephen, R. W.; David, I. S. Biological Applications of Fullerenes. *Bioorganic & Medicinal Chemistry* **1996,** *4*, 767-779.

50) Bose, S.; Kuila, T.; Mishra, A. K.; Rajasekar, R.; Kim N. H.; Lee, J. H. Carbon-Based Nanostructured Materials and Their Composites as Supercapacitor Electrodes. *J. Mater. Chem.* **2012**, *22*, 767-784.

51) Yao, F.; Pham, D. T.; Lee, Y. H. Carbon-Based Materials for Lithium-Ion Batteries, Electrochemical Capacitors, and Their Hybrid Devices, *Chem.Sus.Chem.* **2015,** *8*, 2284–2311,

52) Weir, E.; Lawlor, A.; Whelan, A.; Regan, F. The Use of Nanoparticles in Anti-Microbial Materials and Their Characterization. *Analyst* 2008, *133*, 835-845.

53) Zharov, V. P.; Mercer, K. E.; Galitovskaya, E. N.; Smeltzer, M. S. Photothermal Nanotherapeutics and Nanodiagnostics for Selective Killing of Bacteria Targeted with Gold Nanoparticles. *Biophys. J.* **2006**, *15*, 619- 627.

54) Huang, X.; El-Sayed, I. H.; Qian, W.; El-Sayed, M. A. Cancer Cell Imaging and Photothermal Therapy in the Near-Infrared Region by Using Gold Nanorods. *J. Am. Chem. Soc.* **2006**, *128*, 2115-2120.

55) Mazzola, L. Commercializing Nanotechnology. *Nat. Biotechnol*. **2003**, *21*, 1137-1143.

56) Ghaforyan, H.; Ebrahimzadeh, M.; Ghaffary, T.; Rezazadeh, H.; Sokout, J. Z. Microwave Absorbing Properties of Ni Nanowires Grown in Nanoporus Anodic Alumina Templates. *Chinese J. Phys.* **2014,** *52*, 233-238.

57) Shipway, N. A.; Eugeni, K.; Itamar, W. Nanoparticle Arrays on Surfaces for Electronic, Optical, and Sensor Applications. *Chem. Phys. Chem.* **2000**, *1*, 18-52.

58) Saha, K.; Sarit, S. A.; Chaekyu, K.; Xiaoning, L.; Vincent, M. R. Gold Nanoparticles in Chemical and Biological Sensing. *Chem. Rev.* **2012**, *112*, 2739-2779.

59) Mohammadibilankohi, S.; Ebrahimzadeh, M.; Ghaffary, T. Study of the Properties of Au/Ag Core/Shell Nanoparticles and its Application. *Indian J. Sci. Technol.* **2015**, *8*, 31-33.

60) Choi, Y. J.; Park, H. H.; Kim, H.; Park, H. H.; Chang, H. J.; Jeon, H. Fabrication and Characterization of Direct–Patternable Zno Films Containing Pt Nanoparticles. *Jap. J. Appl. Phys.* **2009,** *48*, 35504–1–35504–4.

61) Daniel, M. C.; Astruc, D. Gold Nanoparticles: Assembly, Supramolecular Chemistry, Quantum-Size-Related Properties, and Applications Toward Biology, Catalysis, and Nanotechnology. *Chem. Rev.* **2004**, 1*04*, 293-346.

62) Boisselier, E.; Astruc, D. Gold Nanoparticles in Nanomedicine: Preparations, Imaging, Diagnostics, Therapies and Toxicity. *Chem. Soc. Rev.* **2009**, *38*, 1759-1782.

63) Haick, H. Chemical Sensors Based on Molecularly Modified Metallic Nanoparticles. *J. Phys. D: Appl. Phys*. **2007**, *40*, 7173- 7186.

64) Ma, Z.; Tian, L.; Wang, T.; Wang C. Optical DNA Detection Based on Gold Nanorods Aggregation. *Anal. Chim. Acta.* **2010**, *673*, 179-84.

65) Sapsford, K. E.; Berti, L.; Medintz, I. L. Materials for Fluorescence Resonance Energy Transfer Analysis: Beyond Traditional Donor-Acceptor Combinations. *Angew. Chem., Int. Ed.* **2006**, *45*, 4562-4589.

66) Jain, P. K.; El-Sayed, I. H.; El-Sayed, M. A. Au Nanoparticles Target Cancer. *Nano Today* **2007**, *2*, 18-29.

67) Katz, E.; Willner, I.; Wang, J. Electroanalytical and Bioelectroanalytical Systems Based on Metal and Semiconductor Nanoparticles. *Electroanalysis* **2004**, *16*, 19-44.

68) Guo, S. J.; Wang, E. K. Synthesis and Electrochemical Applications of Gold Nanoparticles. *Anal. Chim. Acta* **2007**, *598*, 181-192.

69) Pumera, M.; Sanchez, S.; Ichinose, I.; Tang, J. Electrochemical Nano Biosensors, *Sens. Actuat. B Chem.* **2007**, *123*, 1195- 1205.

70) Nie, S. M.; Emory, S. R. Probing Single Molecules and Single Nanoparticles by Surface-Enhanced Raman Scattering. *Science* **1997**, *275*, 1102-1106.

71) Tudos, A. J.; Schasfoort, R. B. M. *Handbook of Surface Plasmon Resonance*; RSC Publishing: United Kingdom, 2008; p 1.

72) Marx, K. A. Quartz Crystal Microbalance: A Useful Tool for Studying Thin Polymer Films and Complex Biomolecular Systems at the Solution-Surface Interface. *Biomacromolecules* **2003**, *4*, 1099- 1120.

73) Nam, J. M.; Park, S. J.; Mirkin, C. A. Bio-Barcodes Based on Oligonucleotide-Modified Nanoparticles. *J. Am. Chem. Soc.* **2002**,*124*, 3820- 3821.

74) Hill, H. D.; Mirkin, C. A. The Bio-Barcode Assay for the Detection of Protein and Nucleic Acid Targets Using DTT-Induced Ligand Exchange. *Nat. Protoc.* **2006**, *1*, 324-336.

75) Edmundson, M. C.; Capeness, M.; Horsfall, L. Exploring the Potential of Metallic Nanoparticles within Synthetic Biology. *New Biotechnol.* **2014,** *31*, 572–578.

76) Qin Y. Silver-Containing Alginate Fibres and Dressings. *Int Wound J.* **2005**, *2*, 172–176.

77) Atiyeh, B. S.; Costagliola, M.; Hayek, S. N.; Dibo, S. A. Effect of Silver on Burn Wound Infection Control and Healing: Review of the Literature. *Burns* **2007,** *33*, 139–48.

78) Lansdown, A. B.; Silver in Health Care: Antimicrobial Effects and Safety in Use. *Curr. Probl. Dermatol.* **2006,** *33,* 17–34.

79) Schultz, S.; Smith, D. R.; Mock, J. J.; Schultz, D. A. Single-Target Molecule Detection with Nonbleaching Multicolor Optical Immunolabels. *Proc. Natl. Acad. Sci. U S A* **2000**, *97*, 996–1001.

80) Elechiguerra, J. L..; Burt, J. L.; Morones, J. R. Bragado, A. C.; Gao, X. Lara, H. H.; Yacaman, M. J. Interaction of Silver Nanoparticles with HIV-1, *J. Nanobiotechnology* **2005**, ***3,*** 6-10.

81) Bulte, J. W.; Zhang, S.; Gelderen, P. V.; Herynek, V.; Jordan, E. K.; Duncan, I. D. Neurotransplantation of Magnetically Labeled Oligodendrocyte Progenitors: Magnetic Resonance Tracking of Cell Migration and Myelination. *Proc. Natl. Acad. Sci. U S A* **1999,** *96*, 15256–61.

82) Chen, H.; Wei, G.; Ispas, A.; Stephen, G.; Hickey, Eychmu¨ller, A. Synthesis of Palladium Nanoparticles and Their Applications for Surface-Enhanced Raman Scattering and Electrocatalysis. *J. Phys. Chem. C* **2010**, *114*, 21976–21981.

83) Noguera, C. *Physics and Chemistry at Oxide Surfaces*; Cambridge University Press: United Kingdom, 1996; p 128.

84) Kung, H.H. *Transition Metal Oxides: Surface Chemistry and Catalysis*; Elsevier: Amsterdam, 1989; p 116.

85) Henrich, V. E.; Cox, P. A. *The Surface Chemistry of Metal Oxides;* Cambridge University Press: Cambridge, UK, 1994; p 85.

86) Wyckoff, R.W.G. *Crystal Structures,* Wiley: New York, 1964; p 52.

87) Ayyub, P.; Palkar, V. R.; Chattopadhyay, S.; Multani, M. Effect of Crystal Size Reduction on Lattice Symmetry and Cooperative Properties. *Phys. Rev. B* **1995**, *51*, 6135- 6138.

88) Pacchioni, G.; Ferrari, A. M.; Bagus, P. S. Cluster and Band Structure ab Initio Calculations on the Adsorption of CO on Acid Sites of the Tio_2 (110) Surface. *Surf. Sci.* **1996**, *350*, 159-175.

89) Mejias, J. A.; Marquez, A. M.; Fernandez-Sanz, J.; Fernández-García, M.; Ricart, J. M.; Sousa, C.; Illas, F. On Modelling the Interaction of CO on the MgO(100) Surface. *Surf. Sci.* **1995**, *327*, 59.

90) Fernández-García, M.; Conesa, J. C.; Illas, F.; Effect of the Madelung Potential Value and Symmetry on the Adsorption Properties of Adsorbate/Oxide Systems. *Surf. Sci.* **1996**, *349*, 207-215.

91) Rodriguez, J. A. Orbital-Band Interactions and the Reactivity of Molecules on Oxide Surfaces: From Explanations to Predictions. *Theor. Chem. Acc.* **2002**, *107*, 117-129.

92) Rodriguez, J. A.; Chaturvedi, S.; Kuhn, M.; Hrbek, J. Reaction of H_2S and S_2 with Metal/Oxide Surfaces: Band-gap Size and Chemical Reactivity. *J. Phys. Chem. B* **1998**, *102*, 5511- 5519.

93) Hoffmann, R. *Solids and Surfaces: A chemist's View of Bonding in Extended Structures*; VCH publishers: New York, 1988; p 142.

94) Lucas, E.; Decker, S.; Khaleel, A.; Seitz, A.; Futlz, S.; Ponce, A.; Li, W.; Carnes, C.; Klabunde, K. J. Nanocrystalline Metal Oxides as Unique Chemical Reagents/Sorbents. *Chem. Eur. J.* **2001**, *7*, 2505- 2510.

95) Anchell, J. L.; Hess, A. C. H_2O Dissociation at Low-Coordinated Sites on $(Mgo)_n$ Clusters, N = 4, 8. *J. Phys. Chem.* **1996**, *100*, 18317- 18321.

96) Richards, R.; Li, W.; Decker, S.; Davidson, C.; Koper, O.; Zaikovski, V.; Volodin, A.; Rieker, T. Onsolidation of Metal Oxide Nanocrystals. Reactive Pellets with Controllable Pore Structure that Represent a New Family of Porous, Inorganic Materials. *J. Am. Chem. Soc.* **2000**, *122*, 4921-4925.

97) Trovarelli, A.; Zamar, F.; Llorca, J.; de Leitenburg, C.; Dolcetti G.; Kiss, J. T. Nanophase Fluorite-Structured CeO_2-ZrO_2 Catalysts Prepared by High-Energy Mechanical Milling. *J. Catalysis* **1997**, *169*, 490-502.

98) Laberty-Robert, C., Long, J. W.; Pettigrew, K. A.; Stroud, R. M.; Rolison, D. R.; Ansart F.; Stevens, P. Synthesis of Pore-Solid Nanoarchitectures via Epoxide-driven Sol-gel Chemistry. *Adv. Mater*.**1997,** *18*, 615-618.

99) Hu, C.; Zhang, Z.; Liu, H.; Gao P.; Wang, Z. L. Direct Synthesis and Structuire Characterization of Ultrafine CeO_2 Nanoparticles. *Nanotechnology* **2006**, *17*, 5983-5987.

100) Jalilpour, M.; Fathalilou, M. Effect of Aging Time and Calcination Temperature on the Cerium Oxide Nanoparticles Synthesis via Reverse Co-Precipitation Method. *Int. J. Phys. Sci.* **2012**, *7*, 944-948.

101) Shukla, D.; Himabindu, K.; Chidambaram, K.; Deshmukh, K.; Ahamed, M. B.; Pasha, S. K. K. Synthesis of CeO_2 Nanoparticles via Solvothermal Route and Their Application in Sensors. *Int. J. Chem. Tech. Res.* **2015**, *8*, 46-53.

102) Marzi, L. D.; Monaco, A.; Lapuente, J. D.; Ramos, D.; Borras, M.; Gioacchino, M. D.; Santucci, S.; Poma, A. Cytotoxicity and Genotoxicity of Ceria Nanoparticles on Different Cell Lines in Vitro. *Int. J. Mol. Sci.* **2013**, *14*, 3065–3077.

103) Shah, V.; Shah, S.; Shah, H.; Rispoli, F. J.; McDonnell, K. T.; Workeneh, S.; Karakoti, A.; Kumar, A.; Seal, S. Antibacterial Activity of Polymer Coated Cerium Oxide Nanoparticles. *PLoS One.* **2012**, *7*, 47827-47830.

104) Manke, A.; Wang, L.; Rojanasakul, Y. Mechanisms of Nanoparticle-Induced Oxidative Stress and Toxicity. *Bio.Med. Research International* **2013**, *2013*. 1-15.

105) Fischer, R.; Maier, O. Interrelation of Oxidative Stress and Inflammation in Neurodegenerative Disease: Role of TNF. *Oxid. Med. Cell. Longev.* **2015**, *2015*, 1-18.

106) Wiener, E. C.; Brechbiel, M. W.; Brothers, H.; Magin, R. L.; Gansow, O. A.; Tomalia, D. A. Dendrimer-based Metal Chelates: A New Class of Magnetic Resonance Imaging Contrast Agents. *Magn. Reson. Med.* **1994**, *31*, 1-8.

107) Fu, H. L.; Cheng, S. X.; Zhang, X. Z.; Zhuo, R. X. Dendrimers/DNA Complexes Encapsulated in a Water Soluble Polymer and Supported on Fast Degrading Star Poly (DL-Lactide) for Localized Gene Delivery. *J. Control. Release* **2007**, *124*, 181-188.

108) Cheng, Y.; Wang, J.; Rao, T.; He, X.; Xu, T. Pharmaceutical Applications of Dendrimers: Promising Nanocarriers for Drug Delivery. *Front. Biosci*. **2008**, *13*, 1447-1471.

109) Mecke, A.; Uppuluri, S.; Sassanella, T. M.; Lee, D. K.; Ramamoorthy, A.; Baker, J. R. Direct Observation of Lipid Bilayer Disruption by Poly (Amidoamine) Dendrimers. *Chem. Phys. Lipids* **2004**, *132*, 3-14.

110) Roy, R. Roy, R. A.; Roy, D. M. Alternative Perspectives on Quasi-Crystallinity: Non-Uniformity and Nanocomposites. *Mater. Lett*. **1986**, *4*, 323-328.

111) Schmidt, D.; Shah, D.; Giannelis, E. P. New Advances in Polymer/Layered Silicate Nanocomposites. *Curr. Opin. Solid State Mater. Sci.* **2002**, *6*, 205-212.

112) Biercuk, M. J.; Llaguno, M. C.; Radosvljevicm, H. J. Carbon Nanotube Composites for Thermal Management. *Appl. Phys. Lett.* **2002**, *80*, 2767-2769.

113) Ounaies, Z.; Park, C.; Wise, K. E.; Siochi, E. J.; Harrison, J. S. Electrical Properties of Single Wall Carbon Nanotube Reinforced Polyimide Composites. *Compos. Sci. Technol.* **2003**; *63*, 1637- 1646.

114) Dalton, A. B.; Coolins, S. Muñoz, E.; Razal, J. M.; Ebron, V. H.; Ferraris, J. P.; Super-Tough Carbon-Nanotube Fibres: These Extraordinary Composite Fibres Can Be Woven into Electronic Textiles. *Nature* **2003**; *423*, 703-703.

115) Choa, Y. H.; Yang, J. K.; Kim, B. H.; Jeong, Y. K.; Lee, J. S.; Nakayama, T. Preparation and Characterization of Metal: Ceramic Nanoporous Nanocomposite Powders. *J. Magn. Magn. Mater.* **2003**, *266*, 12-19.

116) Camargo, P. H. C.; Satyanarayana, K. G.; Wypych, F. Nanocomposites: Synthesis, Structure, Properties and New Application Opportunities. *Materials Research* **2009**, *12*, 1-39.

117) Maiti A.; Bhattacharyya, S. Review: Quantum Dots and Application in Medical Science, *Int. J. Chem. Chem. Eng*. **2013**, *3*, 37-42.

118) Knoss, R.W. *Quantum Dots: Research, Technology and Applications;* Nova Science Publishers: New York, 2008; p 15.

119) Poole, C. P. Owens, F. J. *Introduction to Nanotechnology;* Wiley: New York, 2003; p 25.

120) Sharon, M. and Sharon, M. *Graphene: An Introduction to the Fundamentals and Industrial Applications;* Wiley: New York, 2015; p 39.

121) Chauviré, T.; Mouesca, J. M.; Gasparutto, D.; Ravanat, J. L.; Lebrun, C.; Gromova, M.; Jouneau, P. H.; vin, J. C.; Gambarelli, S.; Maurel, V. Redox Photocatalysis with Water-Soluble Core–Shell Cdse-Zns Quantum Dots. *J. Phys. Chem. C* **2015**, *119*, 17857–17866.

122) Choi, M. K.; Yang, J.; Kang, K.; Kim, D. C.; Choi, C.; Park, C.; Kim, S. J.; Chae, S. I.; Kim, T. H.; Kim, J. H.; Hyeon, T.; Kim, D. H. Wearable Red–Green–Blue Quantum Dot Light-Emitting Diode Array Using High-Resolution Intaglio Transfer Printing. *Nat. Commun.* **2015,** *6*, 7149-7156.

123) Chen, Y.; Rosenzweig, Z. Luminescent CdS Quantum Dots as Selective Ion Probes. *Anal. Chem.* **2002**, *74*, 5132-5138.

124) Barmenkov, Y.O.; Starodumov, A.N.; Lipovskii, A.A. Temperature Fiber Sensor Based on Semiconductor Nanocrystallite-Doped Phosphate Glasses. Appl. Phys. Lett. 1998, 73, 541-543.

125) Patolsky, F.; Gill, R.; Weizmann, Y.; Mokari, T.; Banin, U.; Willner, I. Lighting-Up the Dynamics of Telomerization and DNA Replication by Cdse-Zns Quantum Dots. *J. Am. Chem. Soc.* **2003**, *125*, 13918–13919.

126) Smith, A. M.; Duan, H. W.; Mohs, A. M.; Nie, S. M. Bioconjugated Quantum Dots For in Vivo Molecular and Cellular Imaging. *Adv. Drug Delivery Rev*. **2008**, *60*, 1226–1240.

127) Larson, D. R.; Zipfel, W. R.; Williams, R. M.; Clark, S. W.; Bruchez, M. P.; Wise, F. W.; Webb, W. W. Water-Soluble Quantum Dots for Multiphoton Fluorescence Imaging in Vivo. *Science* **2003**, *300*, 1434–1436.

128) Mel, A. D.; Oh, J. T.; Ramesh. B.; Seifalian, A. M. Biofunctionalized Quantum Dots for Live Monitoring of Stem Cells: Applications in Regenerative Medicine. *Regen. Med.* **2012,** *7*, 335-347.

129) Xu, X. Y.; Ray, R.; Gu, Y. L.; Ploehn, H. J.; Gearheart, L.; Raker K.; Scrivens, W. A. Electrophoretic Analysis and Purification of Fluorescent Single-Walled Carbon Nanotube Fragments. *J. Am. Chem. Soc.* **2004**, *126*, 12736–12737.

130) Sun, Y. P.; Zhou, B.; Lin, Y.; Wang, W.; Fernando, K. A. S.; Pathak, P.; Meziani, M. J.; Harruff, B. A.; Wang, X.; Wang, H. F.; Luo, P. G.; Yang, H.; Kose, M. E.; Chen, B. L.; Veca, L. M.; Xie, S. Y. Quantum Sized Carbon Dots for Bright and Colorful Photoluminescence. *J. Am. Chem. Soc.* **2006**, *128*, 7756–7757.

131) Liu, H. P. Ye, T. Mao, C. D. Fluorescent Carbon Nanoparticles Derived from Candle Soot. *Angew. Chem., Int. Ed.* **2007**, *46*, 6473-6475.

132) Ray, S. C.; Saha, A.; Jana, N. R.; Sarkar, R. Fluorescent Carbon Nanoparticles: Synthesis, Characterization, and Bioimaging Application. *J. Phys. Chem. C* **2009**, *113*, 18546–18551.

133) Bourlinos, A. B.; Stassinopoulos, A.; Anglos, D.; Zboril, R.; Karakassides, M.; Giannelis, E. P. Surface Functionalized Carbogenic Quantum Dots. *Small* **2008**, *4*, 455-458.

134) Zhou, J. G.; Booker, C.; Li, R. Y.; Zhou, X. T.; Sham, T. K.; Sun, X. L.; Ding, Z. F. An Electrochemical Avenue to Blue Luminescent Nanocrystals from Multiwalled Carbon Nanotubes (MWCNTs). *J. Am. Chem. Soc.* **2007**, *129*, 744-745.

135) Bao, L.; Zhang, Z. L.; Tian, Z. Q.; Zhang, L.; Liu, C.; Lin, Y.; Qi, B.; Pang, D. W. Electrochemical Tuning of Luminescent Carbon Nanodots: From Preparation to Luminescence Mechanism. *Adv. Mater.* **2011**, *23*, 5801-5806.

136) Zhu, H.; Wang, X. L.; Li, Y. L.; Wang, Z. J.; Yang F.; Yang, X. R. Microwave Synthesis of Fluorescent Carbon Nanoparticles with Electrochemiluminescence Properties. *Chem. Commun.* **2009**, *34*, 5118-5120.

137) Li, H. T.; He, X. D.; Liu, Y.; Huang, H.; Lian, S. Y.; Lee, S. T.; Kang, Z. H. One-step Ultrasonic Synthesis of Water-Soluble Carbon Nanoparticles with Excellent Photoluminescent Properties. *Carbon* **2011**, *49*, 605-609.

138) Bourlinos, A. B.; Stassinopoulos, A.; Anglos, D.; Zboril, R.; Georgakilas, V.; Giannelis, E. P. Photoluminescent Carbogenic Dots. *Chem. Mater.* **2008**, *20*, 4539-4541.

139) Ming, H.; Ma, Z.; Liu, Y.; Pan, K. M.; Yu, H.; Wang, F.; Kang, Z. H. Large Scale Electrochemical Synthesis of High Quality Carbon Nanodots and Their Photocatalytic Property. *Dalton Trans.* **2012**, *41*, 9526- 9531.

140) Wang, X.; Cao, L.; Yang, S. T.; Lu, F. S.; Meziani, M. J.; Tian, L. L.; Sun, K. W.; Bloodgood M. A.; Sun, Y. P. Bandgap-Like Strong Fluorescence in Functionalized Carbon Nanoparticles. *Angew. Chem., Int. Ed.* **2010**, *49*, 5310-5314.

141) Zheng, L. Y.; Chi, Y. W.; Dong, Y. Q.; Lin, J. P.; Wang, B. B. Electrochemiluminescence of Water-Soluble Carbon Nanocrystals Released Electrochemically from Graphite. *J. Am. Chem. Soc.* **2009**, *131*, 4564- 4565.

142) Shen, J. H.; Zhu, Y. H.; Yang, X. L.; Li, C. Z. Graphene Quantum Dots: Emergent Nanolights for Bioimaging, Sensors, Catalysis and Photovoltaic Devices. *Chem. Commun.* **2012**, *48*, 3686- 3699.

143) Baker, S. N.; Baker, G. A. Luminescent Carbon Nanodots: Emergent Nanolights. *Angew. Chem., Int. Ed.* **2010**, *49*, 6726- 6744.

144) Liu, C.; Zhang, P.; Tian, F.; Li, W.; Li, F.; Liu, W. One-step Synthesis of Surface Passivated Carbon Nanodots by Microwave Assisted Pyrolysis for Enhanced Multicolor Photoluminescence and Bioimaging. *J. Mater. Chem.* **2011**, *21*, 13163-13167.

145) Pan, D. Y.; Guo, L.; Zhang, J. C.; Xi, C.; Xue, Q.; Huang, H.; Li, J. H.; Zhang, Z. W.; Yu, W. J.; Chen, Z. W.; Li, Z.; Wu, M. H. Cutting Sp^2clusters in Graphene Sheets into Colloidal Graphene Quantum Dots with Strong Green Fluorescence. *J. Mater. Chem.* **2012**, *22*, 3314-3318.

146) Li, H. T.; He, X. D.; Kang, Z. H.; Huang, H.; Liu, Y.; Liu, J. L.; Lian, S. Y.; Tsang, C. H. A.; Yang, X. B.; Lee, S. T. Water-Soluble Fluorescent Carbon Quantum Dots and Photocatalyst Design. *Angew. Chem., Int. Ed.* **2010**, *49*, 4430-4434.

147) Esteves da Silva, J. C. G.; Goncalves, H. M. R. Analytical and Bioanalytical Applications of Carbon Dots. *TrAC, Trends Anal. Chem.* **2011**, *30*, 1327-1336.

148) Li, H. Kang, Z. Liu, Y. Lee, S. T. Carbon Nanodots: Synthesis, Properties and Applications, *J. Mater. Chem.* **2012**, *22*, 24230- 24253.

149) Yogeswaran, U.; Chen, S. M. A Review on the Electrochemical Sensors and Biosensors Composed of Nanowires as Sensing Material. *Sensors* **2008**, *8*, 290-313

150) Stradiotto, N. R.; Yamanaka H.; Valnice M.; Zanoni, B.; Electrochemical Sensors: A Powerful Tool in Analytical Chemistry. *J. Braz. Chem. Soc.* **2003,** *14*, 159-173.

151) Shruthi, G. S.; Amitha C. V.; Mathew, B. B. Biosensors: A Modern Day Achievement. *J. Instrum. Technol.* **2014**, *2*, 26-39.

152) P. Malik, V. Katyal, V. Malik, A. Asatkar, G. Inwati, T. K. Mukherjee, Nanobiosensors: Concepts and Variations. *ISRN Nanomaterials* **2013**, *2013*, 1-9.

153) Prabhu, V. V.; Chidambaranathan N.; Gopal, V. A Historical Review on Current Medication and Therapies for Inducing and Inhibiting Angiogenesis. *J. Chem. Pharm. Res.* **2011**, *3*, 526-533.

154) Folkman, J.; Braunwald, E.; Fauci, A. S.; Kasper, D. L. *Harrision's Texbook of Internal Medicine*; McGraw-Hill: New York, 2000; p 132.

155) Prabhu, V. V.; Chidambaranathan, N.; Gopal, V. Evaluation and Quantification of Angiogenesis Activity of Terminalia Bellirica Roxb, By Mice Sponge Implantation Method. *J. Young Pharm.* **2012**, *4*, 22–27.

156) Li, W.; Talcott, K.; Zhai, A.; Kruger, E.; Li, V. The Role of Therapeutic Angiogenesis in Tissue Repair and Regeneration. *Adv. Skin Wound Care.* **2005**, *18*, 491-500.

157) DeAssis, D. N.; Mosqueira, V. C.; Vilela, J. M.; Andrade, M. S.; Cardoso, V. N. Release Profiles and Morphological Characterization by Atomic Force Microscopy and Photon Correlation Spectroscopy of 99m Technetium – Fluconazole Nanocapsules. *Int. J. Pharm.* 2008; 349: 152 –160.

158) Molpeceres, J.; Aberturas, M. R.; Guzman, M. Biodegradable Nanoparticles as a Delivery System for Cyclosporine: Preparation and Characterization. *J. Microencapsul.* **2000**, 17, 599-614.

159) Polakovic M., Gorner T., Gref R., Dellacherie E. Lidocaine Loaded Biodegradable Nanospheres. II. Modelling of Drug Release. *J. Control Release.* **1999**, *60*, 169 -177.

Chapter 2

CeO_2-MWCNTs Nanocomposite Based Electrochemical Sensor for Acetaldehyde

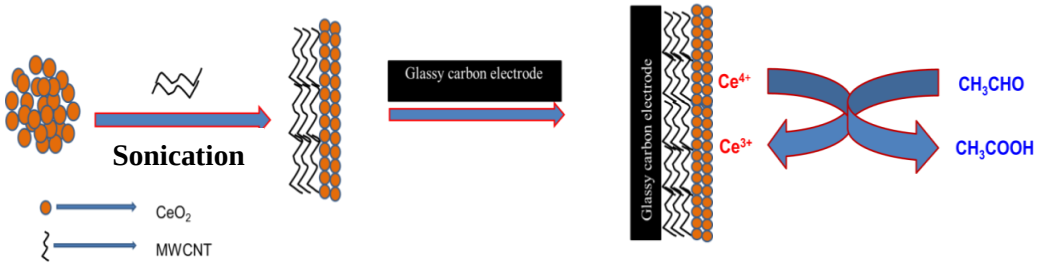

2.1 Abstract

The present study endeavours to build a new, highly sensitive and selective electrochemical sensor with a CeO_2-MWCNTs nanocomposite film, which enhances the sensing platform to detect acetaldehyde. The chemically synthesized CeO_2 nanoparticles (CeO_2NPs) were subjected to adsorb on MWCNTs. Thus the prepared nanocomposite was characterized by XRD, UV-Visible absorption spectroscopy, SEM and electrochemical impedance spectroscopy (EIS). The drop to drop method on glassy carbon electrode (GCE) was employed in the preparation of the CeO_2-MWCNTs nanocomposite modified glassy carbon electrode (CeO_2-MWCNT/GCE) which could sense nanomolar levels of acetaldehyde by cyclic voltammetry (CV). Under optimal conditions, the developed sensor gives linear calibration curve in the concentration range of 0.01 to 10 μM of acetaldehyde with a detection limit of 7.4 nM. In addition, the sensors offers a good precision of 1.6 % at 1μM of acetaldehyde. Moreover, it exhibited reasonably good selectivity towards acetaldehyde in conjunction with different co-existing organic species and was successfully applied to the analysis of synthetic fruit juice samples.

2.2 Introduction

The incomplete combustion of petroleum fuels and biomass produces aldehydes which are ubiquitous air pollutants.[1] Inhalation of acetaldehyde may result in bronchitis, dottiness, protein denaturation and sometimes even death.[2-4] Acetaldehyde is found in many food items including, ripe fruits, beverages, vegetables, cheese and other dairy products. Ripened fruit contains about 80 % more acetaldehyde than unripe fruit. In beverages, it is formed due to the enzymatic oxidation of alcohol. Therefore, the main pathways by which acetaldehyde enter our body includes air, water, alcohol drinking and tobacco smoke. An increased concentration of acetaldehyde in our body favours its reaction with DNA due to its strong electrophilic properties which could induce mutagenesis and carcinogenesis.[5, 6] Being toxic at low concentration and carcinogenic when exposed for a prolonged time, acetaldehyde detection is significantly important for monitoring environmental and domestic pollution[7-9], as well as food sophistication or contamination from packaging. Hence, the development of sensitive, rapid, simple, and low-cost devices for acetaldehyde detection is the need of the day.

There are limited reports available on acetaldehyde detection. Afkhami *et al*. employed a neutral red- sulfite-acetaldehyde system to detect traces of acetaldehyde by developing a kinetic method.[10] Yashuhara and shibamoto detected it using gas chromatography with a nitrogen- phosphorus detector.[11] A gas chromatographic method using an electron capture detector was adopted for the determination of the same by Mori *et al.*[12] High performance liquid chromatography has been used for the same purpose.[13-16] Determination of aliphatic aldehydes in aqueous solution by the inhibition of luminal chemiluminescence induced by hydrogen peroxide in the presence of potassium hexacyanoferrate has been reported.[17] Since all these methods converted acetaldehyde to

some other form to detect it, they are considered to be indirect methods. However, there are studies reported to have detected gaseous acetaldehyde directly by an amperomety based sensor.[18]

Cerium oxides mark their distinctive application as excellent catalysts. Over the years, cerium oxide and cerium oxide-based materials have been investigated as structural and electronic promoters of heterogeneous catalytic reactions. One of the most familiar applications in this field is the utilization of CeO_2 as the key component in three-way catalysts for the treatment of exhaust gas from automobiles.[19] Among different lanthanide oxides, ceric oxides are widely used due to their excellent catalytic properties.[20-22] CeO_2 and its nanocomposite films like CeO_2-$BaTiO_3$, cerium oxide (Nano CeO_2)–chitosan were also explored for applications in electronic devices[23] and biosensors.[24, 25] Composite materials based on CNTs and metal oxide nanomaterials integrate their unique characteristics and functions and may also exhibit some new properties caused by the cooperative effects between the two kinds of materials.[26-30] Therefore, these composite materials have shown very attractive potential applications in many fields.

In this article we describe a direct method for the determination of acetaldehyde with CeO_2-MWCNTs/GCE by cyclic voltammetry. We mainly concentrated on the CeO_2-MWCNTs nanocomposite based on the report that, CeO_2 converts acetaldehyde into acetic acid by donating its labile oxygen atom present in its crystal lattices due to its fluorite structure. Here, Ce^{4+} is reduced into Ce^{3+} by oxidizing molecules on its surface.[31]

2.3 Preparation of CeO_2-MWCNTs nanocomposite and fabrication of CeO_2-MWCNTs/GCE

CeO_2 NPs were synthesized by a chemical method reported in the literature.[32] A $Ce(NO_3)_3$ solution was prepared by dissolving two grams of CeO_2 in a mixture of concentrated HNO_3 and H_2O_2 (10 mL) with a volume ratio of 1:5. The prepared

$Ce(NO_3)_3$ solution was further added dropwise into 2 M ammonia solution until complete precipitation occured. The obtained solution was washed in a centrifuge and the solution pH was regulated as 1.45 by using 1 M HNO_3. Finaly the yellowish CeO_2NPs was obtained by heating the above solution for about 60 ^{0}C on a water bath. A known amount of synthesized CeO_2NPs was further added to an appropriate amount of MWCNTs and sonicated for 30 minutes to form a homogeneous solution. The Van der Waals force of attraction between the CeO_2NPs and MWCNTs made the CeO_2NPs easily attach to the walls of the MWCNTs. This benefit was used for the fabrication of the CeO_2-MWCNTs/GCE. The GCE was polished with an alumina slurry followed by sonication. On to this fine surface of GCE, 5 μL of the above suspension was added by the drop to drop method and air dried to obtain the CeO_2-MWCNTs/GCE. Thus the developed modified electrode was used to detect acetaldehyde in 0.1 M KNO_3 at pH 6.

2.4 Characterization studies

The prepared CeO_2-MWCNTs nanocomposite was characterized by the following methods.

2.4.1 Spectral and morphological characterization

Figure 2.1 shows the XRD patterns of CeO_2NPs and CeO_2-MWCNTs nanocomposite in the range of 10-70^0. The four peaks at 28.5^0, 33.1^0, 47.5^0 and 56.3^0 correspond to (111), (200), (220) and (311) planes of the face centered cubic phase of CeO_2NPs (JCPDS 78–0694). After incorporating MWCNTs two additional peaks are observed at 26.2^0 and 42.1^0 corresponding to the (002) and (101) planes which are clear evidence of the adsorption of CeO_2NPs on the MWCNTs. From the Scherrer formula,

$$D = K\lambda/\beta \cos\theta$$

where D is the crystallite size, K is the Sherrer constant (0.89), λ is the wave length of Cu Kα radiation (0.15406 nm), β is the FWHM (full width of peak intensity at half maximum) in radians, θ is the peak (111) position in degrees, particle size of CeO_2NPs was calculated and was found to be 15-25 nm.

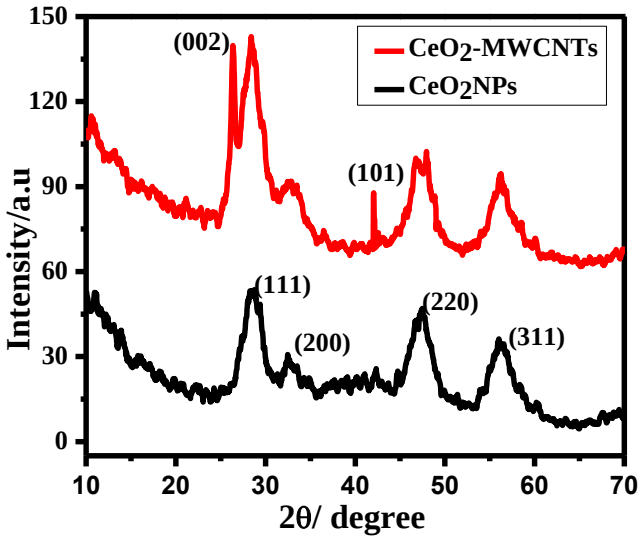

Figure 2.1: *XRD patterns of CeO_2NPs and CeO_2-MWCNTs nanocomposite*

Figure 2.2 shows the UV-Visible absorption spectra of CeO_2NPs and CeO_2-MWCNTs nanocomposite. A well-defined sharp and strong absorbance peak at 300 nm is observed which is due to Ce^{4+}, indicating a narrow and uniform particle size distribution obtained via this route. There was no change in CeO_2NPs absorbance after the addition of MWCNTs, which suggests that MWCNTs have no influence on the size and the structure of CeO_2NPs. Hence, the role of MWCNTs was to provide a better surface for the oxidation of acetaldehyde, thereby increasing the current, which was confirmed from the electrochemical characterization studies.

Figure 2.3 (a), (b), and (c) show the SEM images of CeO_2NPs, MWCNTs and CeO_2-MWCNTs nanocomposite. It is observed that CeO_2NPs possessed a spherical shape with a size of 10-30 nm (a) and MWCNTs were in a tubular form (b). The

spherically shaped CeO_2NPs are adsorbed on the surface of MWCNTs as shown in (c) and this is the concrete indication of the CeO_2-MWCNTs nanocomposite.

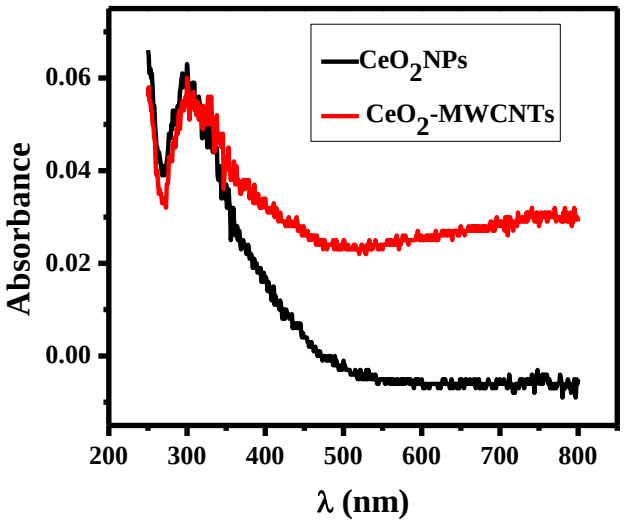

Figure 2.2: *UV-Visible absorption spectra of CeO_2NPs and CeO_2–MWCNTs nanocomposite*

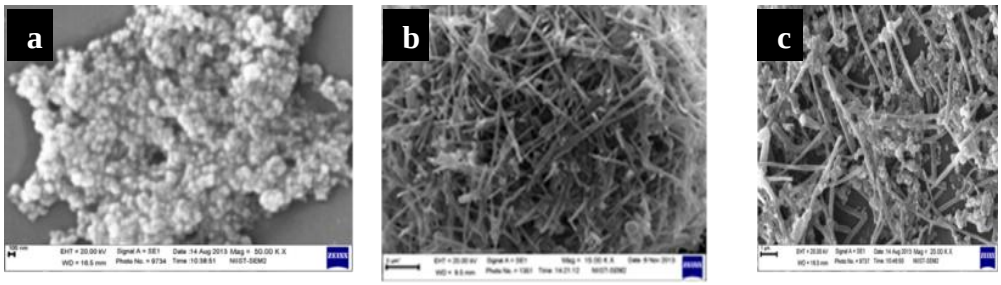

Figure 2.3: *SEM images of* ***(a)*** *CeO_2NPs* ***(b)*** *MWCNTs and* ***(c)*** *CeO_2-MWCNTs naanocomposite*

2.5 Electrochemical characterization

2.5.1 Electrochemical impedance spectroscopy

EIS is a commonly used characterization technique for studying the impedance changes of the electrode surface during the modification process. In a Nyquist plot, the semi-circular or real portion is related to the electron transfer resistance R_{ct} and linear or imaginary part is related to the controlled diffusion process. The electron transfer resistance is dependent on the diameter of the semi-circular portion. A large semicircle with a high R_{ct} means the system has a higher resistance to the flow of electrons. Figure

2.4 shows the EIS of the bare GCE (a), CeO_2NPs/GCE (b) and CeO_2-MWCNTs/GCE (c) in the $[Fe(CN)_6]^{3-/4-}$ system. Inset is the equivalent circuit used to analyse the impedance behavior. The small semicircular portion of the GCE implies that it has a low resistance towards the electron transfer process. After modifying with CeO_2NPs, the diameter of the semicircle increased with an R_{ct} value of 489 Ω, indicating that the CeO_2NPs hindered the electron transfer of the electrochemical probe of $Fe(CN)_6^{3/4-}$ and this hindrance was decreased (R_{ct} =401 Ω) after incorporating MWCNTs with the CeO_2NPs. These results showed the efficiency of the CeO_2-MWCNTs/GCE.

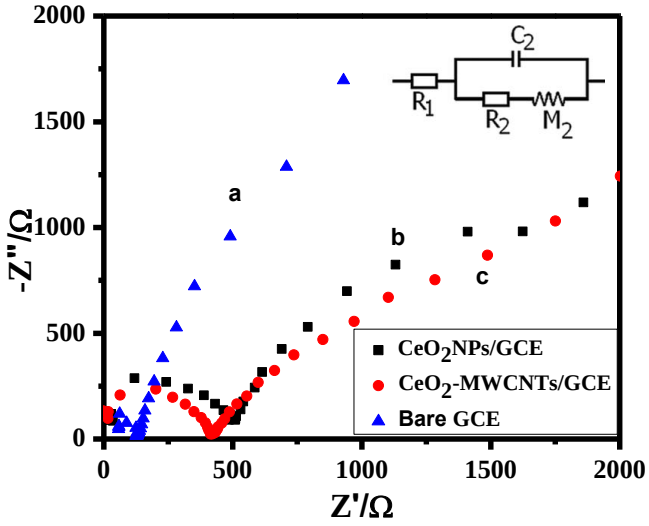

Figure 2.4: A *Nyquist diagram of electrochemical impedance spectra of the bare GCE, CeO_2NPs/GCE and CeO_2-MWCNTs/GCE in 0.1 M KNO_3 solution containing 5.0 mM $[Fe(CN)_6]^{3-/4-}$(1:1). Inset is the equivalent circuit of the CeO_2-MWCNTs/GCE electrochemical impedance measurement system*

2.5.2 Cyclic voltammetric analysis

In comparison to the bare GCE and CeO_2NPs/GCE, CeO_2-MWCNTs/GCE provided more electroactive surface for the oxidation of acetaldehyde. This was confirmed through the cyclic voltammteric experiments of the different electrodes in 1 mM $K_3[Fe(CN)_6]$ solution. Figure 2.5 represents the cyclic voltammograms at the bare

GCE (curve a), CeO_2NPs/GCE (curve b) and CeO_2-MWCNTs/GCE (curve c) in 1 mM $K_3[Fe(CN)_6]$ with 0.1 M KCl as the supporting electrolyte.

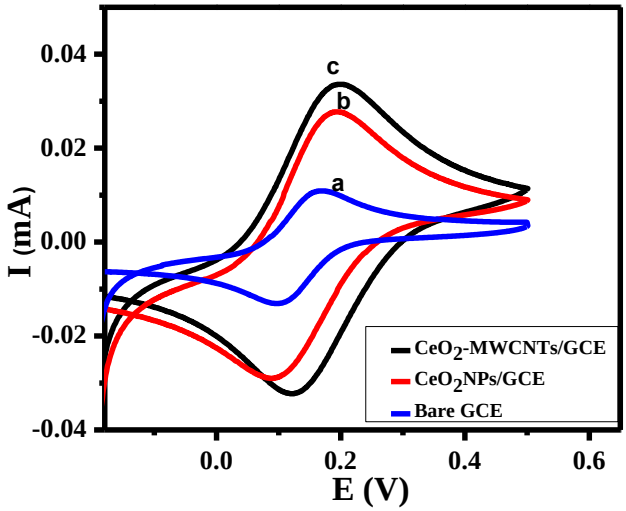

Figure 2.5: *Cyclic voltammograms at the bare GCE,* CeO_2NPs*/GCE and* CeO_2*-MWCNTs/GCE in 1 mM* $K_3[Fe(CN)_6]$ *and 0.1 M KCl as the supporting electrolyte at a scan rate of 50 mV* s^{-1}

At the bare GCE, ferricyanide showed an anodic peak at 160 mV with a peak current of 11 μA and a cathodic peak at 98 mV with 13 μA. ΔE_p at the bare GCE was found to be 62 mV, which was an indication of reversible nature of bare GCE. At the CeO_2NPs/GCE, the anodic peak potential shifted to the more positive side i.e., 196 mV and the cathodic peak potential shifted to the more negative side i.e., 93 mV with ΔE_p of 103 mV. Sensitivity of $K_3[Fe(CN)_6]$ increased remarkably, which could be explained by the change in the particle size and the increase in the electroactive surface area with the CeO_2NPs/GCE, but at the same time the process became quasi reversible. After adding MWCNTs to the CeO_2NPs/GCE, a rapid and a sharp increase in both the anodic (28 μA) and cathodic currents (29 μA) was observed with a shift in both the anodic (193 mV) and cathodic peak (123 mV) potentials. ΔE_p at the CeO_2-MWCNTs/GCE was 70 mV, which implied the electrochemical process had changed to reversible, indicating the

good performance of the modified electrode. Therefore, the electrocatalytic effect is higher with the CeO_2-MWCNTs/GCE as compared to the CeO_2NPs/GCE and bare GCE.

Figure 2.6 showed the cyclic voltammograms of 1 μM acetaldehyde in a potential range of -0.4 to 1.2 V at a scan rate of 50 mV s^{-1} in 0.1 M KNO_3 solution at the bare GCE (curve a), MWCNTs/GCE (curve b) CeO_2NPs/GCE (curve c) and CeO_2-MWCNTs/GCE (curve d). There were no peaks observed at the bare GCE, or MWCNTs/GCE. One broad anodic peak at 0.88 V due to the oxidation of Ce was generated at the CeO_2NPs/GCE, which further sharpened and shifted to 0.8 V with an increase in the current at the CeO_2-MWCNTs/GCE. The broadened reduction peak which appeared at 0.3 V on the CeO_2NPs/GCE was shifted to 0.4 V on the CeO_2-MWCNTs/GCE representing the quasi reversible nature of both the CeO_2NPs/GCE and the CeO_2-MWCNTs/GCE.

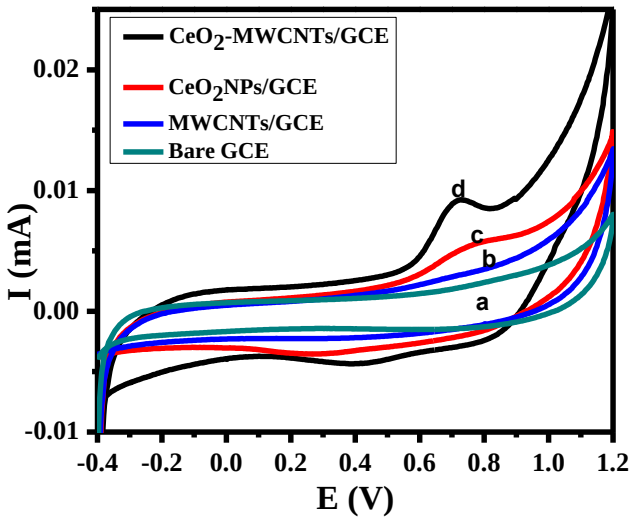

Figure 2.6: *Cyclic voltammograms of acetaldehyde (1 μM) at the bare GCE,* CeO_2NPs*/GCE , MWCNTs/GCE and* CeO_2*-MWCNTs/GCE in 0.1 M* KNO_3 *as the supporting electrolyte at a scan rate of 50 mV* s^{-1}

2.6 Voltammetric analysis of acetaldehyde at the CeO_2-MWCNTs/GCE

Figure 2.7 (a) shows the cyclic voltammetric curves of acetaldehyde at different concentrations in 0.1 M KNO_3 solution of pH 6.0. For each addition of acetaldehyde

there was a decrease in peak current. When the acetaldehyde concentration increased, more CeO_2NPs was used for the conversion of acetaldehyde to acetic acid, this could be the reason for the decrease in the peak current. The plot of peak current Vs [acetaldehyde] (Figure 2.7(b(i))) gives dual linearity, one at a lower concentration range from 0.01 to 0.5 μM and other in a higher concentration range from 1 to 10 μM. This means the fabricated CeO_2-MWCNTs/GCE could be applied for the determination over a wide range of acetaldehyde concentrations.

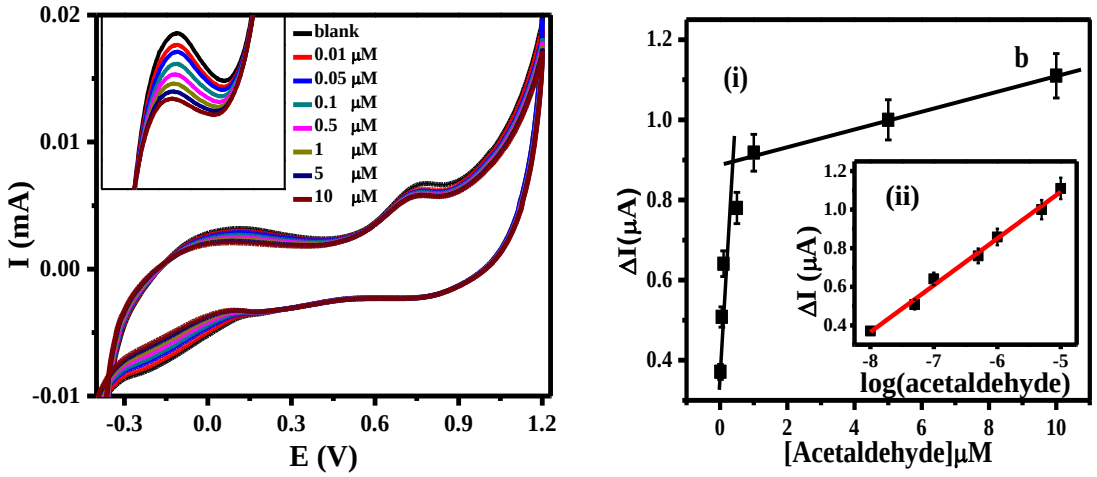

Figure 2.7: ***(a)*** *Cyclic voltammograms at the CeO_2-MWCNTs/GCE in the presence of different concentrations of acetaldehyde, (**b**) calibration curve in the range of 0.01 to 10 μM of acetaldehyde, (i) Ip Vs [acetaldehyde] and (ii) Ip Vs log [acetaldehyde] plots*

For the calculation of the limit of detection, a plot of peak current Vs log [acetaldehyde] was drawn. Again, a good linear graph with a wider range of concentrations, 0.01 to 10 μM was obtained (Figure 2.7(b(ii)). The limit of detection was calculated as 7.4 nM based on 3 times the standard deviation of the blank value. The relative standard deviation was found to be 1.6 % for 10 replicate determinations of 1 μM acetaldehyde, which revealed the extremely high precision of the designed acetaldehyde sensor. Moreover, the developed CeO_2-MWCNTs/GCE was able to produce the same current for a period of one week; this showed the stability of the electrode.

2.7 Mechanism

The Possible mechanism for this electrode process could be explained as follows, Ce^{4+} is reduced itself into Ce^{3+} by oxidizing the acetaldehyde molecules on its surface. The energy between 4f and 5d is almost the same so we can easily switch off Ce^{4+}/Ce^{3+} inter conversion by applying a low potential energy. In the fluorite structure of CeO_2, the oxygen atoms can easily move around the crystal allowing the cerium to reduce or oxidize the molecule on its surface. Hence the CeO_2 can easily convert acetaldehyde into acetic acid by donating its labile oxygen atoms to the acetaldehyde. Scheme 2.1 gives the schematic representation of the fabrication of CeO_2-MWCNT/GCE and its sensing mechanism towards the acetaldehyde.

$$Ce\ (IV) + CH_3CHO \longrightarrow Ce\ (III) + CH_3COOH$$

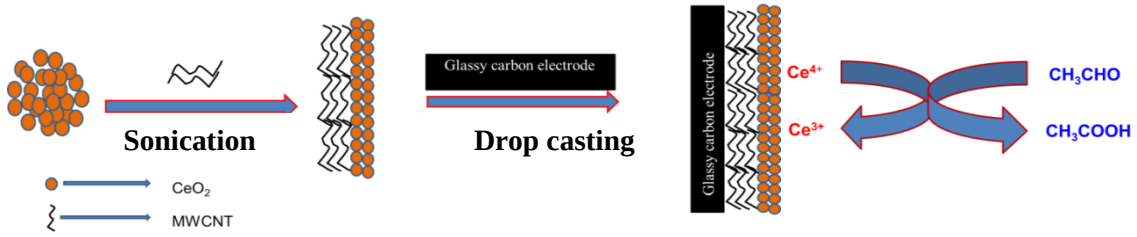

Scheme 2.1: *Preparation of CeO_2-MWCNTs/GCE and its sensing towards the acetaldehyde*

2.8 Effect of scan rate

The effect of scan rate on the electrocatalytic behavior of the modified electrode towards the oxidation of 1 μM acetaldehyde was studied by CV. Figure 2.8 (a) & Figure 2.9 (a) show the cyclic voltammograms of oxidation of acetaldehyde at various scan rates (20 to 90 mV s^{-1}) at the CeO_2-MWCNTs/GCE and CeO_2NPs/GCE respectively. It could be perceived from the CV's that with an increase in scan rate, the peak potential for the electro-oxidation of acetaldehyde shifts to a more positive potentials, suggesting a kinetic limitation on the reaction between the redox sites of the modified electrode and

acetaldehyde. In addition, the catalytic current increases with increasing scan rate, because in short scale experiments there is not enough time for the catalytic reaction to take place completely.

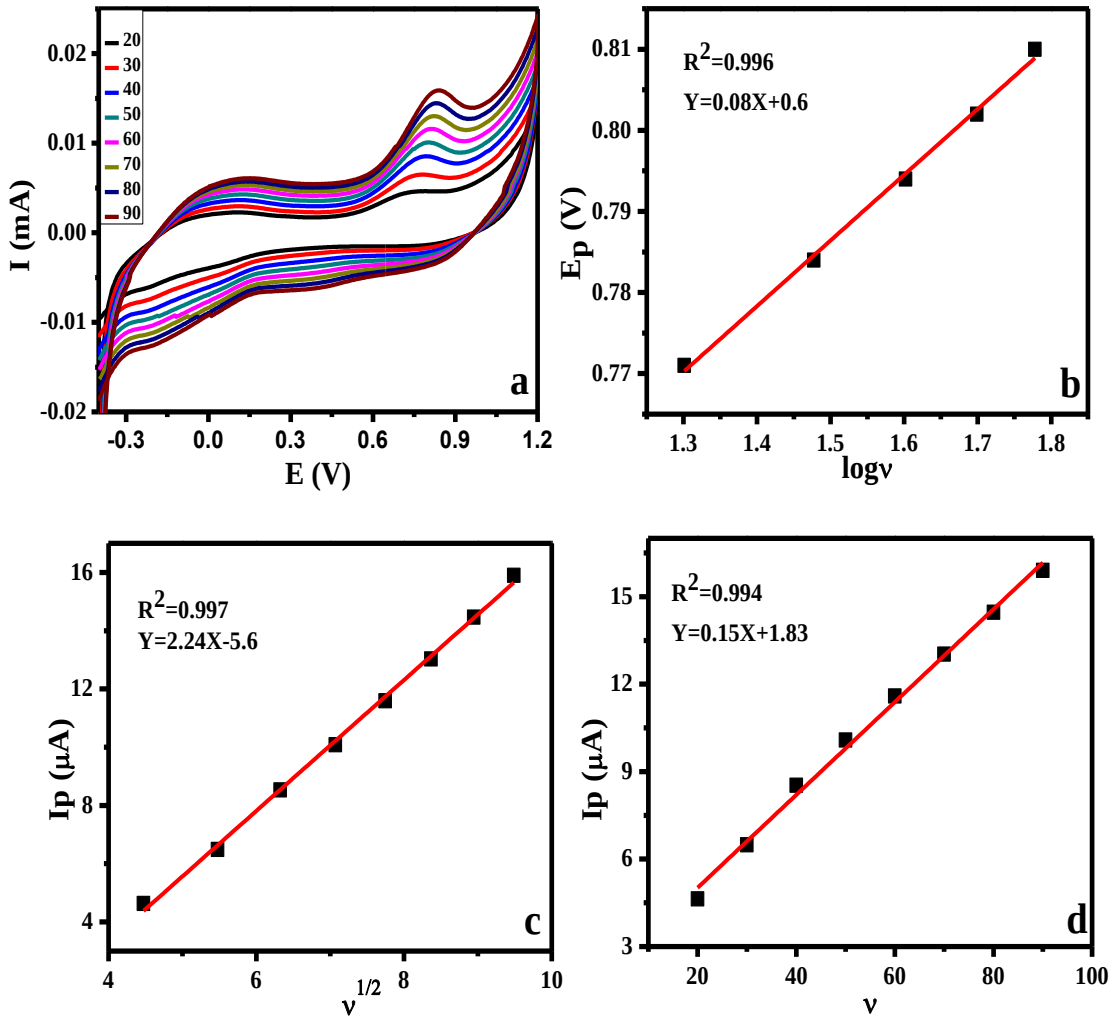

Figure 2.8: ***(a)*** *Cyclic voltammograms of oxidation of acetaldehyde (1 μM) at various scan rates (20 to 90 mV* s^{-1}*) at* CeO_2*-MWCNTs/GCE* ***(b)*** *plot of Ep Vs log ν* ***(c)*** *plot of Ip Vs* $\nu^{1/2}$ *and* ***(d)*** *plot of Ip Vs ν*

In order to obtain information about the rate determining step, the Tafel slope was drawn using the following equation, for a diffusion controlled process,

$$Ep = (2.303RT/n\alpha F) \log \nu + \text{constant}$$

where Ep is potential, R is gas constant, T is the temperature, n is the number of electron transferred and F is the Faraday constant. The electron transfer coefficient (α) was

calculated from the slope of the plot of Ep Vs log ν and was found to be 0.73 for the CeO_2-MWCNTs/GCE (Figure 2.8 (b)). Similarly for the CeO_2NPs/GCE, the α value was 0.59 (Figure 2.9 (b)).

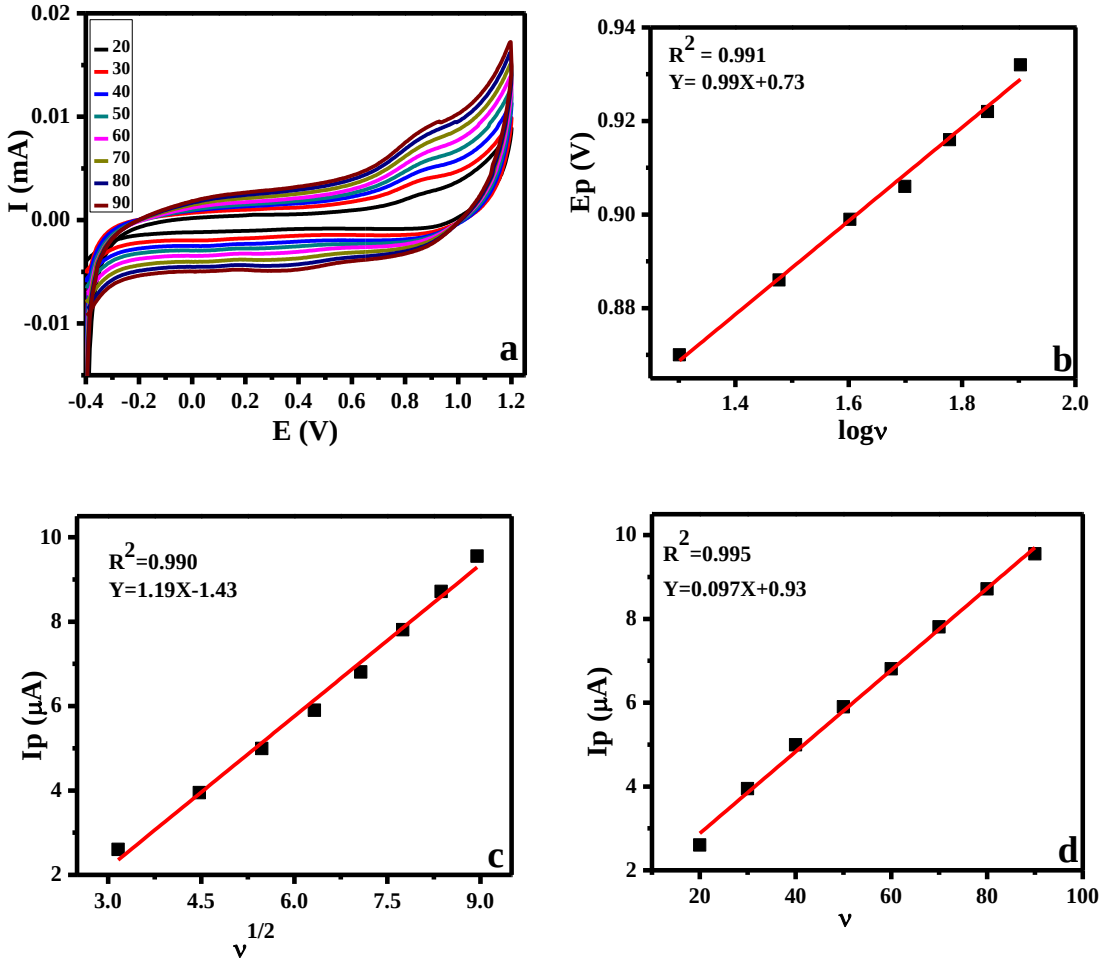

Figure 2.9: ***(a)*** *Cyclic voltammograms of oxidation of acetaldehyde (1 μM) at various scan rates (20 to 90 mV s^{-1}) at CeO_2NPs/GCE,* ***(b)*** *plot of Ep Vs log ν,* ***(c)*** *plot of Ip Vs $ν^{1/2}$ and* ***(d)*** *plot of Ip Vs ν*

On the basis of the slopes of the linear dependence of the anodic peak currents (I_p) on the square root of the potential sweep rates ($ν^{1/2}$) (Figure 2.8 (c), Figure 2.9(c)), using the Randle-Sevcik equation

$$I_p = (2.99 \times 10^5)\, \alpha^{1/2}\, n^{3/2}\, A\, C\, D^{1/2}\, \nu^{1/2}$$

where I_p is the peak current, A is the electrode surface area, D is the diffusion co-efficient

and C is the bulk concentration, the diffusion coefficient of acetaldehyde was calculated to be $5.46x10^{-3}$ cm^2 s^{-1} and $1.55x10^{-2}$ cm^2 s^{-1} for the CeO_2NPs/GCE and CeO_2-MWCNTs/GCE respectively. The reaction (adsorption controlled or diffusion controlled) that controlled acetaldehyde oxidation on the CeO_2NPs/GCE and CeO_2-MWCNTs/GCE was studied from the plots of I_p Vs ν (Figure 2.8 and 2.9 (d)) and I_p Vs $\nu^{1/2}$. In case of CeO_2NPs/GCE, I_p Vs ν is more linear than Ip Vs $\nu^{1/2}$ indicating surface adsorption controlled processes. But in CeO_2-MWCNTs/GCE the greater linearity of the Ip Vs $\nu^{1/2}$ plot indicates the mass transfer being predominately diffusion controlled.

2.9 Optimization studies for the determination of acetaldehyde at the CeO_2-MWCNTs/GCE

In order to attain the maximum sensitivity, the effect of the concentration of CeO_2NPs and the weight percentage of the MWCNTs was studied by varying the volume of CeO_2NPs and the weight percentage of the MWCNTs in the nanocomposite. While keeping the weight percentage of the MWCNTs constant, the volume of the CeO_2NPs suspension was varied from 250-1000 μL. As it can be seen from, Figure 2.10, 500 μL gave the maximum current, with further increment in the concentration of CeO_2NPs from 500 μL the peak current decreased and the anodic peak became broad just like the peak obtained with CeO_2NPs alone, still it senses acetaldehyde from 0.01 μM. By maintaining the concentration of CeO_2NPs at 500 μL we varied the weight percentage of the MWCNTs from 0.15 to 0.90 % and observed a maximum sensitivity at 0.25 %, Figure 2.11 (a). Further increase in weight percentage of the MWCNTs, decreased the sensitivity with an increase in current, this could be due to the fact that the MWCNTs provided its surface area for the adsorbtion of CeO_2NPs and also considerably

contributed to the electron transfer process. Hence 500 μL of CeO_2NPs with 0.25 % MWCNTs was considered to be the optimum conditions for further analysis.

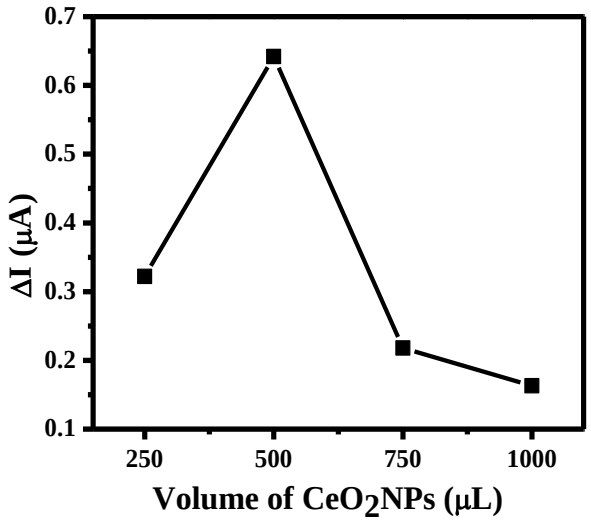

Figure 2.10: *The effect of volume of* CeO_2NPs *in the nanocomposite on the peak current of acetaldehyde*

Likewise, the effect of the drop to drop volume of the nanocomposite on the GCE was optimized and 5 μL exhibited better sensitivity. While increasing the drop to drop volume above 5 μL the sensitivity decreased, this could be attributed to the increasing film thickness and the possibility of it peeling off from the electrode surface (Figure 2.11(b)).

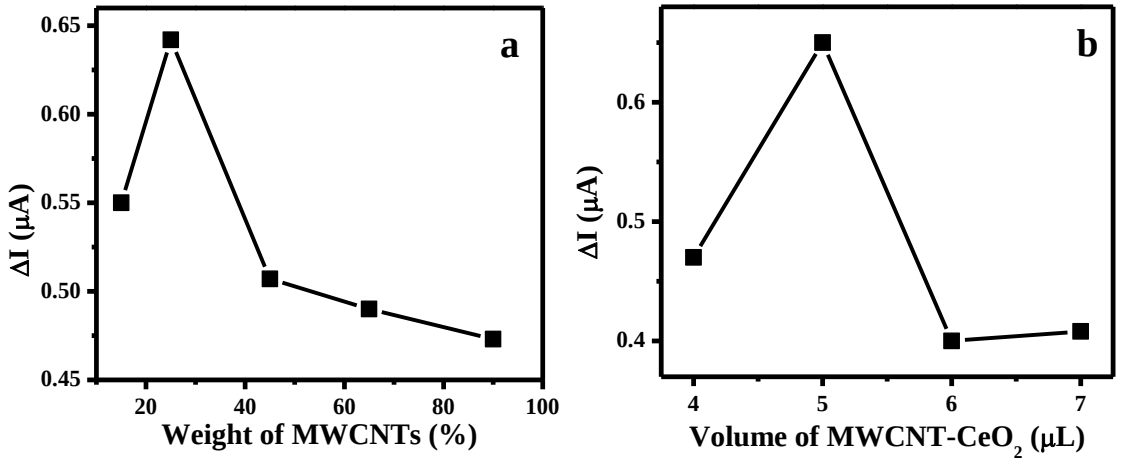

Figure 2.11: ***(a)*** *The* ***e****ffect of weight % of MWCNTs in the nanocomposite and* ***(b)*** *the* ***e****ffect of drop to drop volume of CeO_2-MWCNTs nanocomposite on the peak current of acetaldehyde*

2.10 Effect of electrolyte and pH

The different parameters which may possibly affect the electrochemical determination of acetaldehyde were also studied. The effect of different supporting media including, sodium chloride, potassium chloride, sodium acetate, potassium nitrate, ammonium acetate and sodium dihydrogen phosphate electrolyte towards the electrochemical determination of acetaldehyde on the surface of the CeO_2-MWCNTs/GCE was analysed. Among these media potassium nitrate gave a better response for acetaldehyde sensing and was used as the supporting electrolyte for further analysis.

The effect of the pH of the supporting electrolyte on the electrochemical behaviour of the sensor was investigated over the range of 4.0–9.0. The response current and sensitivity of the sensor increased with increasing pH values from 4.0 to 6.0 and then decreased with a further increase in pH (Figure 2.12). This could be due to the fact that CeO_2NPs would act as a strong oxidising agent when in the acidic medium.

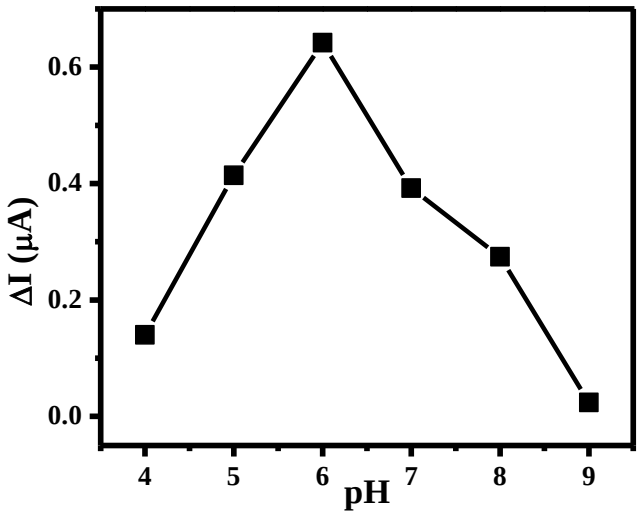

Figure 2.12: *The effect of pH of 0.1 M KNO_3 solution on the peak current of 1 μM acetaldehyde*

2.11 Comparison with reported acetaldehyde sensors

Table 2.1 depicts the comparative studies of the current method with the reported acetaldehyde sensing methods. In comparison with the hitherto reported methods, the current method has a wider calibration range and a lower detection limit. The only sensor which comes close to the developed sensor is the Au-nafion sensor with a limit of detection of 23 nM but it offers only a small calibration range 0.025- 0.5 μM.

Table 2.1: *Comparison with reported acetaldehyde sensing methods*

Method	Modification	Linear calibration Range (μM)	Detection limit (nM)	Reference
HPLC-electrochemistry	GCE	68 to 6800	86	33
Amperometry	Au-nafion	0.025 to 0.50	23	18
Amperometry	AlDH, NADH oxidase and NADs in a polyvinyl alcohol bearing styrylpyridiruum groups (PVA-SbQ) matrix/Pt disk	0.5 to 330	-	34
Amperometry	PNR/sol–gel-AldDH-NADHOx electrodes	10 to 60	2600	35
Cyclic Voltammetry	Copper chloride modified copper electrode	2 to 50	-	36
Amperometry	Aldehyde dehydrogenase and diaphorase on platinum electrode	1 to 500	-	37
Cyclic Voltammetry	CeO_2-MWCNTs/GCE	0.01 to 10	7.4	Present work

2.12 Selectivity studies and analysis of synthetic mixtures of fruit juice

Since acetaldehyde is present in most fruits, the selectivity of the CeO_2-MWCNTs/GCE for acetaldehyde sensing was investigated under optimised conditions by testing the response to several compounds that are usually present in fruit juice.

Among the different interferents, ethanol interferes even in equal amount but glucose, fructose, and glycerol do not interfere up to 100 folds. Cations like K^+ and Na^+ do not interfere with the acetaldehyde oxidation.

Figure 2.13 shows the peak current of 1 μM acetaldehyde and other interferents, which indicates that the developed electrode showed good selectivity towards acetaldehyde from the potential interfering species and could be applied to determine its concentration in the fruit juice samples. Therefore, the developed modified electrode was tested for the determination of acetaldehyde in a synthetic mixture of fruit juice using the standard addition method and the recoveries of acetaldehyde are presented in Table 2.2.

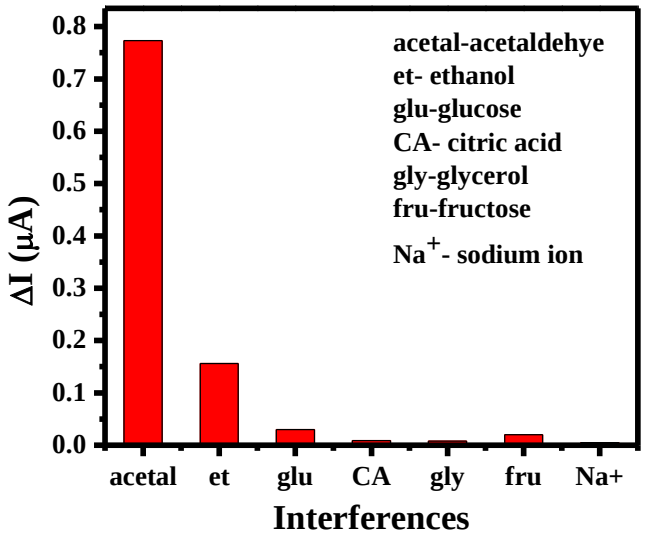

Figure 2.13: *Selectivity studies of acetaldehyde and other organic species*

Table 2.2: *Analysis of the synthetic fruit juice sample*

Synthetic fruit components (g/100ml)	CH_3CHO spiked (M)	CH_3CHO found (M)	Recovery (%)
Glucose: 1 Fructose: 1	10^{-8}	9.88×10^{-9}	98.8
Ethanol : 0.01 Glycerol: 0.01 Potassium: 0.02	10^{-7}	1.01×10^{-7}	101.0

2.13 Experimental

2.13.1 Chemicals and reagents

Acetaldehyde, multi walled carbon nanotube and cerium oxide were purchased from Aldrich, Milwauke, WI, USA. Deionised double distilled water was used in the preparation of working solutions. All other chemicals were of analytical reagent grade (E Merck, Mumbai, India) and were used as received, without any further purification. A potassium nitrate solution of pH 6 was used as the supporting electrolyte in all the electrochemical experiments. A stock solution of 0.1 M acetaldehyde was freshly prepared for each series of experiments.

2.13.2 Instrumentation

The electrochemical measurements were performed using a three-electrode cell, with a GCE (3 mm in diameter) as the working electrode, Pt wire as the auxiliary electrode and a Ag/AgCl electrode as the reference electrode, using a VSP-potentiostat/galvanostat (Biologic Science Instruments). The Oakton pH 700 meter, Germany, was used to measure pH. The size and morphology were examinedwith the aid of a scanning electron microscope (SEM), JEOL, Model JSM 5600 LV, Tokyo, Japan. UV-Visible spectra were recorded with a computer controlled double beam UV-Vis spectrophotometer UV-2401PC (Shimadzu, Kyoto, Japan). The X-ray diffraction (XRD) patterns of the samples were recorded on a Philips X'pert diffractometer (XRD, X'Pert Pro MPD) with CuKα radiation (1.5406A).

2.13.3 Electrochemical measurements

A freshly prepared solution of acetaldehyde (1 μM) was added to an electrochemical cell containing 10 mL of 0.1 M KNO_3 as the supporting electrolyte (pH 6). Cyclic voltammetric curves were plotted by scanning the potential from -0.4 to 1.2 V

at a scan rate of 50 mV s^{-1}. The acetaldehyde quantification was achieved by measuring the decrease in oxidation peak current of Ce^{4+} at 0.78 V.

2.14 Conclusions

A voltammetric sensor based on a CeO_2-MWCNTs nanocomposite was designed for acetaldehyde sensing. MWCNTs can improve the stability of the modified electrode, reduce the agglomeration level of the CeO_2NPs, and increase the electron transfer rate. The catalytic oxidation of acetaldehyde was found to be highly sensitive at the CeO_2-MWCNTs/GCE because of the synergistic effect of the CeO_2NPs and MWCNTs. A lower detection limit of 7.4 nM , wide linear range from 0.01 to 10 μM, excellent selectivity, good stability and repeatability gives it the potential for application in acetaldehyde sensing. Also the interference study showed reasonably good selectivity and hence the developed modified electrode is suitable for the measurement of acetaldehyde in fruit juice samples.

2.15 References

1) Silva, G. D.; Bozzelli, J. W. Enthalpies Of Formation, Bond Dissociation Energies, and Molecular Structures of the N-Aldehydes (Acetaldehyde, Propanal, Butanal, Pentanal, Hexanal, and Heptanal) and Their Radicals. *J. Phys. Chem. A* **2006**, *110*, 13058–13067.

2) O'Brien, P. J.; Siraki, A. G.; Shangari, N. Aldehyde Sources, Metabolism, Molecular Toxicity Mechanisms, and Possible Effects on Human Health. *Crit. Rev. Toxicol.* **2005**, *35*, 609−662.

3) Stein, S.; Lao, Y. B.; Yang, I. Y.; Hecht, S. S.; Moriya, M. Genotoxicity of Acetaldehyde- and Crotonaldehyde-Induced 1,N^2-Propanodeoxyguanosine DNA Adducts in Human Cells. *Mutat. Res.* **2006**, *608*, 1−7.

4) Chen, L.; Wang, M. Y.; Villalta, P. W.; Luo, X. H.; Feuer, R.; Jensen, J.; Hatsukami, D. K.; Hecht, S. S. Quantitation of an Acetaldehyde Adduct in Human Leukocyte DNA and the Effect of Smoking Cessation. *Chem. Res. Toxicol.* **2007**, *20*, 108−113.

5) Uebelacker, M.; Lachenmeier, D. Quantitative Determination of Acetaldehyde in Foods Using Automated Digestion with Simulated Gastric Fluid Followed by Headspace Gas Chromatography. *J. Autom. Methods Manage. Chem.* **2011**, *12*, 13-16.

6) Qiao, Y.; Xie, B. J.; Zhang, Y.; Zhang, Y.; Fan, G.; Yao X. L.; Pan, S. Y. Characterization of Aroma Active Compounds in Fruit Juice and Peel Oil of Jinchen Sweet Orange Fruit (Citrus Sinensis (L.) Osbeck) by GC-MS and GC-O. *Molecules* **2008**, *13*, 1333-1344.

7) Nanto, H.; Yokoi, Y.; Mukai, T.; Fujioka, J.; Kusano, E.; Kinbara, A.; Douguchi, Y. Novel Gas Sensor Using Polymer-Film-Coated Quartz Resonator for Environmental Monitoring. *Mater. Sci. Eng. C* **2000**, *12*, 43-48.

8) Fromme, H.; Heitmann, D.; Dietrich, S.; Schierl, R.; Korner, W.; Kiranoglu, M.; Zapf, A.; Twardella, D. Air Quality in Schools - Classroom Levels of Carbon Dioxide (CO_2), Volatileorganic Compounds (VOC), Aldehydes, Endotoxins and Cat Allergen. *Gesundheitswesen* **2008**, *70*, 88-97.

9) Roche, A. ; Jacob, V.; Garcia, C.; Baussand, P.; Foster, P. A Diffusive Sampler Development and Utilisation for the Measurement of Urban Pollutants (Aldehydes). *Sens. Actuat. B Chem.* **1999**, *59*, 103-107.

10) Afkhami, A.; Parham, H.; Rezaei, M. Kinetic Spectrophotometric Determination of Acetaldehyde. *Anal. Lett.* **2000**, *33*, 527–538.

11) Yasuhara, A.; Shibamoto, T. Gas-Chromatographic Determination of Trace Amounts of Aldehydes in Automobile Exhaust by a Cysteaminederivatization Method. *J. Chromatogr. A* **1994**, *672*, 261–266.

12) Mori, Y.; Tsuji, K.; Setsuda, S.; Goto, S.; Onodera, S.; Matsushita, H. Determination of Aldehydes in Indoor Air Samples by Collection Using O-(2,3,4,5,6-Pentafluorobenzyl) Hydroxylamine Impregnated Silica Gel-Solvent Extraction/Gas Chromatograph Technique. *J. Tox. Env. Health* **1996**, *42*, 500–506.

13) Helmut, S. A New Device for the Automatic Determination of Formaldehyde in Air. *Gefahrstoffe - Reinhaltung der Luft* **1997**, *57*, 75–78.

14) Lipari, F.; Swarin, S. J. Determination of Formaldehyde and Other Aldehydes in Automobile Exhaust with an Improved 2,4-Dinitrophenylhydrazine Method. *J. Chromatogr.* **1982**, *247*, 297–306.

15) Gandelman,M. S.; Birks, J. W. Photooxygenation Chemiluminescence High Performance Liquid Chromatographic Detector for the Determination of Aliphatic Alcohols, Aldehydes, Ethers and Saccharides. *J. Chromatogr*. **1982**, *242*, 21–31.

16) TO-O5, USEPA, Chemical/name index to EPA test methods 600 4-89-017 (2001).

17) Vogin, B.; Baronnet, F.; Andre, J. C. Determination of Aliphatic Aldehydes in Aqueous Solution by Chemiluminescence Measurements. *Anal. Chim.Acta* **1982**, *142*, 293–297.

18) Jacquinot, P.; Hodgson, A. W. E.; Muller, B.; Wehrli, B.; Hauser, P. C. Amperometric Detection of Gaseous Ethanol and Acetaldehyde at Low Concentrations on an Au–Nafion Electrode. *Analyst* **1999**, *124*, 871–876.

19) Trovarelli, A. Catalytic Properties of Ceria and CeO_2-Containing Materials. *Catal. Rev-Sci. Eng.* **1996**, *38*, 439-520.

20) Yao, H. C.; Yao, Y. F. Y. Ceria in Automotive Exhaust Catalysts. *J. Catal.* **1984**, *86*, 254-265.

21) Haneda, M.; Mizushima, T.; Kakuta, N. Behaviour of Oxygen Species Adsorbed of Ai_2O_3-Supported Cerium Oxide Catalysts for Methane Oxidation. *J. Chem. Soc. Faraday Trans.* **1995**, *91*, 4459-4465.

22) Fukui, K.; Namai, Y.; Iwasawa, Y. Imaging of Surface Oxygen Atoms and Their Defect Structures on CeO_2 (111) by Noncontact Atomic Force Microscopy. *Appl. Surf. Sci.* **2002**, *188*, 252-256.

23) Kim, S. M.; Lee, S. Y. Role Of CeO_2 And $BaTiO_3$ Buffer Layers on the Crystallization and the Electrical Property of $Y_1Ba_2Cu_3O_{7-X}$ Thin Film. *Physica C* **2001**, *351*, 42-44.

24) Malhotra, B. D.; Kaushik, A. Metal Oxide-Chitosan Based Nanocomposite for Cholesterol Biosensor. *Thin Solid Films* **2009**, *518*, 614-620.

25) Saha, S.; Arya, S. K.; Singh, S. P.; Sreenivas, K.; Malhotra, B. D.; Gupta, V. Nanoporous Cerium Oxide Thin Film for Glucose Biosensor. *Biosens. Bioelectron.* **2009**, *24*, 2040-2045.

26) Wildgoose, G. G.; Banks, C. E.; Compton, R. G. Metal Nanopartictes and Related Materials Supported on Carbon Nanotubes: Methods and Applications. *Small* **2006**, *2*, 182-193.

27) Georgakilas, V.; Gournis, D.; Tzitzios, V.; Pasquato, L.; Guldi, D. M.; Prato, M. Decorating Carbon Nanotubes with Metal or Semiconductor Nanoparticles. *J. Mater. Chem.* **2007**, *17*, 2679-2694.

28) Hu, X. G.; Dong. S. J. Metal Nanomaterials and Carbon Nanotubes—Synthesis, Functionalization and Potential Applications towards Electrochemistry. *J. Mater. Chem.* **2008**, *18*, 1279-1295.

29) Vairavapandian, D.; Vichchulada, P.; Lay, M. D. Preparation and Modification of Carbon Nanotubes: Review of Recent Advances and Applications in Catalysis and Sensing. *Anal. Chim. Acta.* **2008**, *626*, 119-129.

30) Peng, X.; Chen, J.; Misewich, J. A.; Wong, S. S. Carbon Nanotube–Nanocrystal Heterostructures. *Chem. Soc. Rev.* **2009**, *38*, 1076-1098.

31) Idriss, H.; Ethanol Reactions Over the Surfaces of Noble Metal/Cerium Oxide Catalysts. *Platinum Met. Rev.* **2004**, *48*, 105-115.

32) Yan, W.; Guangfeng, W.; Maoguo, L.; Cong, W.; Bin, F. Determination of Rutin Using a CeO_2 Nanoparticle Modified electrode. *Microchim. Acta* **2007**, *158*, 269–274.

33) Sacks, A. A.; Okumura, L. L.; Oliveira, M. F. D.; Zanoni, M. V. B.; Stradiotto, N. R.; Determination of Acetaldehyde in Fuel Ethanol by High Performance Liquid Chromatography with Electrochemical Detection. *Anal. Sci.* **2005**, *21*, 441-444.

34) Noguer, T.; Marty, J. L. Reagentless Sensors for Acetaldehyde. *Anal. Lett.* **1997**, *30*, 1069-1080.

35) Ghica, M. E.; Pauliukaite, R.; Marchand, N.; Devic, E.; Brett, C. M. A. An Improved Biosensor for Acetaldehyde Determination Using a Bienzymatic Strategy at Poly(Neutral Red) Modified Carbon Film Electrodes. *Anal. Chim. Acta* **2007**, *591*, 80–86.

36) Karim-Nezhad, G.; Dorraji, P. S.; Dizajdizi, B. Z. Electro-Catalytic Oxidation of Formaldehyde and Acetaldehyde on Copper Chloride Modified Copper Electrode. *Anal. Bioanal. Electrochem.* **2011**, *3*, 1-13.

37) Noguer, T.; Marty, J. L. An Amperometric Bienzyme Electrode for Acetaldehyde Detection. *Enzyme Microbial Technol.* **1995**, *17*, 453–456.

Chapter 3

Bimetallic $Au_{90}Pt_{10}$ Alloy Nanoparticles on Glassy Carbon Electrode for the Nanomolar Detection of Phenol

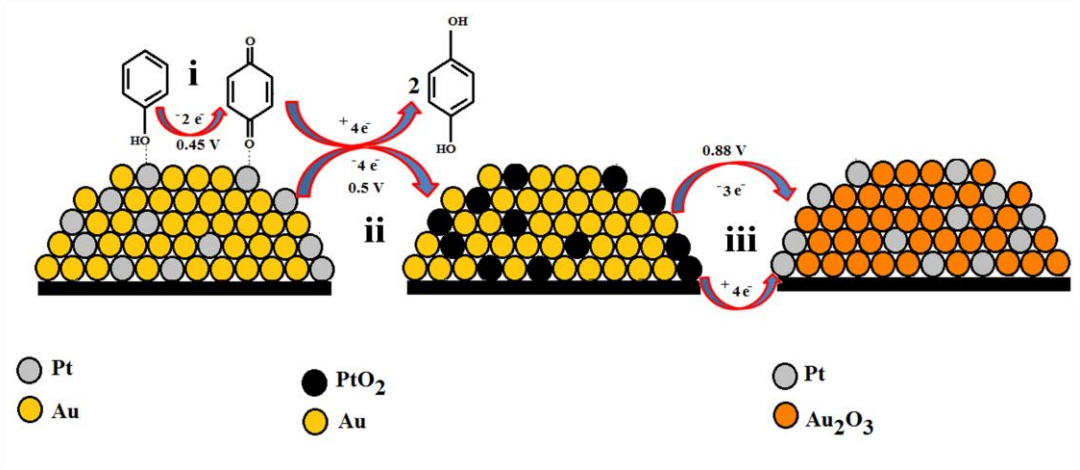

3.1 Abstract

The bimetallic $Au_{90}Pt_{10}$ alloy nanoparticles (AuPtNPs) were synthesized on glassy carbon electrode (GCE) by galvanostatic method. Their surface morphology was characterized by SEM and AFM. XRD, UV-Visible absorption spectroscopy and XPS analysis confirmed the formation of AuPtNPs on GCE. Further, AuPtNPs modified GCE (AuPtNPs/GCE) was employed for the nanomolar detection of phenol in 0.1 M CH_3COONa+0.05 M KCl electrolyte of pH 6.8. Different parameters including concentration of Au and Pt on the formation of AuPtNPs on GCE, deposition time, deposition potential and solution pH were studied. The electrochemical characterization was executed for the calculation of diffusion coefficient, rate constant and electron transfer coefficient. The modified electrode showed a detection limit of 6.5 nM for phenol. The developed $Au_{90}Pt_{10}$NPs/GCE is highly sensitive, selective, precise, and showed a wider calibration range (0.04 to 10 μM) towards phenol. The possible interference from various compounds was also verified on the designed electrode.

3.2 Introduction

The metallic nanoparticles with significant properties and small dimensions have generated an intense research activity in all fields of science.[1-4] This is due to their unique catalytic, magnetic, electrocatalytic, optical, thermal and electrical properties. Several types of nano sized materials of noble metals including, gold, platinum and silver have been explored in the past owing to their interesting practical applications, for example, as signal amplifier in electrochemical sensors.[5] Bimetallic nanomaterials, composed of two distinct metal elements, are exhibiting superior chemical and physical properties than the individual nanomaterials. These bimetallic nanomaterials have a certain chemistry sequence and geometry architecture, and perform specific functions.[6] They perform not only a simple combination or enhancement of the properties associated with their single counterparts, but also many interesting and surprising new properties with a combination of multiple functions and broadened application fields, which is explained by synergistic effects of nanomaterials.[7] Moreover, the physical and chemical performance of bimetallic nanoparticles can be altered by changing their components and morphology.[8] Among the various bimetallic nanoparticles reported, AuPtNPs are of particular interest in catalysis.[9] For example, they exhibit catalytic property in electro oxidation of carbon monoxide, methanol[10], and glucose.[11] Jiang *et al*. reported that AuPtNPs have the potential to act as antibacterial agents and are harmless to human cells.[12] Leung *et al*. demonstrated that AuPtNPs can be used as a high-performance alcohol sensor for analyzing the alcohol concentration in a solution.[13] However, it is very difficult to synthesis AuPtNPs due to the miscibility of Au and Pt in the bulk. At the same time, theoretical calculations of the heat of formation for AuPtNPs suggested that it could be prepared as nanoscale materials.[14] In this paper we propose a new method for the preparation of bimetallic $Au_{90}Pt_{10}$NPs on GCE by applying a constant current (galvanostatic method). This

$Au_{90}Pt_{10}$NPs/GCE was further employed for the nano molar detection of phenol in 0.1 M CH_3COONa+0.05 M KCl solution.

Phenol is considered to be quite toxic. Variety of industries of dyes, plastics, organic chemicals, molding and casting, pharmaceutical, oil refineries, paint, and coke plants etc release phenol as an industrial waste. If they are released into the environment, their accumulation in the soil, ground water, or surface water, thus constitutes environmental hazard.[15, 16] Even at low concentration (ppb) levels, phenol and their derivatives adversely affect the living organisms. Skin and eyes when exposed to them, cause irritation and on acute inhalation, irritation in mucous membranes occurs. Similarly anorexia, weight loss, diarrhea, vertigo, salivation, dark coloration of the urine, blood and liver effects has been reported in long-term exposed humans.[17, 18] It is therefore necessitous to assess the fate of these compounds in the environment and develop effective methods to detect and eliminate them from water.

3.3 Electrochemical preparation of bimetallic AuPtNPs on GCE

A galvanostatic approach was employed for the preparation of AuPtNPs on GCE. A well cleaned GCE was inserted into an electrochemical cell which contained an aqueous solution of 1 mM $HAuCl_4$ and 0.1 mM H_2PtCl_6 in 0.5 M H_2SO_4 as supporting electrolyte. It was observed that a current of -25 μA for 10 minutes was enough for the preparation of AuPtNPs on GCE. The deposited AuPtNPs on the GCE was further peeled off by sonication and characterized by different techniques like SEM, AFM, XRD, XPS and UV-Visible absorption spectroscopy. Similarly individual AuNPs and PtNPs on GCE were also prepared by taking 1 mM $HAuCl_4$ and 0.1 mM H_2PtCl_6 respectively in 0.5 M H_2SO_4 supporting electrolyte.

3.4 Electrochemical characterization of PtNPs/GCE, AuNPs/GCE and AuPtNPs/GCE

Electrochemical experiments were performed for the confirmation of existence of

metal alloy nanoparticles on GCE. Figure 3.1 showed the cyclic voltammograms of individual PtNPs/GCE, AuNPs/GCE and AuPtNPs/GCE in acetate buffer of pH 6.4.

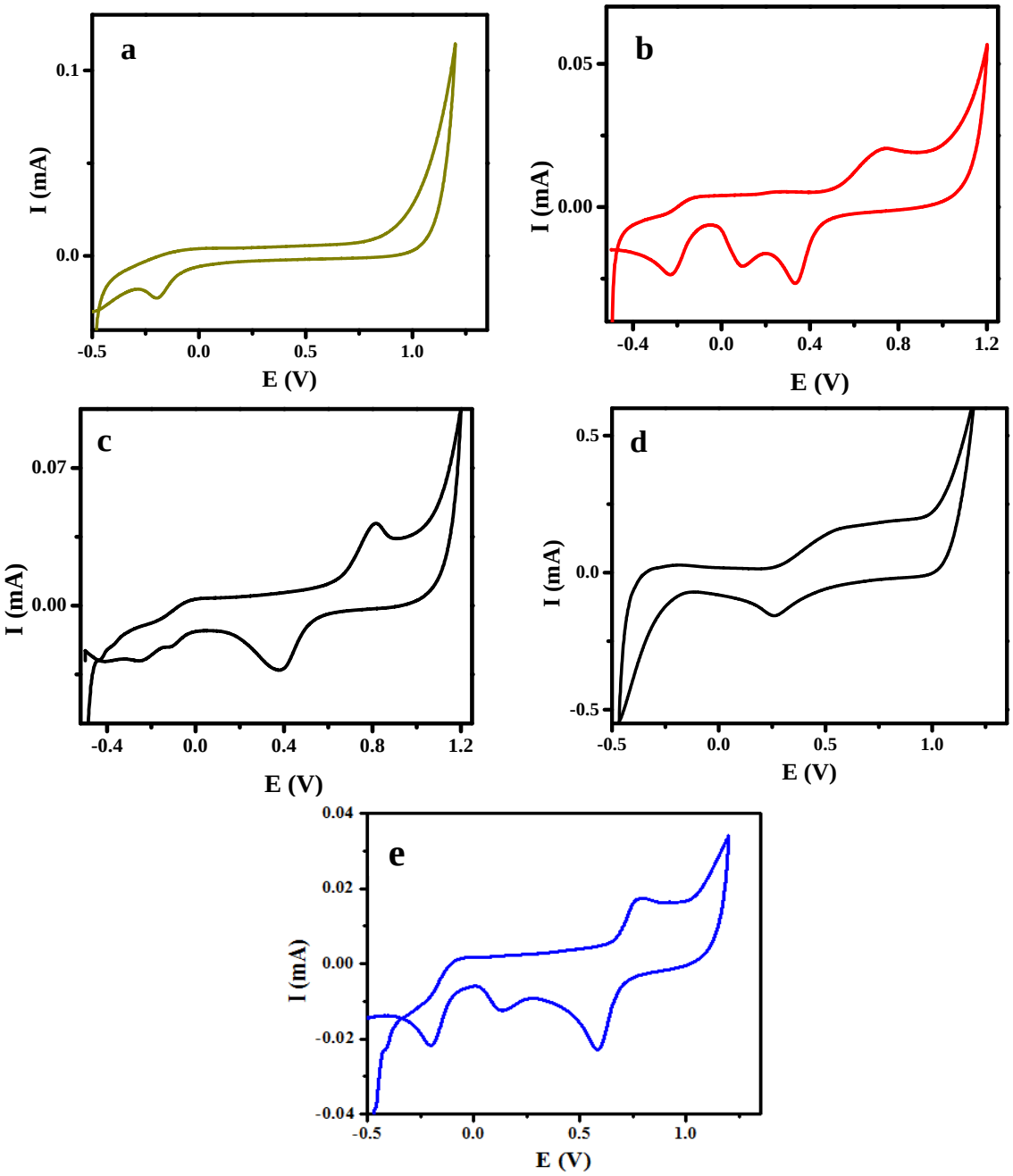

Figure 3.1: *Cyclic voltammograms of* ***(a)*** *PtNPs/GCE* ***(b)*** *AuNPs/GCE,* ***(c)*** *AuPtNPs/GCE* ***(d)*** *AuPtNPs/GCE with higher conc. of Pt and* ***(e)*** *AuPtNPs/GCE with higher conc. of Au in acetate buffer of pH 6.4.*

In acetate buffer solution PtNPs/GCE (a) exhibited one oxidation peak at 0.5 V corresponding to the formation of PtO_2 and the reduction of the formed oxides took place at a potential of -0.3 V. Similarly, AuNPs/GCE (b) generated an oxidation peak at 0.78 V

and a corresponding peak at 0.39 V. Meanwhile the CV of AuPtNPs/GCE (c) in acetate buffer showed evidence of the existence of both nano sized Au and Pt on GCE. All the individual peaks were retained and the redox peak of AuNPs was shifted to a more positive side and the reduction peak corresponding to PtNPs was shifted to a more negative potential side. This is due to the synergistic catalytic effect of AuNPs and PtNPs in the alloy. We also observed that as the concentration of PtNPs in AuPtNPs increases (d), the electrode exhibited only one redox peak corresponding to oxidation and reduction of Pt. Moreover the redox peaks were shifted towards more positive potential side. While the redox peaks of AuNPs were silent. Similar observation was witnessed in the reverse condition (e).

3.5 Morphological and spectral characterizations of AuNPs, PtNPs and AuPtNPs

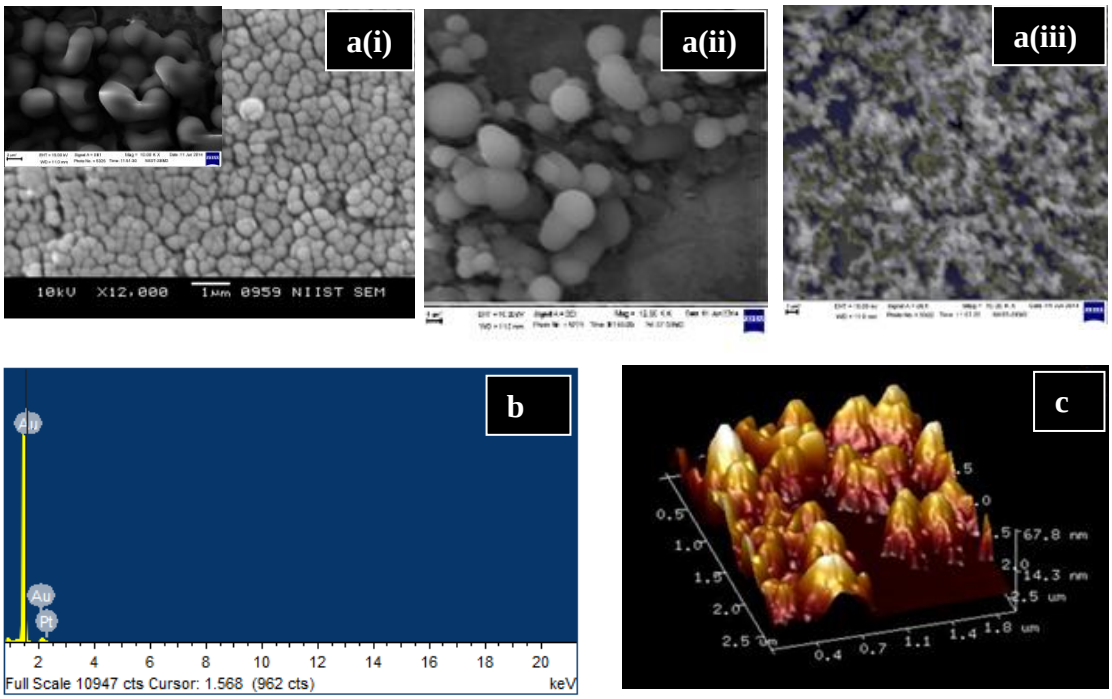

Figure 3.2: ***(a)*** *SEM images of* ***(i)*** *AuPtNPs* ***(ii)*** *AuNPs and* ***(iii)*** *PtNPs* ***(b)*** *EDAX of AuPtNPs and* ***(c)*** *AFM image of AuPtNPs.*

It was experienced that the galvanostatic deposition of these metals on GCE created bimetallic AuPtNPs. SEM image depicted in Figure 3.2a (i) showed that the AuPtNPs have uniform size distribution and exhibited a dumbbell shape with an average

size of 50 nm. Whereas, individual AuNPs and PtNPs showed spherically shaped structure (Figure 3.2a (ii & iii). From EDAX analysis (Figure 3.2b), the composition of Au and Pt in the AuPtNPs were in the ratio $Au_{90}Pt_{10}$. Bimetallic nature of AuPtNPs was further confirmed by AFM analysis. Corresponding AFM measurements were established using the tapping mode as shown in Figure 3.2c.

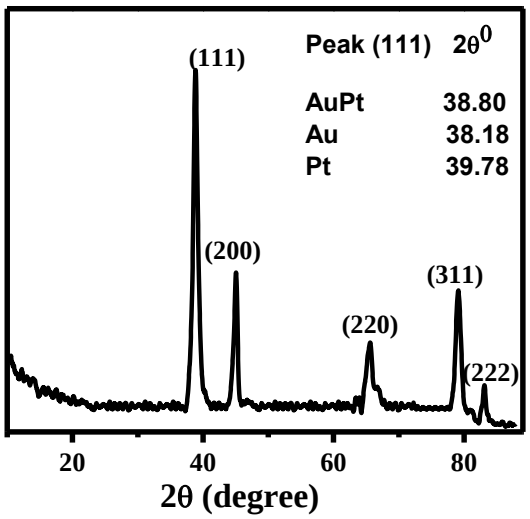

Figure 3.3: *The XRD patterns of AuPtNPs.*

XRD was used to evaluate the structure and composition of AuPtNPs. In Figure 3.3 the XRD pattern of AuPt particles exhibited five major peaks at 38.8^0, 45.0^0, 65.63^0, 79.06^0 and 83.14^0 corresponding to (111), (200), (220), (311), and (222) planes of the face-centered cubic lattice of AuPt alloy. The peak corresponding to (111) plane of AuPtNPs was in between that of AuNPs (38.18^0) and PtNPs (39.78^0), which indicated the formation of bimetallic AuPtNPs on GCE. The corresponding lattice parameters and interplanar d spacing were calculated and depicted in the Table 3.1. Similarly we also calculated the above parameters corresponding to AuNPs and PtNPs. From the Debye scherrer formula,

$$D = K\lambda/\beta \cos\theta$$

where D is the crystallite size, K is the Sherrer constant (0.89), λ is the wave length of Cu Kα radiation (0.15406 nm), β is the FWHM (full width of peak intensity at half maximum) in radians, θ is the peak (111) position in degrees, the crystallite size of the

AuPtNPs corresponding to (111) plane was calculated as 48 nm, which is in great concurrence with SEM measurement.

Table 3.1: *Lattice parameter and d spacing of AuNPs, PtNPs ans AuPtNPs*

Parameter	AuNPs	PtNPs	AuPtNPs
Lattice parameter (A^0)	4.078	3.923	4.016
d spacing (nm)	0.235	0.227	2.319

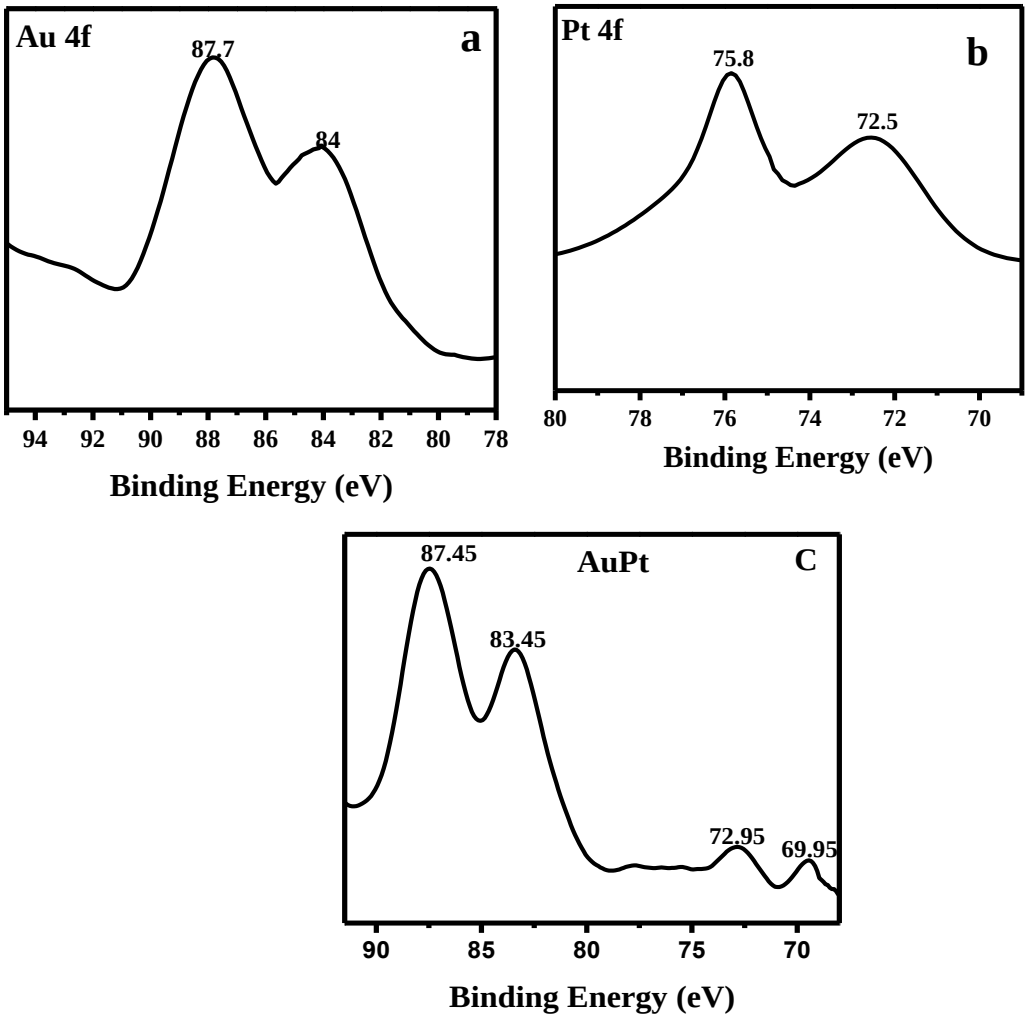

Figure 3.4: ***(a)*** XPS spectra for the Au *4f* ***(b)*** *Pt 4f region of monometallic samples and* ***(c)*** *XPS spectra of the AuPt NPs in the Pt 4f and Au 4f regions*

Further, the resulting AuPtNPs were subjected to XPS analysis to confirm the underlying surface composition. For AuNPs (Figure 3.4a), peaks at 87.7 and 84 eV represented Au 4f 5/2 and Au 4f 7/2 respectively. Similarly for PtNPs (Figure 3.4b), peaks at 75.8 eV and 72.5 eV represented Pt 4f 5/2 and Pt 4f 7/2 was also observed. But

for AuPtNPs (Figure 3.4c) Au and Pt peaks were shifted towards lower side (87.45 & 83.45 for Au and 72.95 & 69.95 for Pt respectively). This shifting could be explained by the d band theory. When AuPt alloys are formed there will be a decrease in their binding energy due to the expansion of d band center of Pt by the Au [19].

UV-Visible absorption spectroscopic study revealed that AuNPs showed a strong absorption band at 525 nm (Figure 3.5). At the same time no absorption band was observed for both PtNPs and AuPtNPs in the investigating range. If the formed bimetallic nanoparticles were arranged in the core shell or phase segregated form there should be an absorption band at around 525 nm corresponding to Au. The absence of absorption band of Au in the bimetallic nano particles implied the existence of bimetallic nano particles on GCE are in the alloy form.

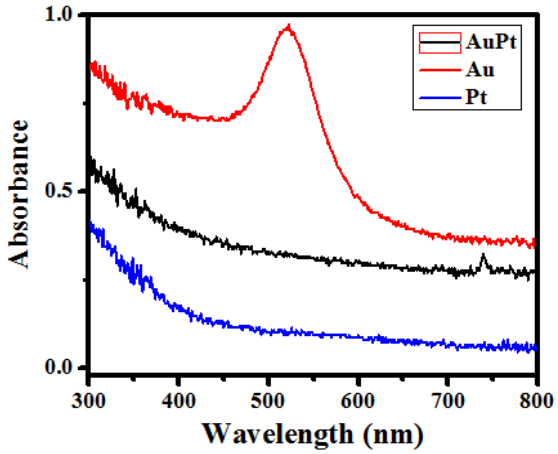

Figure 3.5: *UV-Visible absorption spectra of PtNPs, AuNPs and AuPtNPs*

3.6 Electrochemical behaviour of bare GCE, PtNPs/GCE, AuNPs/GCE and AuPt/GCE in $K_3[Fe(CN)_6]$

Figure 3.6 showed the electrochemical performance of fabricated AuPtNPs/GCE in comparison with bare GCE, PtNPs/ GCE and AuNPs/GCE in 1 mM $K_3[Fe(CN)_6]$ with KCl as suppoting electrolyte. From the CV it was evident that the AuPtNPs/GCE showed better sensitivity than all the other mentioned electrodes. On bare GCE, $K_3[Fe(CN)_6]$ in KCl undergoes an oxidation at a potential of 60 mV with peak current 6.8 μA and reduction at 0.001 with peak current 2 μA. It was also observed that on all the other

electrodes the oxidation potential was shifted towards a small positive potential side. This was maximum for PtNPs/GCE (77.2 mV) and minimum for AuNPs/GCE (65 mV). On AuPtNPs/GCE, K_3[$Fe(CN)_6$] in KCl undergoes oxidation at 70 mV (in between that of AuNPs/GCE and PtNPs/GCE) with a peak current of 15.67 μA and reduction at 0.001 V with a peak current of -17.29 μA. This could be attributed to the synergetic effects of Au and Pt towards the electron flow of $K_3[Fe(CN)_6]$. This confirmed the higher electrocatalytic activity of AuPtNPs/GCE towards the electrochemical oxidation of K_3[$Fe(CN)_6$] in KCl supporting medium.

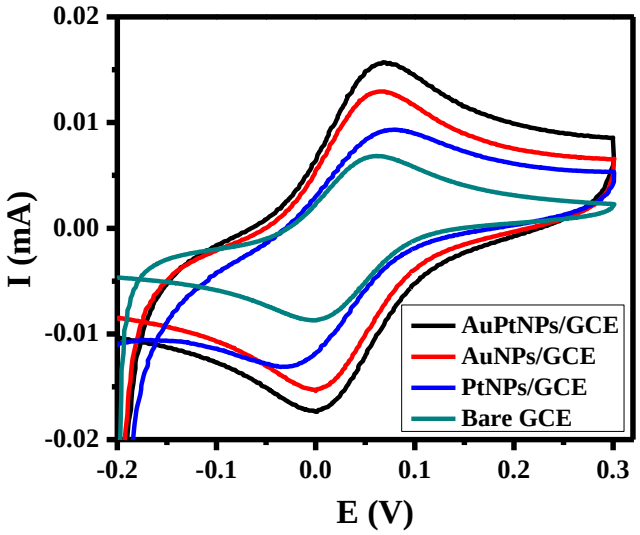

Figure 3.6: *Cyclic voltammograms at the bare GCE, PtNPs/GCE, AuNPs/GCE and AuPtNPs/GCE in 1 mM $K_3[Fe(CN)_6]$ and 0.1 M KCl as the supporting electrolyte at a scan rate of 50 mV s^{-1}.*

3.7 Kinetic studies

In order to calculate the diffusion coefficient of AuPtNPs/GCE, CV of 1 μM phenol in 0.1 M CH_3COONa+0.05 M KCl solution of pH 6.8 with different scan rates was plotted (Figure 3.7a). While increasing the scan rate from 10 to 100 mV s^{-1}, both the oxidation and reduction peaks increased simultaneously. Further a good linear graph was obtained for Ip Vs $\nu^{1/2}$. The corresponding slope of the plot for the graph and from the Randles–Sevcik equation $Ip = (2.99x10^5)\ \alpha^{1/2}\ n^{3/2} A\ C\ D^{1/2}\ \nu^{1/2}$ where I_p is the peak current, A is the electrode surface area, D is the diffusion co-efficient and C is the bulk

concentration, diffusion coefficient (D) of the phenol on AuPtNPs/GCE was calculated as 0.7888×10^{-5} cm^2 s^{-1} (Figure 3.7b).

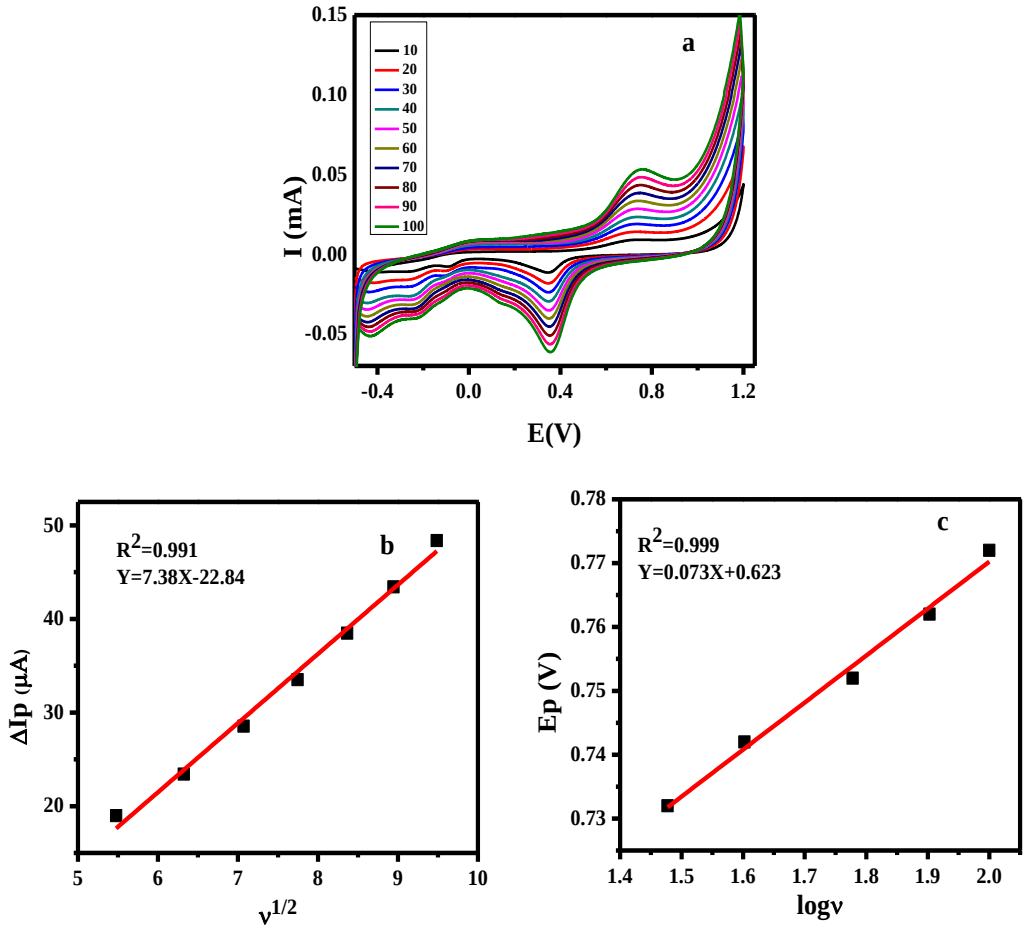

Figure 3.7: ***(a)*** *Cyclic voltammograms of oxidation of phenol (1μM) at various scan rates (10 to 100 mV* s^{-1}*) at AuPtNPs/GCE* ***(b)*** *plot of Ip Vs* $v^{1/2}$ *and* ***(c)*** *plot of Ep Vs log v*

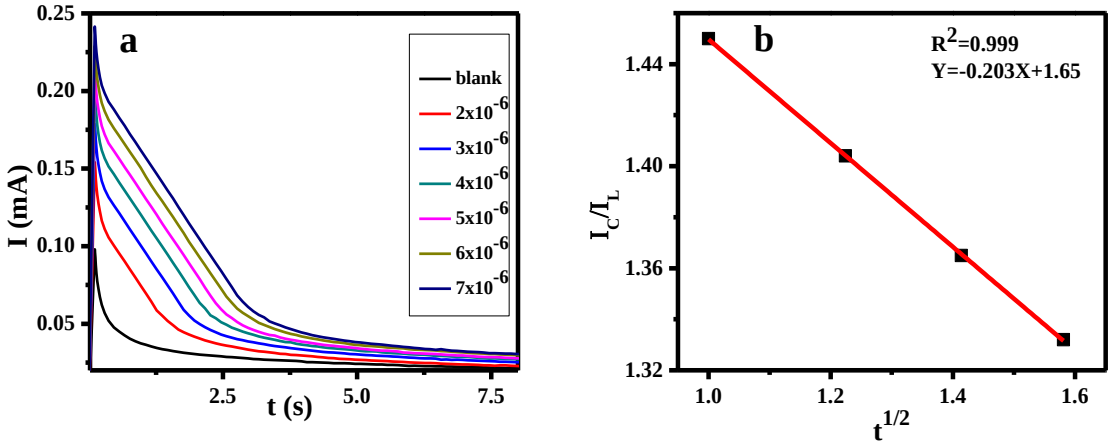

Figure 3.8: ***(a)*** *Current-time transients of AuPtNPs/GCE in absence and presence of different concentrations of phenol in 0.1 M* CH_3COONa*+0.05 M KCl and* ***(b)*** *dependence of* I_C/I_L *Vs (time)* $^{1/2}$

Electron transfer coefficient (α) of AuPtNPs/GCE was also calculated from the Tafel plot which was drawn by the equation, Ep = (2.303RT/nαF) logν+ constant where Ep is potential, R is gas constant, T is the temperature, n is number of electron transferred and F is the Faraday constant. From the slope of the plot of Ep Vs log ν, α was calculated as 0.81 (Figure 3.7c). For the understanding of charge transfer rate constant for the oxidation of phenol, a single step chronoamperogram was recorded with a fixed potential of 1.2 V (Figure 3.8a). From the equation $I_C/I_L = \pi^{1/2}(kCt)^{1/2}$, (where I_C is the catalytic current, I_L is the limiting current, C is the bulk concentration) a plot of I_C/I_L against $t^{1/2}$ was plotted and from the slope, rate constant (k) was calculated as 1.31×10^7 cm^3 mol^{-1} s^{-1} (Figure 3.8b). Similarly D, α and k for AuNPs/GCE, PtNPs/GCE and bare GCE were also calculated and the values were tabulated in Table 3.2.

Table 3.2: *D, α and k values of bare GCE, PtNPs/GCE, AuNPs/GCE and AuPtNPs/GCE*

Electrode	Diffusion coefficient (cm^2 s^{-1})	Electron transfer coefficient	Rate constant (cm^3 mol^{-1} s^{-1})
Bare GCE	0.88×10^{-6}	0.59	3.99×10^6
PtNPs/GCE	0.55×10^{-5}	0.65	5.48×10^6
AuNPs/GCE	0.69×10^{-5}	0.71	6.88×10^6
AuPtNPs/GCE	0.78×10^{-5}	0.81	1.31×10^7

3.8 Electrochemical performance of bare GCE, PtNPs/GCE, AuNPs/GCE and AuPtNPs/GCE in 0.1 M CH_3COONa+0.05 M KCl

Cyclic voltammetry was used to study the electrochemical behaviour of AuPtNPs/GCE. Figure 3.9 showed the cyclic voltammograms of bare GCE, PtNPs/GCE, AuNPs/GCE and AuPtNPs/GCE in 0.1 M CH_3COONa+0.05 M KCl solution of pH 6.8 with a scan rate of 50 mV s^{-1}. In supporting electrolyte, bare GCE doesn't give any significant peaks in this experimental range. At the same time PtNPs/GCE exhibited one broad oxidation peak at 0.5 V due to the formation of PtO_2 and the corresponding reduction peak was obtained at -0.195 V. Similarly, AuNPs/GCE exhibited one sharp

oxidation peak at 0.73 V owing to Au_2O_3 formation and three reduction peaks at 0.345 V, 0.095 V and -0.224 V corresponding to the reduction of Au_2O_3, hydrogen adsorption and hydrogen evolution. On AuPtNPs/GCE, a sharp anodic peak at 0.88 V appeared due to the Au_2O_3 formation and the reduction of Au_2O_3 is appeared at 0.389 V and the hydrogen adsorption peak were shifted to a negative potential side and there wasn't any change in the peak corresponding to hydrogen evolution. Moreover, there was a considerable shift in the reduction potential of platinum towards more negative side as observed (-0.41 V) on the modified electrode. All these observations revealed that the modified electrode provided an entirely different surface than that of the AuNPs, PtNPs and bare GCE surface. Altogether, these results confirmed the formation of bimetallic AuPtNPs on GCE.

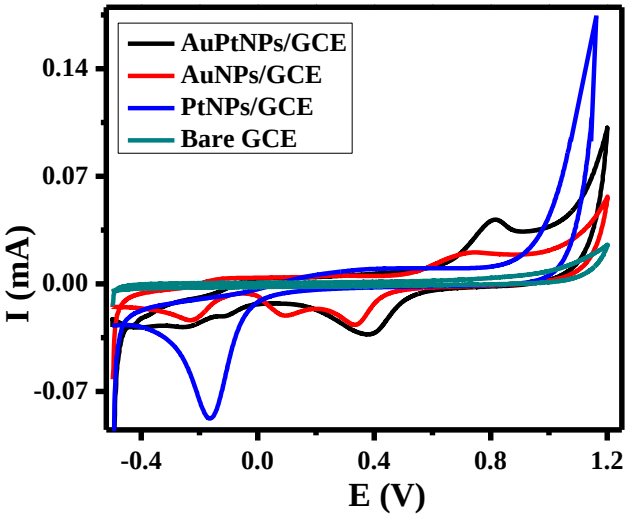

Figure 3.9: *Cyclic voltammograms of bare GCE, PtNPs/GCE, AuNPs/GCE and AuPtNPs/GCE in 0.1 M CH_3COONa+0.05 M KCl solution of pH 6.8 with a scan rate of 50 mV s^{-1}.*

3.9 Optimization of experimental conditions for the preparation of AuPtNPs on GCE

In order to attain the maximum performance, the effect of concentration of gold and platinum, the deposition time, and the deposition current was analyzed. When the concentration of Pt was lower than that of Au, the prepared electrode showed sharp oxidation peak at a potential of 0.73 V itself. This indicated that Pt concentration was not sufficient for the formation of bimetallic nanoparticles, i.e. AuNPs dominated on the

electrode surface. When excess Pt concentration was taken for the preparation, a broadened oxidation peak was obtained at 0.34 V, seemed to be PtNPs dominated over AuNPs on the electrode surface. Through observation it was clear that the performance was very poor at high and low concentrations of platinum. The concentration studies revealed that 0.1 mM Pt and 1 mM Au was suitable for the preparation of bimetallic AuPtNPs on GCE. At this concentration ratio it showed maximum combined effect i.e., a sharp oxidation peak at a potential of 0.88 V.

The performance of AuPtNPs was greatly dependent up on the deposition time. While varying the deposition time from 5 – 12 minutes, the oxidation peaks showed fluctuation. Initially for 5 minutes the oxidation peak was at 0.73 V and peak nature was similar when AuNPs alone was taken in the solution. Gradually this oxidation peak started shifting towards the positive side and the peak obtained was extra sharpened when the deposition time was 10 minutes. During this time, platinum was deposited along with AuNPs and this modified film had extra stability when compared to AuNPs film formed in the absence of platinum. Beyond this time, there wasn't any change in the nature of all the peaks and therefore 10 minutes was considered as the optimum deposition time for further analysis (Figure 3.10a).

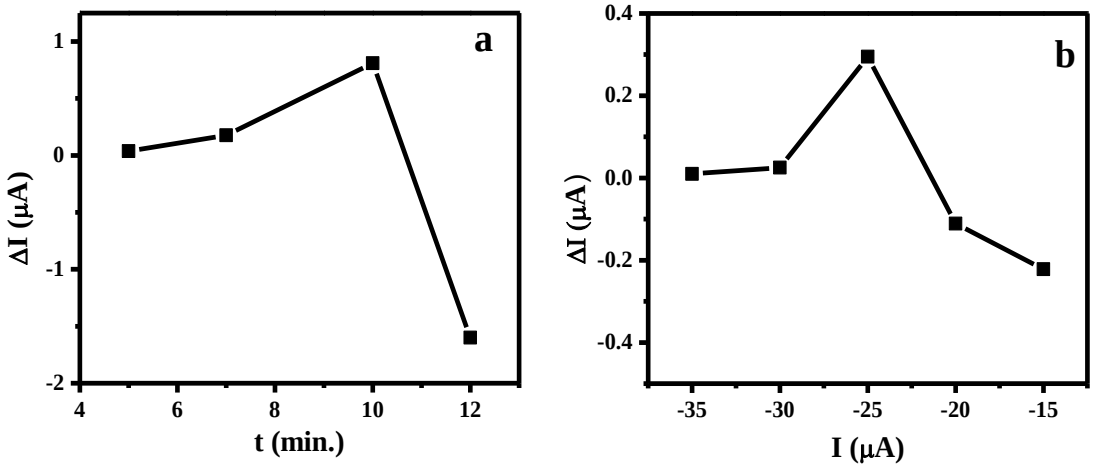

Figure 3.10: ***(a)*** *The effect of deposition time and* ***(b)*** *deposition current on the peak current of AuPtNPs/GCE*

Since the galvanostatic current was another parameter which largely depended on the preparation of AuPtNPs, the careful optimization of current for the formation of AuPtNPs was also performed. From this it was found that -25 μA was the suitable current for the formation of AuPtNPs on GCE (Figure 3.10b). The investigated and optimized conditions were shown in Table 3.3.

Table 3.3: *Investigated and optimized conditions for the preparation of AuPtNPs on GCE*

Parameters	Investigated range	Optimized conditions
Conc. of Au and Pt (M)	10^{-2} – 10^{-5} (Au)	10^{-3} Au/10^{-4} Pt
	10^{-3} – 10^{-5} (Pt)	
Deposition time (min.)	5 – 12	10
Deposition current (μA)	-15 – -35	-25

3.10 Application of fabricated AuPtNPs/GCE towards the detection of phenol

The modified electrode was further applied for the nano molar level detection of phenol by CV. Figure 3.11 showed the typical CV of the bare GCE and the modified electrode without and with the presence of phenol in 0.1 M CH_3COONa+0.05 M KCl of pH 6.8.

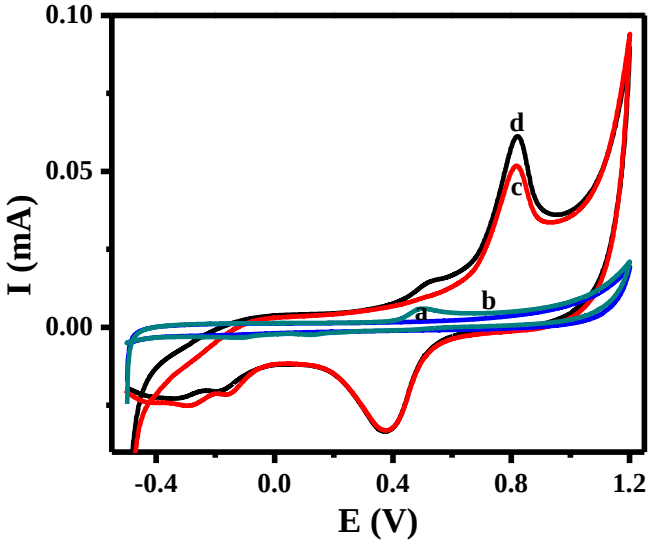

Figure 3.11: *Cyclic voltammograms of bare GCE and AuPtNPs/GCE in 0.1 M CH_3COONa+0.05 M KCl electrolyte with and without the presence* of 10 μM phenol.

On bare GCE, up to 9 μM phenol, there were no peaks observed (curve a), meanwhile phenol with concentration above 9 μM could produce oxidation peak at 0.45 V on GCE (curve b). As mentioned earlier, the modified electrode generated one oxidation and three reduction peaks in 0.1 M CH_3COONa+0.0 5M KCl of pH 6.8 (curve c). When 0.04 μM phenol was added to the supporting electrolyte, the oxidation peak current of AuPtNPs/GCE increased considerably. This oxidation peak further increased as the concentration of phenol increased. This enhancement in oxidation peak was due to the catalytic effect of phenol towards the oxidation of AuPtNPs on GCE. It was also observed that when the concentration of phenol reached above 9 μM, a peak corresponding to phenol oxidation at 0.45 V also appeared (curve d). Such kind of enhancement in Au peak current was not observed on AuNPs/GCE (Figure 3.12 a). Mean while on PtNPs/GCE only a broad oxidation peak due to the combined oxidation of both Pt and phenol was experienced (Figure 3.12b).

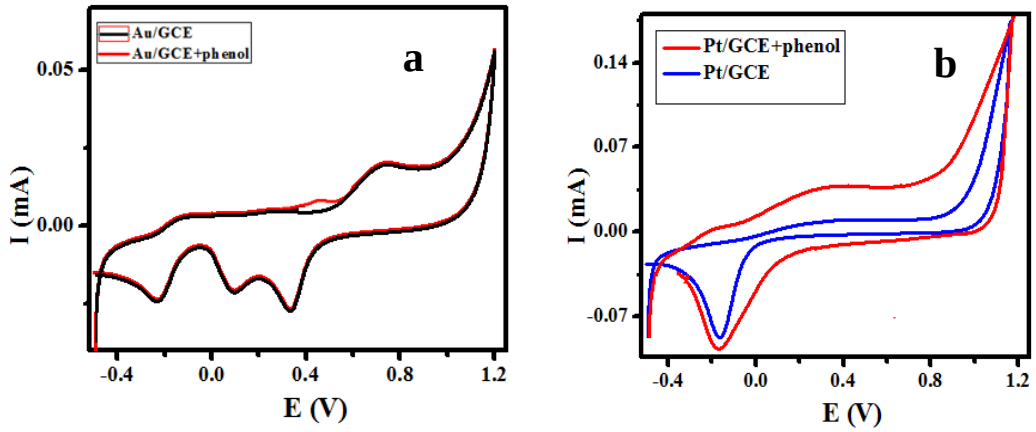

Figure 3.12: (a) *Cyclic voltammograms of AuNPs/GCE and* ***(b)*** *PtNPs/GCE in 0.1 M CH_3COONa+0.05 M KCl electrolyte with and without the presence of 10 μM phenol.*

The probable mechanism for this electrode process could be explained as follows. In presence of Au, phenol molecules were adsorbed to a greater extent on the Pt surface. During the forward scan, phenol was oxidized into hydroquinone at around 0.45 V, thus formed hydroquinone accelerated the oxidation capability of Pt. Hence at a potential of 0.5 V, the hydroquinone formed would oxidize the Pt into PtO_2 by undergoing self

reduction into quinol. The formed PtO_2 intern accelerated the oxidation of Au into Au_2O_3 by reducing itself in to platinum at a potential of 0.88 V. In fact due to all this process the oxidation current of Au got enhanced in presence of phenol and this increase in peak current was directly proportional to the phenol concentration. So the fabricated electrode could be used as a phenol sensor. The probable oxidation mechanism for this enhancement effect was explained in Scheme 3.1. The corresponding balanced equation is depicted below.

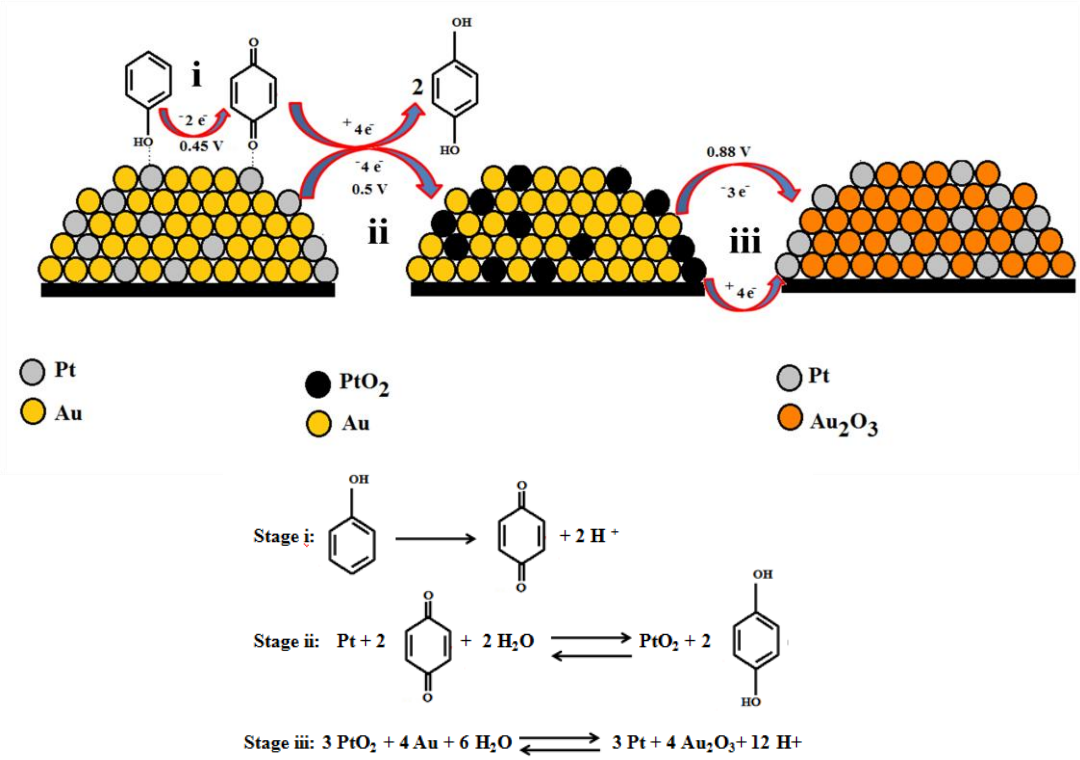

Scheme 3.1: *Mechanism of overall electrochemical process of phenol on AuPtNPs/GCE*

3.11 Effect of electrolyte and solution pH on the detection of phenol

Experiments were carried out in various sample media such as CH_3COONa, CH_3COONH_4, KCl, NaCl, NaH_2PO_4, and a mixture of CH_3COONa+KCl, CH_3COONa+NaCl and CH_3COONa+NaH_2PO_4. In all the cases, except for 0.1 M CH_3COONa+0.05 M KCl, a less sensitive, broad oxidation peaks were observed and were not even reproducible. Figure 3.13 showed the cyclic voltammetry of AuPtNPs/GCE in 0.1 M CH_3COONa with KCl of different concentrations. In 0.1 M

CH_3COONa+0.05 M KCl mixture the phenol oxidation peak was sharp with enriched peak current (curve b) and it could detect phenol from 0.04 μM onward. From this figure it was also understood that the phenol oxidation peak current was reduced further for the mixture of CH_3COONa+0.1 M KCl buffer (curve c) and the current was minimum for the mixture of CH_3COONa+0.2 M KCl (curve d). A shift in oxidation peak potential towards the negative potential was also recorded during this variation. It was also observed that in the absence of KCl, the modified electrode showed less sensitive oxidation peak current and it could detect phenol only after adding 0.2 μM to the supporting electrolyte (curve a). Therefore 0.1M CH_3COONa+0.05 M KCl mixture was selected as an appropriate supporting electrolyte for further analysis.

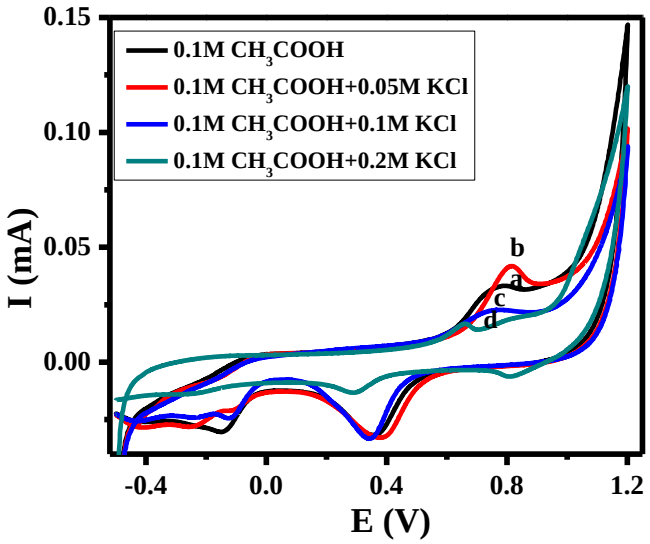

Figure 3.13: *Cyclic voltammograms of oxidation of phenol at AuPtNPs/GCE in 0.1 M CH_3COONa with different concentrations of KCl.*

The effect of the pH (6-7.5) of the electrolyte on the electrochemical behaviour of the sensor was also studied by varying the pH from 6.8 to 7.5 (Figure 3.14) and was found that below 6.8 and above 7.25, the modified electrode had no response on phenol. Between 6.8 and 7.25, pH of 6.8 gave maximum peak current and response to phenol. So it was fixed for further analysis of phenol.

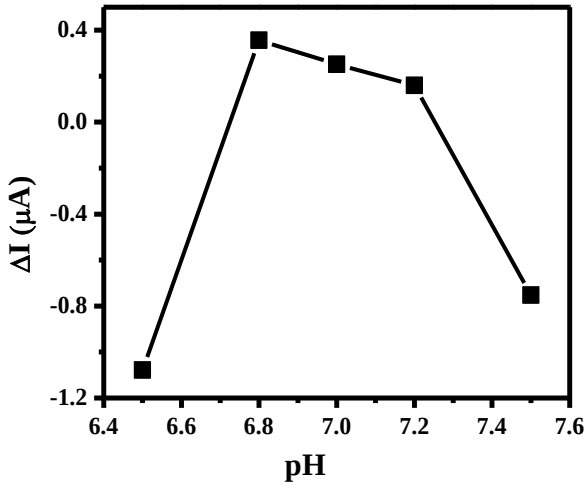

Figure 3.14: *The effect of solution pH on the peak current of 1μM phenol*

3.12 Effect of phenol concentration on AuPtNPs/GCE

Figure 3.15a showed the CV of AuPtNPs/GCE towards the different concentrations of phenol in 0.1 M CH_3COONa+0.05 M KCl of pH 6.8 as electrolyte. While increasing the concentration from 0.04 to 10 μM the oxidation peak currents increased drastically. From the calibration plot of Ip Vs [phenol], two linearities were obtained (Figure 3.15b). One in the lower concentration range (0.04 to 0.8 μM) and other in the higher concentration range (1 to 10 μM). From this plot the correlation coefficients of these two plots were 0.998 and 0.996. Limit of detection based on 3 times the standard deviation (s) of the blank value was found to be 6.5 nM. The relative standard deviation was 1.6 % for 10 replicate determination of 0.2 μM of phenol, which revealed the extremely high precision of designed phenol sensor. Further, the performance of the modified electrode was compared with the previously reported electrodes and the results were tabulated in Table 3.4.

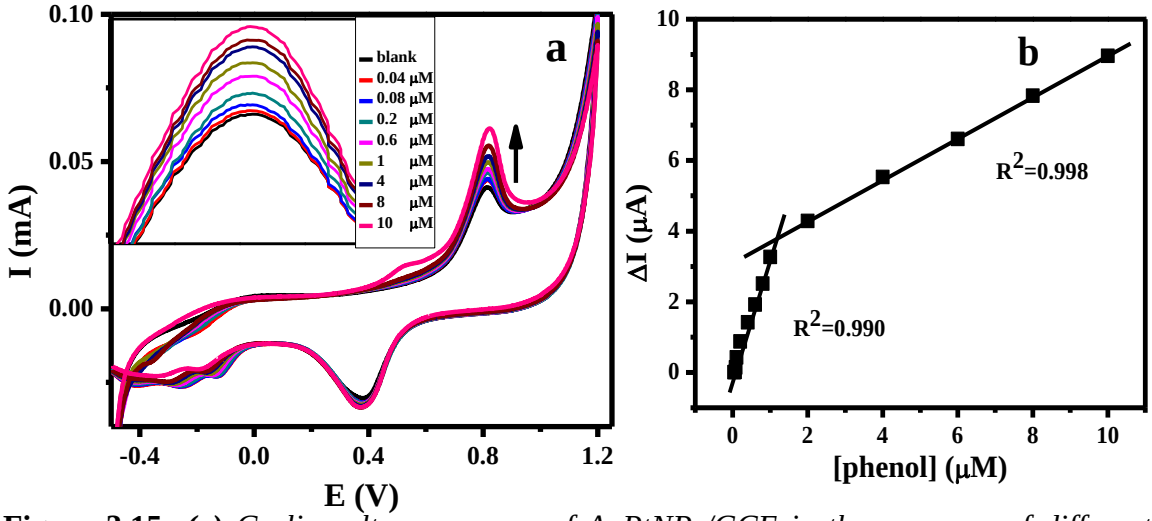

Figure 3.15: ***(a)*** *Cyclic voltammograms of AuPtNPs/GCE in the presence of different concentrations of Phenol and* ***(b)*** *the calibration curve in the range of 0.04 µM to 10 µM of phenol.*

Table 3.4: *Comparison with reported phenol sensing methods*

Method	Modification	Linear Calibration Range (µM)	Detection Limit (µM)	Reference
Cyclic Voltammetry	Pt/PPy-FeCN	5 to 100	5	20
Amperometry	Pt/(PDMA-PSA) polymer	-	2089	21
Amperometry	Carbon nanotube modified GCE	-	15	22
Amperometry	Nafion membrane doped with [$CuDipyCl_2$]/GCE	40 to 600	9	23
Cyclic Voltammetry	Pt/RuO_2/C	0.007 to 0.05	0.001	24
Cyclic Voltammetry	AuPtNPs/GCE	0.04 to 0.8 & 1 to 10	0.0065	Present work

3.13 Selectivity and reproducibility studies

The selectivity of the AuPtNPs/GCE for phenol sensing was demonstrated with other phenol compouds like catechol, p-chlorophenol, o-chlorophenol and tri chlorophenol. The compound with a group in the para position was not interfering on the Au oxidation peak up to 20 folds. It was found that the complete elimination of possible

interference from ortho substituted phenol and catechol on the oxidation of phenol was not possible beyond 10 folds. It was also observed that tri substituted phenol had no effect on the oxidation peak current of Au. This result also justified the authenticity of the proposed mechanism. Figure 3.16 showed the electrochemical signals of 1 μM concentrations of phenol and above listed species. 96 % of the initial current response was observed after 15 days storage at room temperature, indicating the stability of the fabricated electrode.

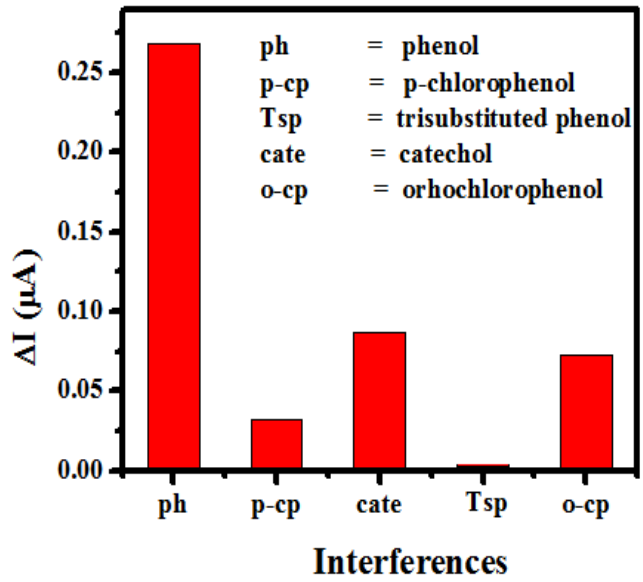

Figure 3.16: *Selectivity studies of phenol and other interferences*

3.14 Real sample analysis

The fabricated electrode was tested by the triplicate analysis of river and well water samples by standard addition method. The results were listed in Table 3.5. The recoveries for the determinations vary from 97.6 % to 102.3 %, suggesting the proposed electrode can be used to reliably determine phenol in real samples.

Table 3.5: Analysis of real water samples

Sample	Phenol spiked (M)	Phenol found (M)	Recovery (%)
Well water	$8x10^{-8}$	$7.8x10^{-8}$±0.04	97.6±0.5
River water	$4x10^{-7}$	$4.1x10^{-7}$±0.12	102.3±0.3

3.15 Experimental

3.15.1 Chemicals and reagents

Phenol, Hydrogen tetrachloroaurate trihydrate ($HAuCl_4.3H_2O$), and Hexachloroplatinic acid hexahydrate ($H_2PtCl_6.6H_2O$) were purchased from Aldrich, Milwauke, WI, USA. 4-chlorophenol, 2- chlorophenol, 2, 4, 6-trichlorophenol and catechol were from Merck, Darmstadt, Germany. All the chemicals were of analytical reagent grade (E Merck, Mumbai, India) and were used without further purification. Deionized double distilled water was used for the preparation of working solutions. Acetate buffer solution (0.1 M sodium acetate +0.05 M potassium chloride and adjusted to pH 6.8 with HCl) of pH 6.8 was used as the supporting electrolyte in all electrochemical experiments.

3.15.2 Instrumentation

Electrochemical measurements were performed on a three-electrode cell (20 ml) fitted with a glassy carbon electrode (3 mm in diameter) as working electrode, a Pt wire as auxiliary electrode, and saturated calomel electrode (SCE) as reference electrode. Electrochemical measurements were performed with a VSP-potentiostat/galvanostat (Biologic Science Instruments). The pH values were measured with Oakton pH 700 meter, Germany. The X-ray diffraction (XRD) patterns of the samples were recorded on a Philips X'pert diffractometer (XRD, X'Pert Pro MPD) with CuKα radiation (1.5406 °A). XPS studies were carried out by x-ray photoelectron spectroscopy (XPS) (model ESCALAB220IXL) equipped with an Axis Ultra, Kratos (1486.7 eV) monochromatic source for excitation. XPS spectra over a binding energy (BE) range of 0–1200 eV was obtained using analyzer pass energy of 117.4 eV. The size and morphology was studied by a scanning electron microscope (SEM), JEOL, Model JSM 5600 LV, Tokyo, Japan and AFM was performed on Bruker's Scan Asyst and Peak Force Tapping AFM with NSG 10 Tip and golden silicon probe. UV- Visible spectra were recorded with a

computer controlled double beam UV-Vis spectrophotometer UV-2401PC (Shimadzu, Kyoto, Japan).

3.16 Conclusions

Galvanostatic method was used for the fabrication of bimetallic $Au_{90}Pt_{10}$NPs on GCE surface. The prepared hybrid bimetallic nanoparticles possessed alloy nature. The fabricated $Au_{90}Pt_{10}$NPs/GCE was highly sensitive, selective, precise, and showed a wider calibration range (0.04 to 10 μM) towards phenol. Possible interference from various compounds was also tested and found that the compound with a group in the para position did not interfere in the phenol determination at lower concentration (upto 20 folds). Even in the presence of tri substituted phenols, the fabricated electrode could detect 10 μM phenol. So, it can be concluded that the AuPtNPs modified glassy carbon electrode can be used for the quantitative determination of phenol with high selectivity, which are commonly found in well and river water.

3.17 References

1) Zhang, W.; Saliba, M.; Stranks, S. D. Sun, Y.; Shi, X.; Wiesner, U.; Snaith, H. J. Enhancement of Perovskite- Based Solar Cells Employing Core Shell Metal Nanoparticles. *Nano. Lett.* **2013,** *13,* 4505-4520.
2) Ando, J.; Yano, T.A.; Fujita, K.; Kawata, S. Metal Nanoparticles for Nano- Imaging and Nano Analysis. *Phys. Chem. Chem. Phys.* **2013,** *15,* 13713-13722.
3) Rodriguez, P.; Plana, D.; Fermin, D. J.; Koper, M. T. M. New Insight in to the Activity of Gold Nanoparticles for CO Oxidation in Electrochemical Media. *J. Catal.* **2014,** *311,* 182-189.
4) Nantaphol, S.; Chailapakul, O.; Siangproh, W. Sensitive and Selective Electrochemical Sensor Using Silver Nanoparticles Modified Glassy Carbon Electrode for Determination of Cholesterol in Bovin Serum. *Sens. Actuators, B* **2015,** *207,* 193-198.
5) Lei, J.; Ju, H. *Applications of Nanomaterials in Sensors and Diagnostics;* Springer: New York, 2013; p 20.
6) Duan, S.; wang, R.; Bimetalic Nanostructures with Magnetic and Noble Metals and Their Physiocochemical Applications. *Prog. Nat. Sci.* **2013,** *23,* 113-126.
7) Mott, D.; Luo, J.; Njoki, P. N.; Lin, Y.; Wang, L.; Zhong, C. J. Synegistic Activity of Gold- Platinum Alloy Nanoparticles Catalysts. *Catal. Today* **2007,** *122,* 378-385.
8) Ming, C. H.; Chieh, P. H.; Shi, L. R.; Fen, H. S.; Shuenn, S. H. Morphology and Surface Plasma Changes of Au-Pt Bimetallic Nano Particles. *J. Nanosci. Nanotechnol.* **2006,** *6,* 1411-14115
9) Zhao, L.; Thomas, J. P.; Heining, N. F.; Ellaah, M. A.; Wang X.; Leung, K.T.; Au-Pt Alloy Nanocatalysts for Electro Oxidation of Methanol and Their Application for Fast Response Non Enzymatic Alcohol Sensing. *J. mater. Chem. C* **2014,** *2,* 2707.

10) Suntivich, J.; Xu, Z.; Carlton, C.; Kim, J.; Han, B.; Lee, S. W.; Bonnet, N.; Marzari, N.; Allard, L. F.; Gasteir, H. A. Surface Composition Tuning of Au-Pt Bimetallic Nanoparticles for Enhanced Carbon Monoxide and Methanol Electro-Oxidation. *J. Am. Chem. Soc.* **2013,** *135*, 7985-7991.

11) Zhang, H.; Toshima, N. Synthesis of Au/Pt Bimetallic Nanoparticles with a Pt-Rich Shell and Their High Catalytic Activities for Aerobic Glucose Oxidation. *J. Colloid Interface Sci.* **2013,** *394*, 166–176.

12) Zhao, Y.; Ye, C.; Liu, W.; Chen, R.; Jiang, X. Tuning the Composition of AuPt Bimetallic, Nanoparticles for Antibacterial Application. *Angew. Chem. Int. Ed.* **2014,** *53*, 8127 – 8131.

13) Zhao, L.; Thomas, J. P.; Heinig, N. F.; Abd-Ellah, M.; Wang, X.; Leung, K. T. Au–Pt Alloy Nanocatalysts for Electro-Oxidation of Methanol and Their Application for Fast-Response Non- Enzymatic Alcohol Sensing. *J. Mater. Chem. C* **2014,** *2*, 2707-2714.

14) Zhao, L.; Heining, N.; Leung, K. T. Formation of Au-Pt Alloy Nanoparticles on a Si Substrate by Simple Dip- Coating at Room Temperature. *Langmuir* **2013,** *29*, 927-931.

15) Gogate, P. R. Treatment of Wastewater Streams Containing Phenolic Compounds Using Hybrid Techniques Based on Cavitation: A Review of the Current Status and the Way Forward. *Ultrason. Sonochem.* **2008,** *15*, 1–15.

16) Wang, Y.; Gu, B.; Xu, W. Electro-Catalytic Degradation of Phenol on Several Metaloxideanodes. *J. Hazard. Mater.* **2009,** *162*, 1159–1164.

17) Fang, Z.; Zhang, Y.; Lü, Y.; Ma, G.; Chen, J.; Liu, D.; Ye, X. Phenolic Compounds and Antioxidant Capacities of Bayberry Juices. *Food Chem.* **2009,** *113*, 884–888.

18) Martus, P.; Puttmann, W.; Formation of Alkylated Aromatic Acids in Groundwater by Anaerobic Degradation of Alkylbenzenes. *Sci. Total Environ.* **2003,** *307*, 19–33.

19) Altavilla C.; Ciliberto, E.; *Inorganic Nanoparticles: Synthesis, Applications, and Perspectives*; CRC Press: New York, 2011; p 1.

20) Lupu, S.; Ion, I.; Ion, A.C.; Voltammetric Determination of Phenol at Platinum Electrodes Modified with Polypyrrole Doped with Ferricyanide. *Revue Roumaine de Chimie* **2009,** *54*, 351–357.

21) Klink, M. J.; Iwuoha, E. I.; Ebenso, E. E.; The Electro-Catalytic and Redox-Mediator Effects of Nanostructured PDMA-PSA Modified-Electrodes as Phenol Derivative Sensors. *Int. J. Electrochem. Sci.* **2011,** *6*, 2429 – 2442.

22) Wang, J.; Deo, R. P.; Musameh, M.; Stable and Sensitive Electrochemical Detection of Phenolic Compounds at Carbon Nanotube Modified Glassy Carbon Electrodes. *Electroanalysis* **2003,** *15*, 23-24.

23) Sotomayor, M. D. P. T.; Tanaka, A. A.; Kubota, L. T.; Development of an Amperometric Sensor for Phenol Compounds Using a Nafion® Membrane Doped with Copper Dipyridyl Complex as a Biomimetic Catalyst. *J. Electroanal. Chem.* **2002**, *536*, 71-81.

24) Tzang, C. H.; Li, C.W.; Zhao, J.; Yang, M.; Electrocatalytic Phenol Oxidation on Mixed Pt-RuO_2 Nanoparticle Modified Electrode. *Anal. Lett.* **2005,** *38*, 1735–1746.

Chapter 4

One step green synthesis of carbon quantum dots and its application towards the bioelectroanalytical and biolabelling studies

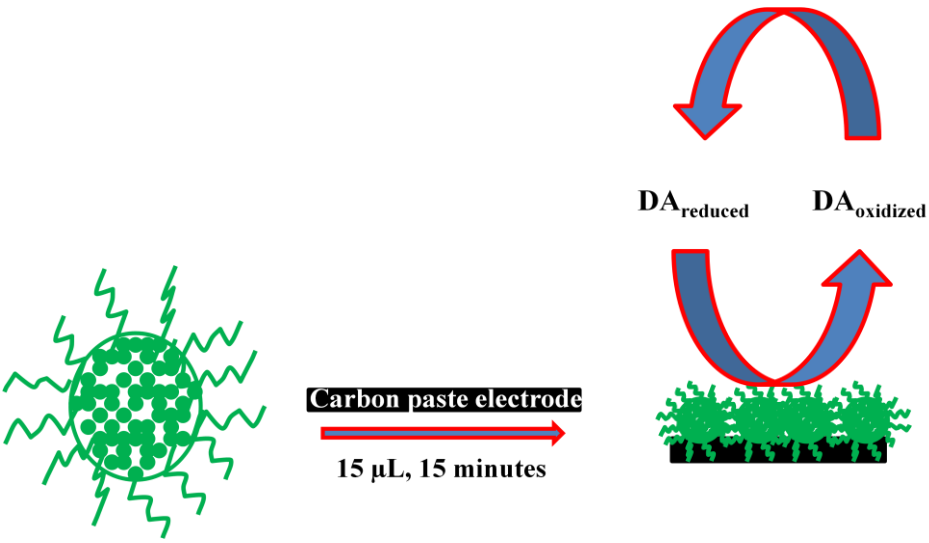

4.1 Abstract

A green luminescent carbon quantum dots (CQDs) were prepared from maltose by Microwave assisted method followed by passivation with NaOH (pH=7.4). The TEM measurement confirmed the average size of prepared CQDs to be 2 nm. Surface characterization such as UV-Visible absorption spectroscopy, PL spectroscopy, XPS, FTIR and Raman spectroscopy confirm that the functional groups (C=O, C-OH) were attached on the surface of sp^2 hybridized carbon. Electrochemical characterization studies on carbon paste electrode (CPE) revealed that the synthesized CQDs showed higher electrocatalytic property, conductivity and surface area. Therefore, herein we report the synthesis of green CQDs which could find its applicability as an electrochemical sensor for the detection of neurotransmitter, dopamine (DA). Cyclic voltammetry (CV) and differential pulse voltammetry (DPV) were employed for the detection of DA in presence of common interferents like uric acid (UA) and ascorbic acid (AA) with CQDs modified CPE (CQDs/CPE). The developed sensor was effectively applied for the real sample analysis with satisfactory results. Moreover, biological studies in He La cell lines proclaimed that the cell viability was unaffected (100 % viability) on incubation with the CQDs. Significant cellular uptake as revealed by fluorescence imaging makes them suitable for cell labeling studies.

4.2 Introduction

In the year 2004, during the purification of single-walled carbon nanotubes by preparative electrophoresis, a new type of carbon material with size below 10 nm was obtained. This newly obtained carbon material exhibited high fluorescence and were highly soluble in water. It is now well recognized that CQDs is an emerging star in the world of nano materials.[1] Till date there are so many methods adopted for the synthesis of carbon quantum dots including arc discharge[1], electrochemical synthesis,[2, 3] combustion/thermal/hydrothermal/acidic oxidation,[4-7] cage-opening of fullerene,[8] supported synthesis,[9-11] microwave/ultrasonic,[12, 13] laser ablation[14, 15] and electrochemical oxidation methods[16, 17] and so on. CQDs gained greater acceptance because of their wide application for instance in bioimaging,[18, 19] nanomedicine,[20, 21] photocatalysis,[22, 23] electrocatalysis,[24, 25] biosensing,[26, 27] and chemical sensing.[28, 29] It was also used as Hg^{2+}, Cu^{2+}, Fe^{3+}, Pb^{2+} and Ag^{+} sensors.[30-34] These dots were also reported with its application as pH sensors by Jia *et al.*[35] Li *et al.* stated that the Nitrogen-doped graphene quantum dots supported by graphene sheets have been found to possess superior electrocatalytic ability.[36] Recently, in 2015, Xu *et al.* reported Sulfur-doped graphitic carbon nitride decorated with graphene quantum dots which could be used as an efficient metal-free electrocatalyst.[37]

DA is an important biomolecule belongs to the catecholamine family. Being monoamine neurotransmitter, that plays a critical role in the function of the central nervous, hormonal, and cardiovascular systems.[38, 39] Since its discovery, DA has attracted a great deal of attention in clinical fields because its abnormal levels indicate various diseases, such as Parkinson's disease, senile dementia, and schizophrenia.[40] Over the past several decades, tremendous effort has been made and various techniques have been developed, such as fluorimetry, chemiluminescence, capillary electrophoresis, and ion

chromatography.[41-44] Being electrochemically active electrochemical detection of DA could be possible. This approach got much more attention due to its fast detection, simplicity, reproducibility, impressive cost-effectiveness, and potential for miniaturization.[45] However, the electrochemical response to DA can easily be affected by AA, UA, and other molecule due to the closeness of their oxidation potential. Various approaches have been made for the detection of DA individually and simultaneously. Unfortunately most of the fabricated electrodes failed to detect them in the nano molar level.

In this work, we are proposing a one step green synthesis of green luminescent CQDs from maltose, which was further utilized for cell labelling studies. Electrochemical characterization studies using CPE revealed that CQDs provided higher surface area, conductivity and electrocatalytic activity. By taking advantage of this characteristic, CQDs modified CPE (CQDs/CPE) was successfully applied for the determination of nano molar level of DA individually and in the presence of AA and UA by CV, further it was confirmed by DPV. To our knowledge, this is the first report on the application of CQDs/CPE for electrochemical sensing.

4.3 Synthesis of carbon quantum dots

Maltose was digested in a microwave oven for 20 minutes. The charring product was stirred for half an hour at 800 rpm with a much diluted solution of NaOH of pH 7.4 as passivating agent. During this process more and more –OH groups will attach on the sp^2 hybridized carbon surface, which will lead to the enrichment of quantum yield of CQDs. The unreacted and other impurities were eliminated by centrifugation. The resultant solution was then sonicated and filtered with Whatmann filter paper. The obtained CQDs were stored at room temperature.

4.4 Preparation of CQDs/CPE

CQDs/CPE was prepared by manually grinding 70 % graphite powder and 30 % silicon oil in an agate mortar for about 30 minute to get a homogenous mixture. The paste was packed into the cavity of CPE and smoothened on weighing paper. 15 µL CQDs was drop casted on the surface of CPE for 15 min. After this, the electrode was washed with water and data were recorded in pH 7.4 PBS.

4.5 Surface and spectral characterization

The size of the CQDs was found to be 2.49 nm from DLS (Figure 4.1a). In addition, TEM analysis (Figure 4.1b) reveals that highly monodispersed and spherical CQDs with an average size of 2 nm were obtained, which was further summarized in PSD (Figure 4.1c).

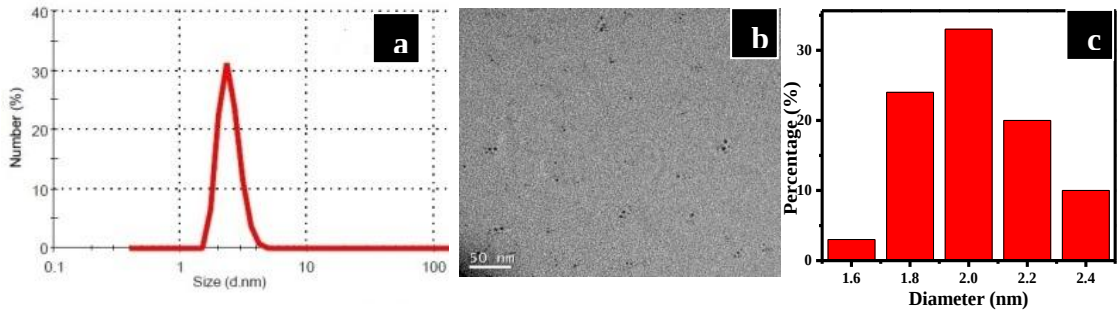

Figure 4.1: ***(a)*** *DLS* ***(b)*** *TEM image and* ***(c)*** *particle size distribution of CQDs.*

Figure 4.2a (inset) shows the physical characteristics of prepared CQDs under visible and UV light. UV-Visible absorption spectroscopy (Figure 4.2a) gave two characteristic peaks, one at 220 nm corresponding to $\pi - \pi^*$ transition of the conjugated C=C band and another at 280 nm corresponding to $n - \pi^*$ transition of C=O band. The PL spectra (Figure 4.2b) reveal that maximum emission intensity was observed at 436 nm when excited at 360 nm. In addition to that, a regular bathochromic shift (up to 600 nm) in the emission maxima was observed when the excitation window was changed from 360 to 480 nm. Tang *et al.*

suggested that this kind of bathochromic shift is a common characteristic of carbon-based QDs.[46]

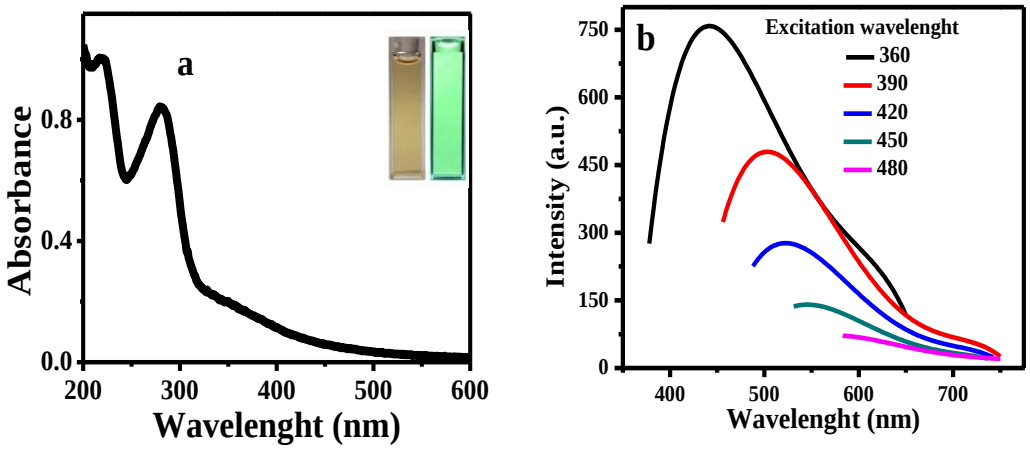

Figure 4.2: (a) *UV-Vis spectra and inset shows appearance of CQDs in absence and presence of UV light and* ***(b)*** *PL spectra of the CQDs at different wavelength*

Quantum yields (QYs) of the CQDs were calculated using the equation

$$\Phi_s = \Phi_R \, A_R \, n_S^2 \, I_S / A_S \, n_R^2 \, I_R$$

Where, Φ_S and Φ_R are quantum yields of sample and reference respectively; A_R and A_S are absorbance of the reference and sample at excitation wavelengths; n_S and n_R are refractive indices of the sample medium and reference medium respectively; I_S and I_R are integrated fluorescence intensities of sample and reference respectively and was found to be 8 % which is comparable with the reported data.[46] (Quinine sulfate (Φ=0.54) was used as reference to determine QYs of CQDs).

Further, CQDs were subjected to XPS analysis in order to obtain information about the functional group present on them. XPS spectra (Figure 4.3a) show a peak at 284.8 eV and another at 532 eV corresponding to graphitic C1s and O1s respectively. The deconvolution of the dominated C1s spectra (Figure 4.3c) show three peaks corresponding to C=C (284.5 eV), C-O (286.5 eV) and C=O (288.6 eV) respectively.

Figure 4.4a displays Raman spectra of CQDs. Two major peaks at 1578 cm^{-1} and 1331 cm^{-1} corresponding to G band and D band and a minor peak at 2654 cm^{-1} corresponding to 2D band which confirmed the sp^2 nature of CQDs. In order to get

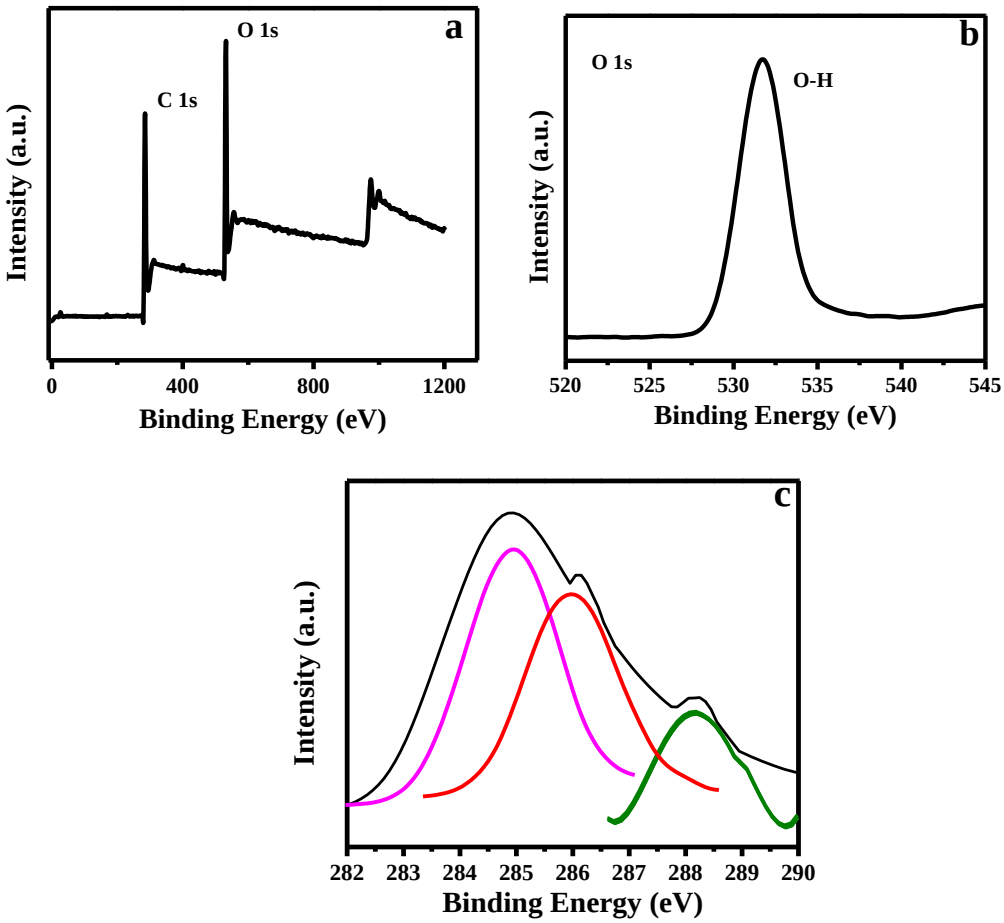

Figure 4.3: ***(a)*** *XPS wide spectra of CQDs* ***(b)*** *XPS of O 1s and* ***(c)*** *C 1s spectra of CQDs.*

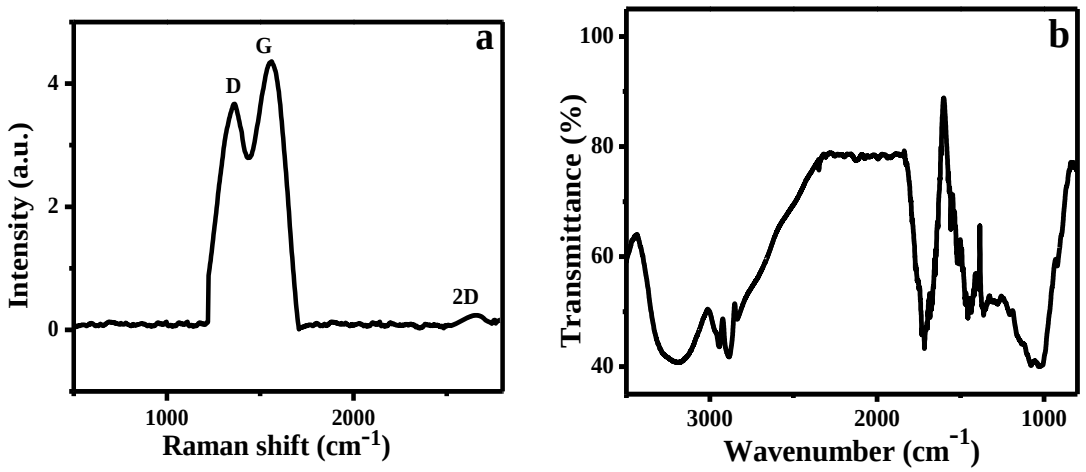

Figure 4.4: ***(a)*** *Raman and* ***(b)*** *FTIR spectra of the CQDs*

structural insight, FTIR spectra of CQDs was recorded. A peak corresponding to C=O group at 1691 cm^{-1} and another peak corresponding to aromatic C=C (ring stretching) at 1625 cm^{-1} was depicted clearly by Figure 4.4b. Similarly, a broad peak at 3340 cm^{-1}

could be assigned to –O-H stretching frequency. The peaks due to C–O stretching and bending vibrations appeared at 1031 and 1143 cm^{-1}, respectively. A peak corresponding to C-OH emerged in the range 1353 cm^{-1}.

4.6 Electrochemical characterization

Electrochemical experiments were performed to examine the electrocatalytic activity of CQDs/CPE. Figure 4.5 (i) showed the cyclic voltammogram of bare carbon paste electrode (BCPE) and CQDs/CPE (curve a & b) in 1 mM $K_3[Fe(CN)_6]$ with 0.1 M KCl as the supporting electrolyte. The CQDs/CPE in $K_3[Fe(CN)_6]$ electrochemical redox probe showed an anodic peak potential (Epa) at 0.210 V and a cathodic peak potential (Epc) at 0.147 V. ΔEp (Epa-Epc) was 60 mV, which showed the reversibility of the modified electrode. Comparing both the anodic (23.27 μA) and cathodic peak current (-32.18 μA) at BCPE, a drastic change in anodic (208.80 μA) and cathodic peak current (-240.89 μA) was observed at CQDs/CPE which approved the fact that CQDs lifted the conductivity of BCPE.

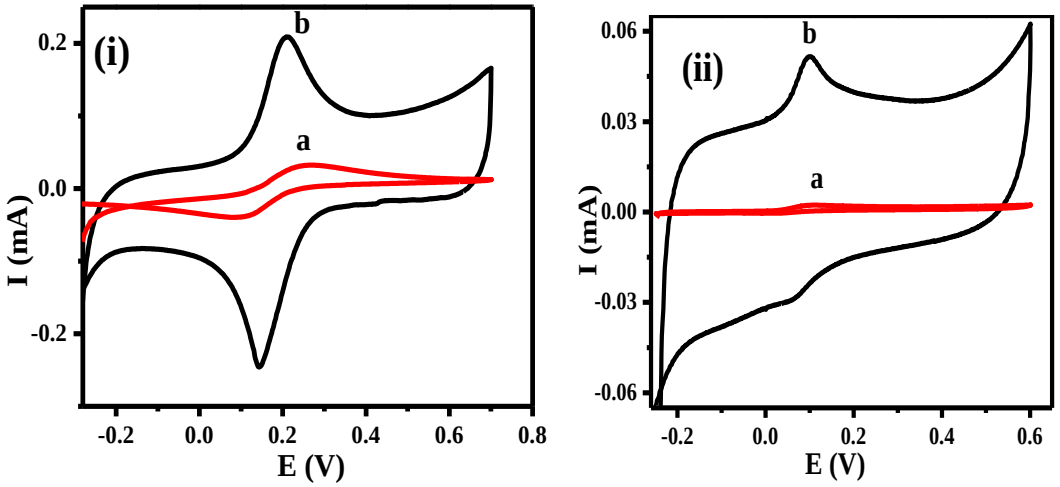

Figure 4.5: ***(i)*** *Cyclic voltammograms of BCPE (curve a), CQDs/CPE (curve b) in 0.1 M KCl containing 1 mM $K_3[Fe(CN)_6]$ and* ***(ii)*** *in 0.1 M PBS containing 1μM DA*

In order to compare the surface area of BCPE and CQDs/CPE cyclic voltammogram of $K_3[Fe(CN)_6]$ in 0.1 M KCl with varying scan rate from 50 to

150 mV s^{-1} were plotted (Figure 4.6a & 4.7a). As per the Randles–Sevcik equation,

$$Ip = 2.69 \times 10^5 n^{3/2} A C_o D_R^{1/2} \nu^{1/2}$$

Where, Ip is the peak current, n is the number of electrons transferred, A is the surface area of the electrode (cm^2), D_R is the diffusion coefficient of the molecule in solution (cm^2 s^{-1}), ν is the scan rate (mV s^{-1}) and C_o corresponds to the bulk concentration of the probe (mol dm^{-3}). The surface area could be calculated from the slope of the plot of Ip Vs $\nu^{1/2}$ (for 1 mM $K_3[Fe(CN)_6]$, n =1, $D_R = 7.6 \times 10^{-6}$ cm s^{-1}) and was found to be 0.0429 cm^2 (from Figure 4.6b) for CQDs/CPE and 0.00817 cm^2 (from Figure 4.7b) for BCPE. All this results approved that CQDs provide larger surface area and high conductivity.

4.7 Electrochemical behaviour of DA on CQDs/CPE

The prepared CQDs/CPE was employed for the analysis of 1 μM of DA in 0.1 M PBS of pH 7.4. The poor sensitivity of BCPE towards the redox reaction of DA was improved with CQDs/CPE, Figure 4.5(ii). DA undergoes oxidation at a potential of 0.113 V with peak current 2.26 μA and reduction at a potential 0.022 V with peak current 0.37 μA on the surface of BCPE (curve a). On the other hand oxidation (0.102 V) and reduction peak potentials (0.06 V) of DA on CQDs/CPE (curve b) were shifted to less positive sides. In spite of this, a strong increase in oxidation (51.5 μA) and reduction peak current (29.15 μA) was also observed. This suggested the higher sensitivity and catalytic activity of CQDs/CPE towards the electrochemical oxidation of DA.

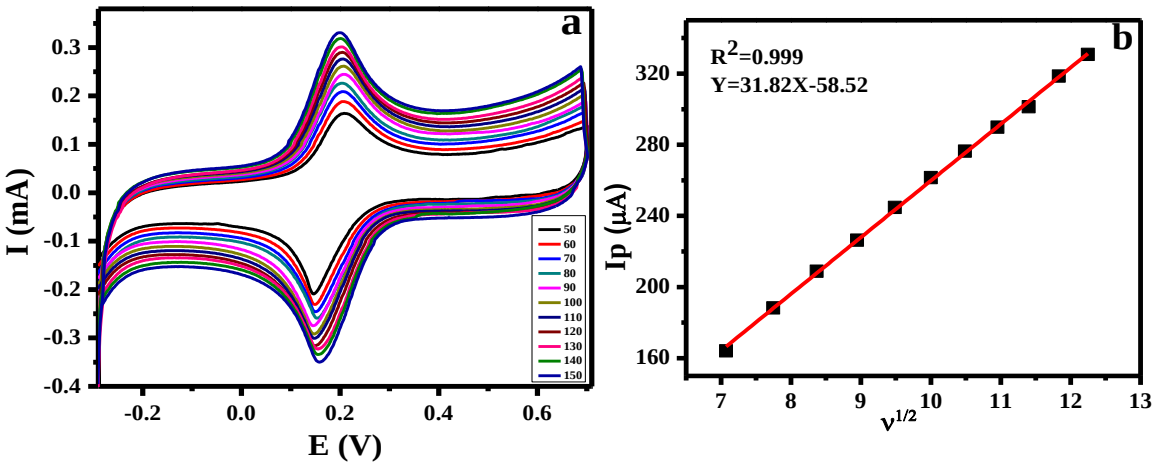

Figure 4.6: ***(a)*** *Cyclic voltammograms of 0.1 mM $K_3[Fe(CN)_6]$ in 0.1M KCl with various scan rates (50 to 150 mV s^{-1}) at CQDs/CPE and* ***(b)*** *plot of Ip Vs $\nu^{1/2}$*

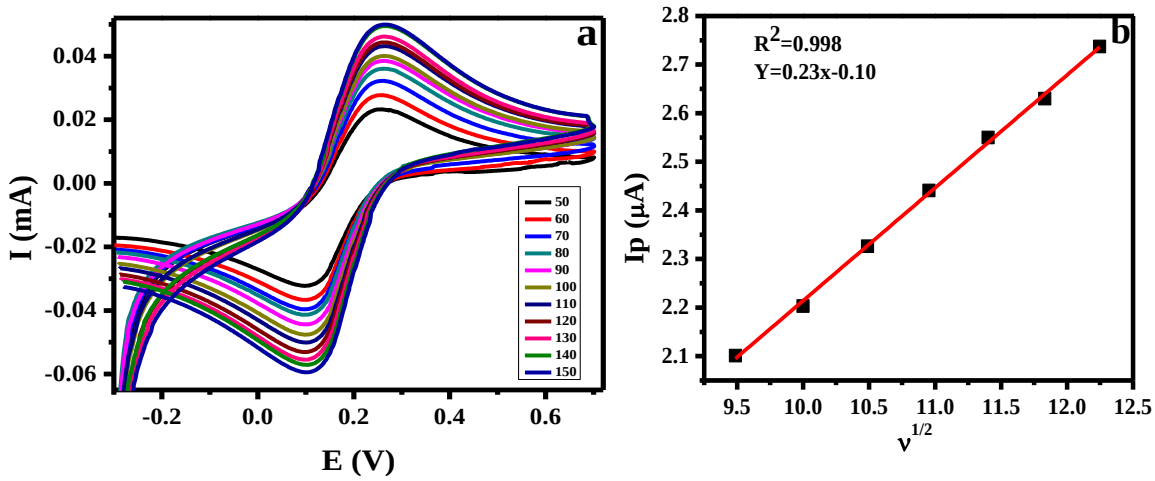

Figure 4.7: ***(a)*** *Cyclic voltammograms of 0.1mM $K_3[Fe(CN)_6]$ in 0.1M KCl with various scan rates (50 to 150 mV s^{-1}) at BCPE and* ***(b)*** *plot of Ip Vs $\nu^{1/2}$*

4.8 Kinetics studies

The effect of scan rate (ν) on the oxidation of DA on CQDs/CPE and BCPE in 0.1 M PBS of pH 7.4 were studied by CV (Figure 4.8a & 4.9a). While increase in the scan rate from 70-150 mV s^{-1} both the oxidation and reduction peaks of DA increased without shift in potential.

From the equation

$$Ep = (2.303RT/n\alpha F) \log \nu + \text{constant}$$

where Ep is potential, R is gas constant, T is the temperature, n is number of electron

transferred and F is the Faraday constant, electron transfer coefficient (α) was calculated from the slope of the plot of Ep Vs log υ and was found to be 0.69 for CQDs/CPE and 0.59 for BCPE (Figure 4.8b & 4.9b).

On the basis of the slopes of the linear dependence of the anodic peak currents on the square root of the potential sweep rates, by the Randel–Sevcik equation,

$$Ip = (2.99 \times 10^5)\, \alpha^{1/2}\, n^{3/2}\, A\, C\, D^{1/2}\, \nu^{1/2}$$

Where Ip is the peak current, A is the electrode surface area, D is the diffusion co-efficient and C is the bulk concentration, the diffusion coefficient of DA was calculated to be 0.929 $cm^2\, s^{-1}$ for CQDs/CPE and 0.096 $cm^2\, s^{-1}$ for BCPE (Figure 4.8c & 4.9c).

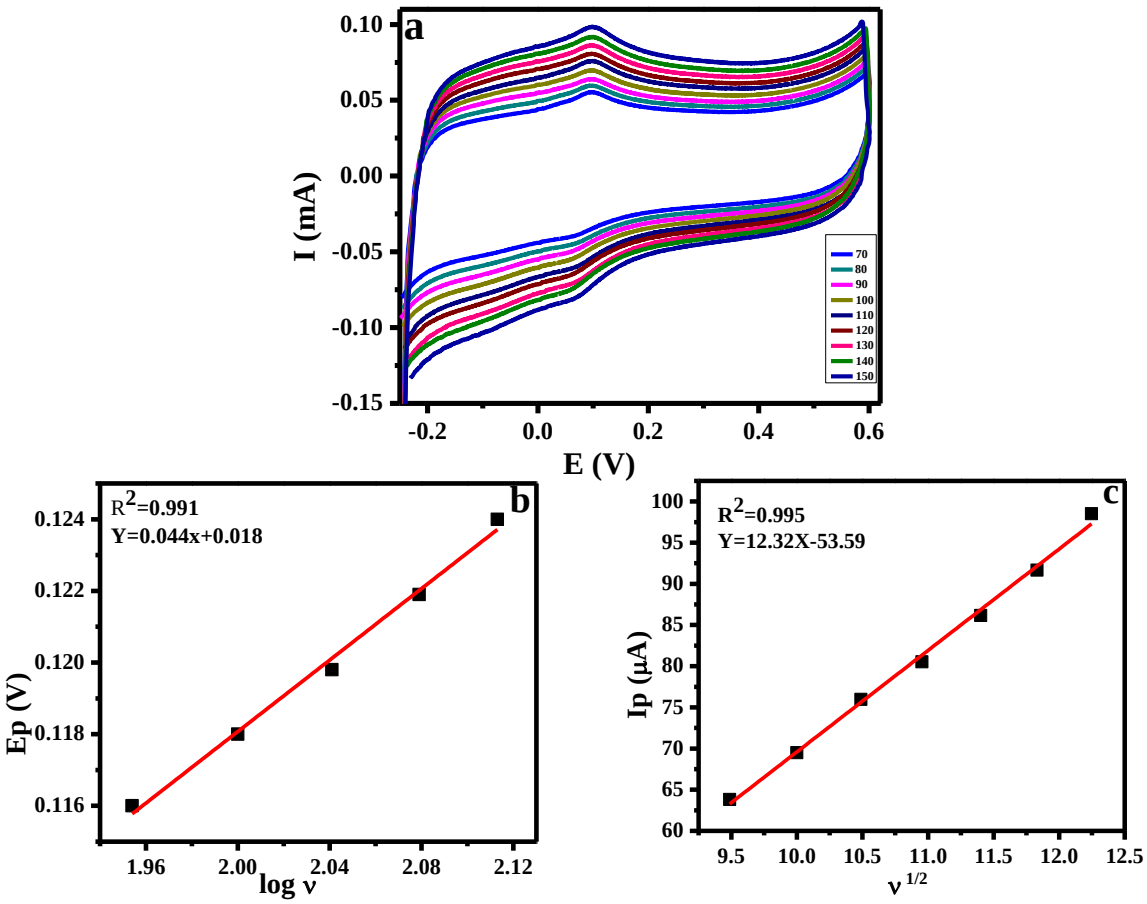

Figure 4.8: ***(a)*** *Cyclic voltammograms of oxidation of DA (1μM) at various scan rates (70 to 150 mV s^{-1}) at CQDs/CPE* ***(b)*** *plot of Ep Vs log ν and* ***(c)*** *plot of Ip Vs $\nu^{1/2}$*

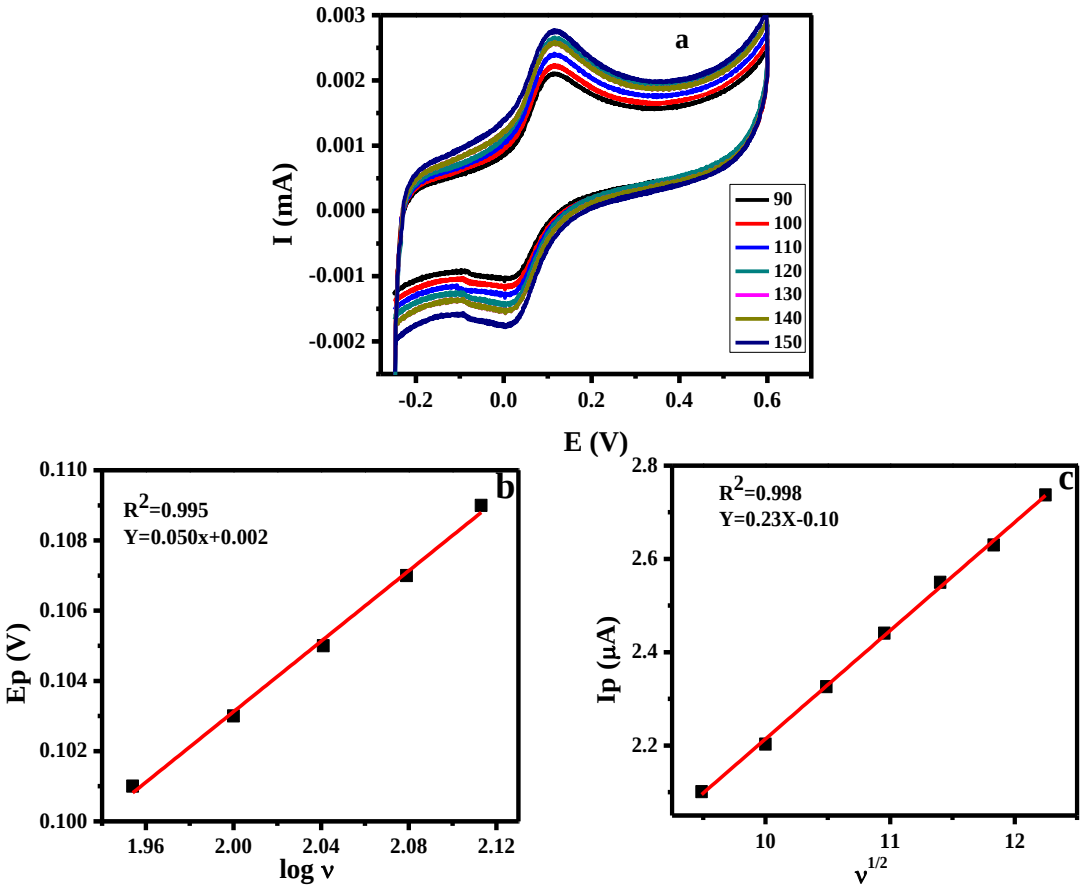

Figure 4.9: ***(a)*** *Cyclic voltammograms of oxidation of DA (1μM) at various scan rates (90 to 150 mV* s^{-1}*) at BCPE* ***(b)*** *plot of Ep Vs log ν and* ***(c)*** *plot of Ip Vs* $ν^{1/2}$

Single step potential chronoamperometry was employed to investigate the electrochemical process at the bare and modified electrodes. Figure 4.10 & 4.11a show the current–time curves of CQDs/CPE and BCPE in 0.1 M PBS with and without DA by applying a potential of 1.2 V. Rate constant was calculated from the plot I_C/I_L Vs $t^{1/2}$ obtained from the equation

$$I_C/I_L=\pi^{1/2}(kCt)^{1/2}$$

where I_C is catalytic current and I_L is limiting current, k is rate constant, C is concentration of the analyte in mol dm^{-3} and t is time and was found to be 2.796 x 10^8 and 2.408 x 10^7 cm^3 mol^{-1} s^{-1} for CQDs/CPE and BCPE respectively (Figure 4.10b & 4.11b).

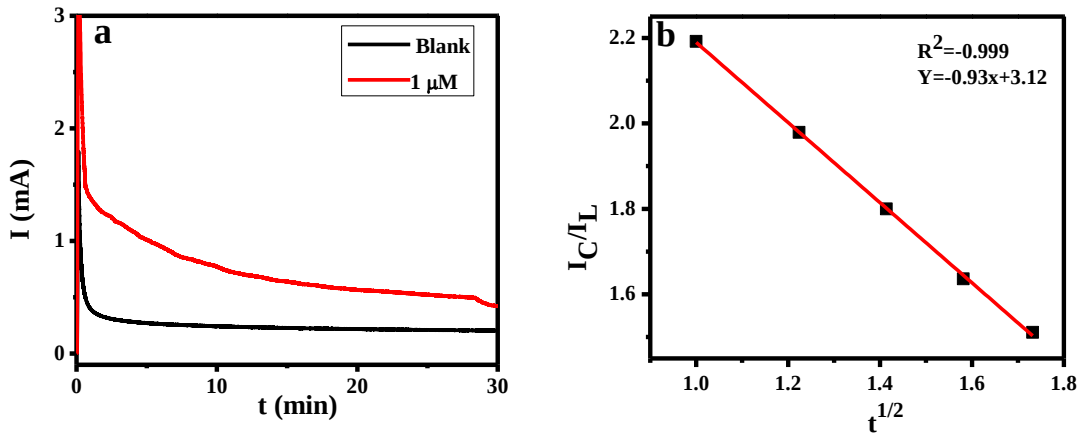

Figure 4.10: ***(a)*** *Current-time transients of CQDs/CPE in absence and presence of 1μM of DA in 0.1M PBS and* ***(b)*** *dependence of I_C/I_L Vs $t^{½}$*

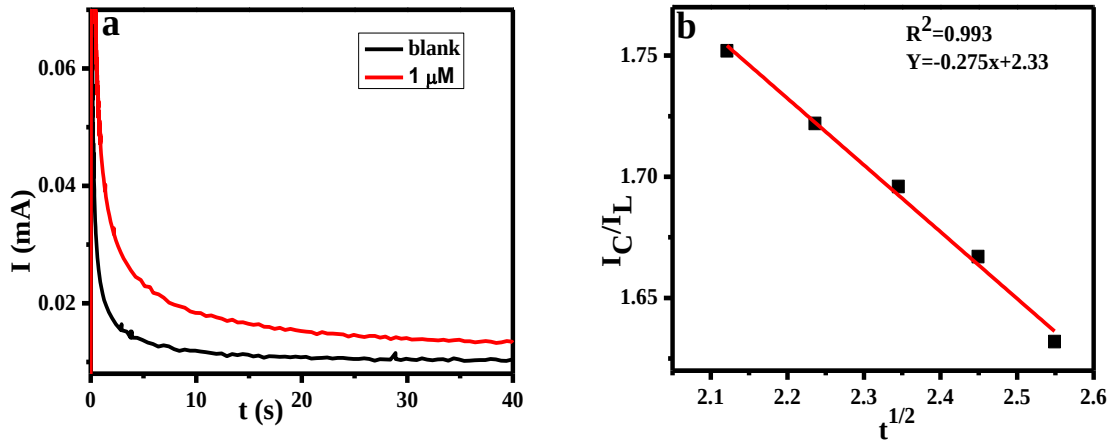

Figure 4.11: ***(a)*** *Current-time transients of BCPE in absence and presence of 1μM of DA in 0.1M PBS and* ***(b)*** *dependence of I_C/I_L Vs $t^{1/2}$*

4.9 Effect of solution pH on the oxidation behaviour of DA

pH studies revealed that the redox reaction of DA on the surface of CQDs/CPE was largely dependent on pH of the solution. The effect of pH on the electrode signal and oxidation potential of 1 μM DA in solution was investigated using CV. As shown in Figure 4.12a, with increase in pH, the peak potential (Epa) of DA became more negative on CQDs/CPE. The plot of Epa versus pH was linear with a slope of 63 mV/pH and the equation of best fit being: Epa = 0.063 pH+ 0.54 (R^2 = 0.995). The involvement of equal number of protons and electrons in the electrochemical process could be inferred from this result. Moreover, the plot of Epa Vs pH graph clearly indicated that there is a

catalytic peak shift to a more negative potential with increasing pH. From Figure 4.12b, a gradual increase in the peak current of DA with the increase of pH from 5.4 to 7.4 was observed with a maximum value at pH 7.4, which drastically decreased with further increase in pH.

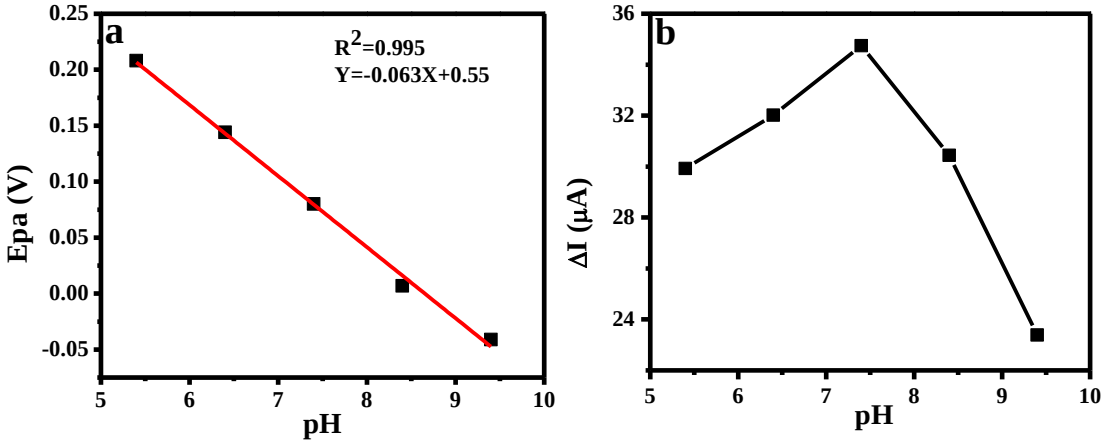

Figure 4.12: ***(a)*** *The effect of pH on the anodic peak potential of 1μM DA and* ***(b)*** *the effect of pH on the peak current of 1μM M DA*

4.10 Analytical performance characteristics

Chronoamperometric experiments were used to evaluate the analytical performance of the modified electrode. Chronoamperometric responses for the increasing concentrations of DA added at regular intervals along the ranges of concentration from 0.01 to 500 μM in 0.1 M PBS at 1.2 V was displayed in Figure 4.13a.The corresponding calibration graph of current Vs DA concentration portrayed linearity in the lower concentration region (0.01 to 1 μM) with R^2=0.999 as well as in the higher concentration range (5 to 500 μM) with R^2=0.999 (Figure 4.13b). The detection limit for DA was determined from the calibration graph to be 0.004 μM based on thrice the standard deviation of blank. The analytical performance of CQDs/CPE was compared with the reported electrodes and it is depicted in Table 4.1.

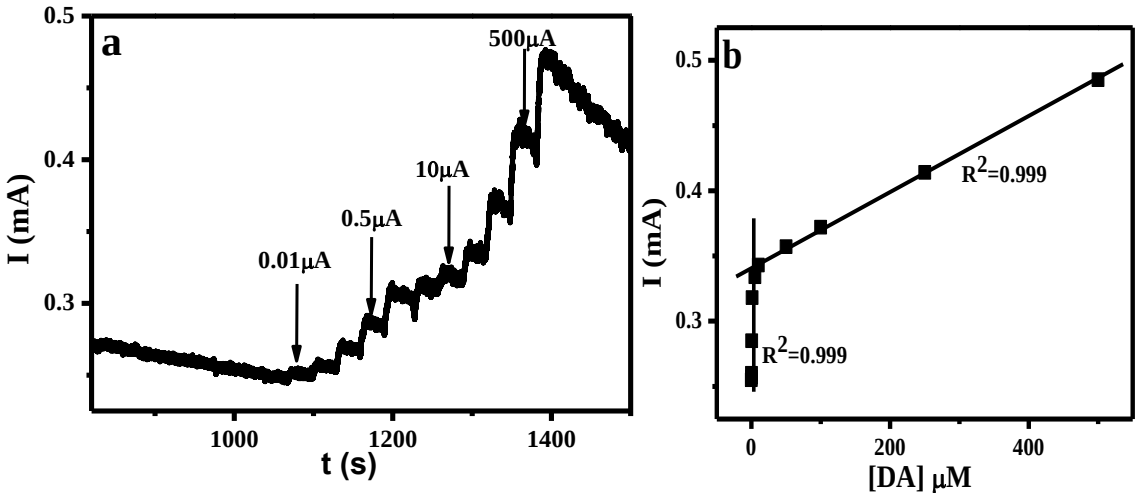

Figure 4.13: ***(a)*** *Chronoamperometric determination of DA with different concentration with a time interval of 30 seconds and* ***(b)*** *plot of concentration of DA Vs Current*

Table 4.1: *Comparison of CQDs/CPE with reported methods*

Electrode	Detection limit (μM)	Linear range (μM)	Method	Reference
Multi-walled carbon nanotube/poly(glycine) modified carbon paste electrode	0.012	0.5 to 40	DPV	47
Fe-Ag CTAB Nanoparticles Carbon Paste Electrode	0.01	1000 to 6230	DPV	48
Graphene–chitosan nanocomposite modified carbon paste electrode	0.098	100 to 0.2	DPV	49
DNA-doped poly(3,4-ethylenedioxythiophene)/carbon paste electrode	0.074	0.25 to 66	CA	50
Alizarin Modified Carbon Paste Electrode	0.237	50 to 500	CV	51
CQDs/CPE	0.004	0.01 to 1 5 to 500	CA	This work

4.11 Analytical performance of CQDs/CPE towards DA in presence of AA and UA as interferents

The CQDs/CPE was introduced for the electrochemical analysis of ternary system consisting 1 μM DA, 1 mM AA and 0.1 mM UA in 0.1M PBS of pH 7.4 with a scan rate of 50 mV s^{-1} (Figure 4.14 (i)). On the surface of BCPE (curve a) all the three analytes exhibited an overlapped voltammogram at a potential of 0.125 V. This was further converted to three well separated oxidation peaks on CQDs/CPE (curve b). On CQDs/CPE AA, DA and UA undergo oxidation at -0.112 V, 0.106 V and 0.180 V respectively which was further confirmed by DPV (inset). The peak to peak separation for DA-AA and UA-DA were 0.218 V and 0.08 V respectively, which were large enough to identify them simultaneously. Interference studies using DPV reveal that the increase in concentration of DA was not interfering with the oxidation of other analytes (Figure 4.14(ii)). Furthermore, even at higher concentration of AA and UA oxidation peak of DA did not alter. This was strong evidence to the capability of the fabricated electrode towards the electrochemical analysis of DA in presence of AA and UA.

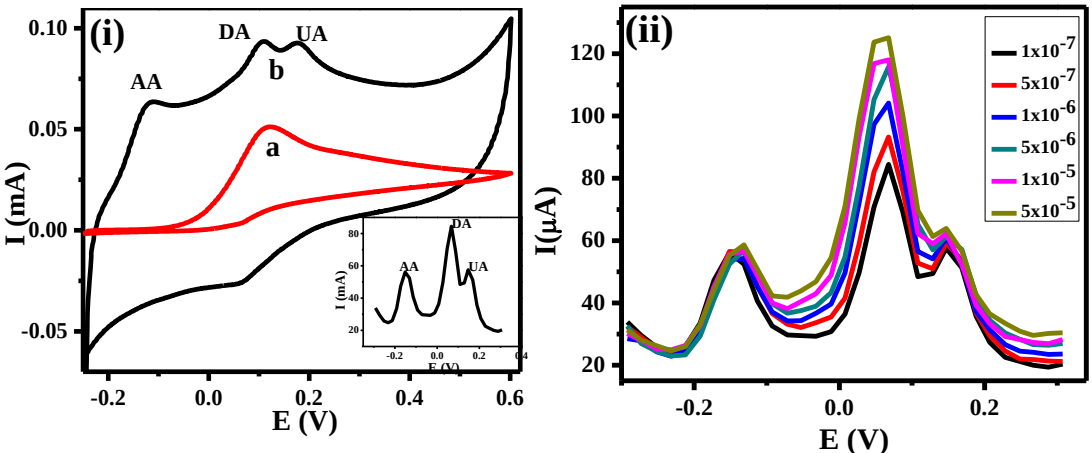

Figure 4.14: ***(a)*** *Cyclic voltammograms of 1 mM AA, 1.0 μM DA and 0.1 mM UA at BCPE (curve a) and on CQDs/CPE (curve b) DPV of same analytes on CQDs/CPE (inset).* ***(b)*** *DPVs of 1 mM AA and UA in the presence of different concentration of DA (from 0.1μM to 500 μM) at CQDs/CPE in pH 7.4 PBS.*

4.12 Mechanism

The prepared CQDs/CPE poses a negatively charged surface due to the hydroxyl groups present on the carbon quantum dots. Hence the positively charged dopamine will interact with the negative layer on the electrode surface (Scheme 4.1). This electrostatic interaction will be the driving force for the rapid oxidation and reduction processes of dopamine in 0.1 M PBS of pH of 7.4.

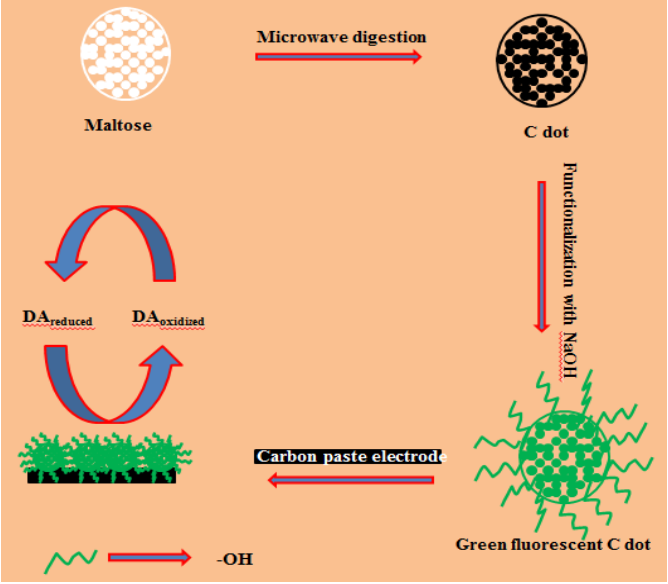

Scheme 4.1: *Preparation of CQDs/CPE and its sensing mechanism towards DA*

4.13 Reproducibility and Stability of CQDs/CPE

The relative standard deviation of 5 successive measurements for DA level of 1 μM was 2.0 %. When not in use, the CQDs/CPE was stored in air at room temperature. After one week of storage at room temperature, 95 % of the initial response was observed, indicating the stability and reproducibility.

4.14 Application of CQDs/CPE towards real sample analysis

The applicability of CQDs/CPE was tested by introducing it for the detection of DA in blood serum sample, which revealed acceptable results (Table 4.2). Serum samples were obtained from Amrita Institute of Medical Science and Research centre, Cochin, Kerala, India. 5 mL of blood sample was centrifuged (1000 rpm for 20 minutes)

to remove plasma. Appropriate aliquot (200 μL) of clear serum samples was used for the recovery studies of DA. Recovery studies were performed by spiking known amounts of standard solutions of DA to the diluted (100 times) serum samples followed by the analysis using the modified electrode under optimized analytical conditions. The appreciable recovery and R.S.D. suggested that the proposed methods could be efficiently used for the determination of DA in serum with recovery in the range 99.8–101.1 %.

Table 4.2: *Application of CQDs/CPE into real sample analysis*

Sample	Added (mg ml^{-1})	Found (mg ml^{-1})	Recovery (%)
1	10	9.98 ± 0.21	99.8 ± 2.1
2	10	10.02 ± 0.11	100.2 ± 1.1
3	10	10.11 ± 0.03	101.1 ± 0.3

4.15 Application of CQDs towards the cell labelling

Biological studies were carried out in He La cell line model to evaluate cellular uptake and cytotoxicity, on incubation with the CQDs. The CQDs with no functionalization were found to enter the cells, evident from the localization of green fluorescence inside the cells (Figure 4.15). Cell viability was found to be unaffected after incubation of the cells with CQDs for a 24 h time period. Detailed protocols have been given in below.

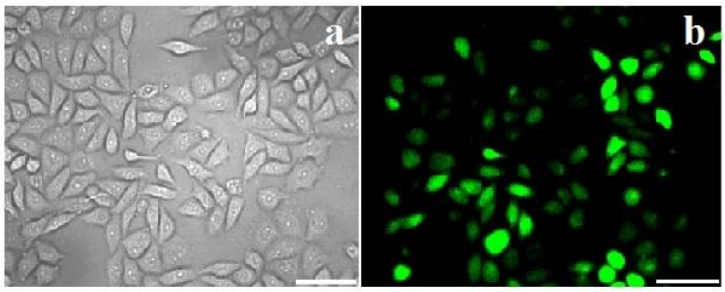

Figure 4.15: (a) *Transmitted light image and* ***(b)*** *fluorescent image of HeLa cell after incubation with green CQDs for 24 h*

4.15.1 Cell line maintenance

HeLa cell lines (cervical cancer cell lines) were obtained from Prof S. Murty Srinivasula of Indian Institute for Science Education and Research (IISER), Thiruvananthapuram, India. For maintenance of cell lines, Dulbeccos Modified Eagle's Medium (DMEM) *(Sigma)* containing 10 % fetal bovine serum (FBS) *(Gibco)*, antibiotics (100 U/ml Penicillin and 100 µg/ml streptomycin) and amphotericin (0.25 µg/ml) *(HiMedia)* was employed. The cells were maintained in CO_2 incubators at 37 ^oC with 5 % CO_2 in air and 99 % humidity. Passaging of cells when confluent was carried out using 0.25 % trypsin and 0.02 % EDTA *(HiMedia)* in phosphate buffered saline (PBS). Experiments were performed after 36 h of seeding the cells at appropriate density in suitable well plates.

4.15.2 MTT assay

Cell viability after incubating the cells with different concentrations of CQDs was determined by methylthiazolyltetrazolium (MTT) assay. It is a colorimetric assay based on the ability of live, but not dead cells to reduce MTT (yellow) to a purple for mazan product. The cells were spread in 96-well plates at a density of 10^4 cells/well. After 36 h of seeding, they were incubated with the test substances for 24 h. Subsequently, the cells were exposed to MTT at a concentration of 50 µg/well for 2.5 to 3 hrs at 37 ^oC in CO_2 incubator. The working solution of MTT was prepared in Hanks balanced salt solution (HBSS). After viewing for mazan crystals under the microscope, the crystals were solubilized by treating the cells with DMSO: isopropanol at a ratio of 1:1 for 20 min at 37 ^oC. Plate was read at an absorbance of 570 nm. The relative cell viability in percent was calculated as: Absorbance of treated /Absorbance of control x 100. Control samples used were cells without the test substances. Cell viability of control cells were kept as 100 %.

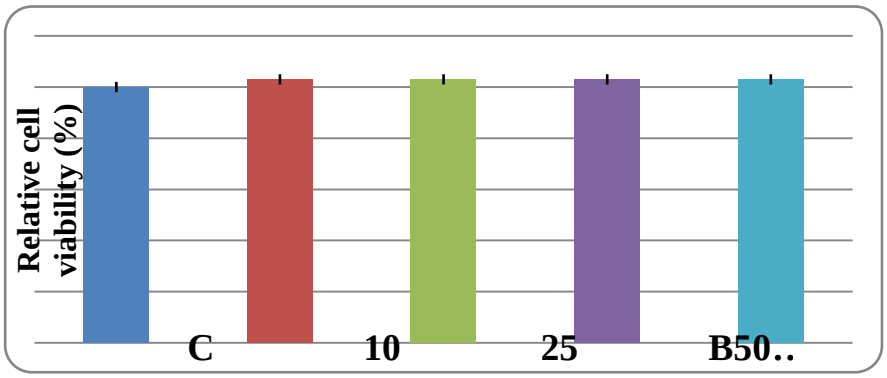

4.15.3 Cellular uptake studies of CQDs by fluorescence imaging

Cellular uptake studies were executed by fluorescence imaging of adherent cells based on the intrinsic fluorescent property of CQDs. The cells were seeded at a density of 10^4 cells/ well of 96 well black plates *(BD Biosciences, USA)* for the purpose. After 36 h of seeding, the cells were incubated with CQDs in HBSS for 1 h. Subsequently, the cells were washed thrice with HBSS and subjected to imaging. Images of the cells were collected by high-content spinning disk facility *(BD Pathway 855; BD Biosciences)* using *AttoVision 1.5.3 software.* Filters used were A488/10 nm excitation filter and 515 nm LP emission filter.

4.16 Experimental

4.16.1 Reagents and Chemicals

Maltose was purchased from Merck, Mumbai, India. Dopamine hydrochloride and UA were purchased from sigma-aldrich, Milwauke, WI, USA. AA was purchased from Riedel-de haen chemicals. DA stock solution was prepared in 0.1 M perchloric acid; whereas UA and AA in double distilled water. Afore mentioned chemicals were of analytical reagent grade and were used without any further purification. Standard method was employed in the preparation of phosphate buffer solution (PBS). The water used was double distilled. All the experiments were performed at room temperature.

4.16.2 Apparatus

Maltose was digested with a Panasonic Model NN-GT231M microwave oven. The size and morphology was studied by a high-resolution transmission electron microscopy (HRTEM) on a FEI, TECNAI 30G2 S-TWIN microscope with an accelerating voltage of 300 kV. XPS studies were carried out by x-ray photoelectron spectroscopy (XPS) (model ESCALAB220IXL) equipped with an Axis Ultra, Kratos (1486.7 eV) monochromatic source for excitation. XPS spectra over a binding energy (BE) range of 0–1200 eV were obtained using analyzer pass energy of 117.4 eV. UV-Visible spectra were recorded with a Shimadzu computer controlled double beam UV-Vis spectrophotometer UV-2401PC (Shimadzu, Kyoto, Japan), The photoluminescence (PL) spectrum of the C-dot was recorded on a Spex-Fluorolog FL22 spectrofuorimeter equipped with a double grating 0.22 m Spex 1680 monochromator and a 450 W Xe lamp as the excitation source. The IR spectra were recorded as KBr pellets on a Perkin-Elmer Spectrum One FT-IR spectrometer operating between 4500 and 400 cm^{-1}. Raman spectra were recorded with a confocal Raman microscope WITec alpha 300R (WITec GmbH, Ulm, Germany). A laser beam with 633 nm from air cooled argon was used for excitation. The Electrochemical measurements were performed using a three-electrode cell (20 ml) fitted with a CQDs/CPE or CPE (3 mm in diameter) as working electrode, Pt wire as auxiliary electrode, and saturated calomel electrode (SCE) as reference electrode using a VSP-potentiostat/galvanostat (Biologic Science Instruments).

4.17 Conclusions

A green luminescent CQDs of 2 nm diameter was prepared from maltose. Electrochemical studies revealed that the CQDs show high electro catalytic activity, high conductivity and provide large surface area. CQDs/CPE, a new type of electrochemical sensor could detect nanomolar levels of DA. It is to be noted

that the CQDs/CPE could be used for the simultaneous analysis of DA, UA and AA. The developed CQDs/CPE was successfully applied to real sample analysis. Being non cytotoxic, the fluorescence property of the CQDs is useful for cell imaging application. These CQDs enter into cell without any further functionalization and fluorescence property of the particle could be used to track their position in cell using conventional fluorescence microscope. The fabricated CQDs/CPE and its application will unambiguously lead to more research in the field of biosensors.

4.18 References

1) Xu, X. Y.; Ray, R.;Gu, Y. L.; Ploehn, H. J.; Gearheart, L.; Raker, K.; Scrivens, W. A. Electrophoretic Analysis and Purification of Fluorescent Single-Walled Carbonnanotube Fragments. *J. Am. Chem. Soc.* **2004,** *126*, 12736-.

2) Lu, J.; Yang, J. X.; Wang, J.; Lim, A.; Wang, S.; Loh, K. P. One-pot Synthesis of Fluorescent Carbon Nanoribbons, Nanoparticles, and Graphene by the Exfoliation of Graphite in Ionic Liquids. *ACS Nano* **2009**, *3*, 2367.

3) Zhao, Q. L.; Zhang, Z. L.; Huang, B. H.; Peng, J.; Zhang, M.; Pang, D. W. Facile Preparation of Low Cytotoxicity Fluorescent Carbon Nanocrystals by Electrooxidation of Graphite. *Chem. Commun.* **2008,** *41*, 5116.

4) Liu, H. P.; Ye, T.; Mao, C. D. Fluorescent Carbon Nanoparticles Derived from Candle Soot. *Angew. Chem. Int. Ed.* **2007**, *46*, 6473.

5) Ray, S. C.; Saha, A.; Jana, N. R.; Sarkar, R. Fluorescent Carbon Nanoparticles: Synthesis, Characterization, and Bioimaging Application. *J. Phys. Chem. C* **2009**, *113*, 18546.

6) Bourlinos, A. B. Stassinopoulos, A. Anglos, D. Zboril, R. Karakassides, M.Giannelis, E. P. Surface Functionalized Carbogenic Quantum Dots. *Small* **2008**, *4*, 455.

7) Tian, L.; Ghosh, D.; Chen, W.; Pradhan, S.; Chang, X.; Chen, S. Nanosized Carbon Particles from Natural Gas Soot. *Chem. Mater.* **2009**, *21*, 2803.

8) Lu, J.; Yeo, P. S. E.; Gan, C. K.; Wu, P.; Loh, K. P. Transforming C_{60} Molecules Intographene Quantum Dots. *Nat. Nanotechnol.* **2011**, *6*, 247.

9) Bourlinos, A. B.; Stassinopoulos, A.; Anglos, D.; Zboril, R.; Georgakilas, V.; Giannelis, E. P. Photoluminescent Carbogenic Dots. *Chem. Mater.* **2008**, *20*, 4539.

10) Liu, R. L.; Wu, D. Q.; Liu, S. H.; Koynov, K.; Knoll, W.; Li, Q. An Aqueous Route to Multicolour Photoluminescent Carbon Dots Using Silica Spheres as Carriers. *Angew. Chem. Int. Ed.* **2009**, *48,* 4598.

11) Zong, J.; Zhu, Y. H.; Yang, X. L.; Shen, J. H.; Li, C. Z. Synthesis of Photoluminescentcarbogenic Dots Using Mesoporous Silica Spheres as Nanoreactors. *Chem. Commun.* **2011**, *47*, 764.

12) Li, H. T.; He, X. D.; Liu, Y.; Yu, H.; Kang, Z. H.; Lee, S. T. Synthesis of fluorescent Carbon Nanoparticles Directly from Active Carbon via a One-Step Ultrasonic Treatment. *Mater. Res. Bull.* **2011**, *46,* 147.

13) Wang, X. H.; Qu, K. G.; Xu, B. L.; Ren, J. S.; Qu, X. G. Microwave Assisted One-Step Green Synthesis of Cell-Permeable Multicolour Photoluminescent Carbon Dots Without Surface Passivation Reagents. *J. Mater. Chem.* **2011**, *21*, 2445.

14) Hu, S. L.; Bai, P. K.; Cao, S. R.; Sun, J. Preparation of Fluorescent Carbon Nanoparticles by Pulsed Laser. *Chem. J. Chin. Univ.* **2009**, *30*, 1497.

15) Hu, S. L.; Niu, K. Y.; Sun, J.; Yang, J.; Zhao, N. Q.; Du, X. W. One-Step Synthesis ff Fluorescent Carbon Nanoparticles by Laser Irradiation. *J. Mater. Chem.* **2009**, *19,* 484.

16) Zhou, J. G.; Booker, C.; Li, R. Y.; Zhou, X. T.; Sham, T.-K.; Sun, X. L.; Ding, Z. F. An Electrochemical Avenue to Blue Luminescent Nanocrystals from Multiwalled Carbon Nanotubes (MWCNTS). *J. Am. Chem. Soc.* **2007**, *129*, 744.

17) Ming, H.; Ma, Z.; Liu, Y.; Pan, K. M.; Yu, H.; Wang, F.; Kang, Z. H. Large Scale Electrochemical Synthesis of High Quality Carbon Nanodots and Their Photocatalytic Property. *Dalton Trans.* **2012**, *41,* 9526.

18) Hsu, P.-C.; Chen, P.-C.; Ou, C.-M.; Chang, H.-Y.; Chang, H.-T. Extremely High Inhibition Activity of Photoluminescent Carbon Nanodots toward Cancer Cells. *J. Mater. Chem. B* **2013**, 1, 1774.

19) Qiao, Z.-A.; Wang, Y. F.; Gao, Y.; Li, H. W.; Dai, T. Y.; Liu, Y. L.; Huo, Q. S. Commercially Activated Carbon as the Source for Producing Multicolour Photoluminescent Carbon Dots by Chemical Oxidation. *Chem. Commun.* **2010**, *46*, 8812.

20) Bechet, D.; Couleaud, P.; Frochot, C.; Viriot, M.-L.; Guillemin, F.; Barberi-Heyob, M. Nanoparticles as vehicles for delivery of photodynamic therapy agents. *Trends Biotechnol.* **2008**, *26*, 612.

21) Yang, K.; Gong, H.; Shi, X. Z.; Wan, J. M.; Zhang, Y. J.; Liu, Z. In Vivo Biodistribution and Toxicology of Functionalized Nano-Graphene Oxide in Mice after Oral and Intraperitoneal Administration. *Biomaterials* **2013**, *34*, 2787.

22) Li, H. T.; Liu, R. H.; Lian, S. Y.; Liu, Y.; Huang, H.; Kang, Z. H. Near-Infrared Light Controlled Photocatalytic Activity of Carbon Quantum Dots for Highly Selective Oxidation Reaction. *Nanoscale* **2013**, *5*, 3289.

23) Liu, R. H.; Huang, H.; Li, H. T.; Liu, Y.; Zhong, J.; Li, Y. Y.; Zhang, S.; Kang, Z. H. Metal Nanoparticle/Carbon Quantum Dot Composite as a Photocatalyst for High-Efficiency Cyclohexane Oxidation. *ACS Catal.* **2014**, *4*, 328.

24) Morozan, A.; Jaouen, F. Metal Organic Frameworks for Electrochemical Applications. *Energy Environ. Sci.* **2012**, *5*, 9269.

25) Yang, S. B.; Feng, X. L.; Wang, X. C.; Mu¨llen, K. Graphene-Based Carbon Nitride Nanosheets as Efficient Metal-Free Electrocatalysts for Oxygen Reduction Reactions. *Angew. Chem., Int. Ed.* **2011,** *50*, 5339.

26) Posthuma-Trumpie, G. A. Wichers, J. H. Koets, M. Berendsen, L. B. J. M. van Amerongen, A. Amorphous Carbon Nanoparticles: A Versatile Label for Rapid Diagnostic (Immuno) Assays. *Anal. Bioanal. Chem.* **2012**, *402*, 593.

27) Gordon, J.; Michel, G. Analytical Sensitivity Limits for Lateral Flow Immunoassays. *Clin. Chem.* **2008**, *54*, 1250.

28) Yan, F. Y.; Zou, Y.; Wang, M.; Mu, X. L.; Yang, N.; Chen, L. Highly Photoluminescent Carbon Dots-Based Fluorescent Chemosensors for Sensitive and Selective Detection of Mercury Ions and Application of Imaging in Living Cells. *Sens. Actuators, B* **2014**, *192*, 488.

29) Barman, S.; Sadhukhan, M. Facile Bulk Production of Highly Blue Fluorescent Graphitic Carbon Nitride Quantum Dots and Their Application as Highly Selective and Sensitive Sensors for the Detection of Mercuric and Iodide Ions in Aqueous Media. *J. Mater. Chem.* **2012**, *22*, 21832.

30) Huang, H.; Lv, J.-J.; Zhou, D.-L.; Bao, N.; Xu, Y.; Wang, A.-J.; Feng, J.-J. One-Pot Green Synthesis of Nitrogen-Doped Carbon Nanoparticles as Fluorescent Probes for Mercury Ions. *RSC Adv.* **2013**, *3*, 21691.

31) Liu, J. M.; Lin, L. P.; Wang, X. X.; Lin, S. Q.; Cai, W. L.; Zhang, L. H.; Zheng, Z. Y. Highly Selective and Sensitive Detection of Cu^{2+} with Lysine Enhancing Bovine Serum Albumin Modified-Carbon Dots Fluorescent Probe. *Analyst* **2012**, 137, 2637.

32) Zhang, Y.-L.; Wang, L.; Zhang, H.-C.; Liu, Y.; Wang, H.-Y.; Kang, Z.-H.; Lee, S.-T. Graphitic Carbon Quantum Dots as a Fluorescent Sensing Platform for Highly Efficient Detection of Fe^{3+} Ions. *RSC Adv.* **2013**, *3*, 3733.

33) Wee, S. S.; Ng, Y. H.; Ng, S. M. Synthesis of Fluorescent Carbon Dots via Simple Acid Hydrolysis of Bovine Serum Albumin and Its Potential as Sensitive Sensing Probe for Lead (II) Ions. *Talanta* **2013**, *116*, 71.

34) Qian, Z. S.; Ma, J. J.; Shan, X. Y.; Feng, H.; Shao, L. X.; Chen, J. R. Highly Luminescent N-Doped Carbon Quantum Dots as an Effective Multifunctional Fluorescence Sensing Platform. *Chem. – Eur. J.* **2014**, *20,* 2254.

35) Jia, X. F.; Lia, J.; Wang, E. K. One-Pot Green Synthesis of Optically Ph-Sensitive Carbon Dots with Upconversion Luminescence. *Nanoscale* **2012**, *4*, 5572.

36) Li, Y.; Zhao, Y.; Cheng, H.; Hu, Y.; Shi, G.; Dai, L.; Qu, L. Nitrogen-Doped Graphene Quantum Dots with Oxygen-Rich Functional Groups. *J. Am. Chem. Soc.* **2012**, *134*, 15.

37) Xu, C.; Han, Q.; Zhao, Y.; Wang, L.; Li, Y.;Qu, L. Sulfur-Doped Graphitic Carbon Nitride Decorated with Graphene Quantum Dots for an Efficient Metal-Free Electro Catalyst. *J. Mater. Chem. A* **2015**, *3,* 1841.

38) Levesque, D. Rouillard, C. Nur77 and Retinoid X Receptors: Crucial Factors in Dopamine-Related Neuroadaptation. *Trends Neurosci.* **2007**, *30*, 22.

39) Hayashi, K.; Iwasaki, Y.; Kurita, R.; Sunagawa, K.; Niwa, O.; Tate, A. The Highly Sensitive Detection of Catecholamines Using a Microfluidic Device Integrated with an Enzyme-Modified Pre-Reactor for Interferent Elimination and an Interdigitated Array Electrode. *J. Electroanal. Chem.* **2005**, 579, 215.

40) Hong, C. J.; Liu, H. C.; Liu, T. Y.; Liao, D. L.; Tsai, S. J. Association Studies of the Adenosine A2a Receptor (1976T > C) Genetic Polymorphism in Parkinson's Disease and Schizophrenia. *J. Neural Transm.* **2005**, *112*, 1503.

41) Nohta, H.; Yukizawa, T.; Ohkura, Y.; Yoshimura, M.; Ishida, J.; Yamaguchi, M. Aromatic Glycinonitriles and Methylamines as Pre-Column Fluorescence Derivatization Reagents for Catecholamines. *Anal. Chim. Acta* **1997**, *344*, 233.

42) Wang, L.; Liu, Y.; Xie, H.; Fu, Z. Trivalent Copper Chelate-Luminol Chemiluminescence System for Highly Sensitive CE Detection of Dopamine in Biological Sample After Clean-Up using SPE. *Electrophoresis* **2012**, *33*, 1589.

43) Jin, W.; Jin, L. T.; Shi, G. Y.; Ye, J. N. Determination of Monoamine Transmitters and their Metabolites by Capillary Electrophoresis with Electrochemical Detection. *Anal. Chim. Acta* **1999**, *382*, 33.

44) Tong, C. L.; Zhu, Y.; Guo, D.; Xiang, G. H.; Ye, M. L. Determination of Dopamine and Epinephrine by Ion Chromatography with Fluorescence Detector. *Chin. J. Anal. Chem.* **2001**, 29, 1237.

45) Guo, Z.; Seol, M. L.; Kim, M. S.; Ahn, J. H.; Choi, Y. K.; Liu, J. H.; Huang, X. J. Sensitive and Selective Electrochemical Detection of Dopamine using an Electrode Modified with Carboxylated Carbonaceous Spheres. *Analyst* **2013**, *138*, 2683.

46) Tang, L.; Ji, R.; Cao, X.; Lin, J.; Jiang, H.; Li, X.; Teng, K. S.; Luk, C. M.; Zeng, S.; Hao, J.; Lau, S. P. Deep Ultraviolet Photoluminescence of Water-Soluble Self-Passivated Graphene Quantum Dots. *ACS Nano.* **2012**, *6*, 5102.

47) Thomas, T.; Mascarenhas, R. J.; Swamy, B. E.; Martis, P.; Mekhalif, Z.; Sherigara, B. S. Multi-walled Carbon Nanotube/Poly(Glycine) Modified Carbon Paste Electrode for the Determination of Dopamine in Biological Fluids and Pharmaceuticals. *Colloids Surf. B Biointerfaces* **2013,** *110*, 458.

48) Lavanya, M.; Reddy, Y. V. M.; Rao, V. P.; Madhavi, G. Simultaneous Determination of Dopamine in Presence of Ascorbic Acid with Fe-Ag CTAB Nanoparticles Carbon Paste Electrode. *Chem. Sci. Trans.* **2014**, *3*, 1404.

49) Liu, C.; Zhang, J.; Yifeng, E.; Yue, J.; Chen, L.; Li, D. One-Pot Synthesis of Graphene–Chitosan Nanocomposite Modified Carbon Paste Electrode for Selective Determination of Dopamine. *Electron. J. Biotechnol.* **2014**, *17*, 183.

50) Xu, G.; Wang, W.; Li, B.; Luo, Z.; Luo, X. A. Dopamine Sensor Based on a Carbon Paste Electrode Modified with DNA-Doped Poly (3, 4-Ethylenedioxythiophene). *Microchim. Acta* **2015**, *182*, 679.

51) Mahanthesha, K. R.; Swamy, B. E. K.; Pai, K. V.; Chandra, U.; Sherigara, B. S. Cyclic Voltammetric Investigations of Dopamine at Alizarin Modified Carbon Paste Electrode. *Int. J. Electrochem. Sci.* **2010**, *5*, 1962.

Chapter 5

Angiogenic Profiling of Synthesized Carbon Quantum Dots

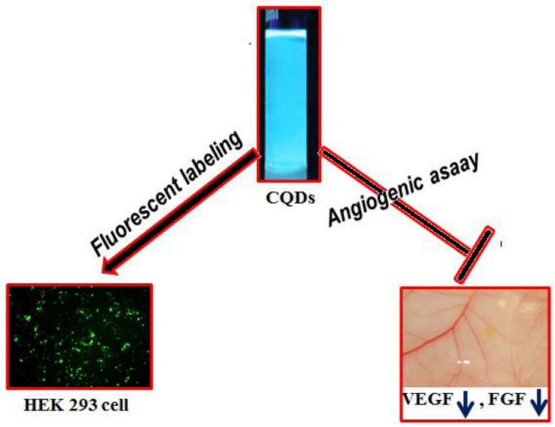

5.1 Abstract

A simple method was employed for the synthesis of green luminescent carbon quantum dots (CQDs) from styrene soot. The CQDs were characterized by TEM, UV-Visible absorption spectroscopy, PL spectroscopy, FTIR, Raman Spectroscopy and XPS. The prepared CQDs did not show cellular toxicity and could successfully be used for labelling cells. We also evaluated the effects of CQDs on the process of angiogenesis. Results of ChorioAllantoic Membrane assay (CAM) revealed the significant reduction in the density of branched vessels after the treatment with CQDs. Further application of CQDs significantly down regulated the expression levels of pro-angiogenic growth factors like VEGF and FGF. Expression of VEGFR2 and levels of hemoglobin were also significantly lower in CAMs treated with CQDs, indicating that the CQDs inhibit angiogenesis. Data presented here also show that CQDs can selectively target cancer cells and therefore holds potential in the field of cancer therapy.

5.2 Introduction

Angiogenesis is the process of development of new blood capillaries from the preexisting ones. It occurs either by one of the two main processes; (a) endothelial cell migration (sprouting) (b) splitting of vessels (intussusceptions).[1] Some physiological events comprising, embryo development, wound healing, ovulation and several pathological conditions including, cancer, diabetic retinopathy etc. relies on the process of angiogenesis.[2] VEGF and FGF are the major pro angiogenic factors, which gets up-regulated during pro angiogenic conditions. In the case of tumors, angiogenesis plays an important role that tumors cannot grow beyond 1-2 cubic millimeter without inducing angiogenesis and the nutrients and oxygen cannot diffuse that long distances. The tumor responds to a hypoxic environment by secreting pro-angiogenic factors, triggering angiogenesis. The new vessels formed due to angiogenesis, facilitate supply of oxygen and nutrients to the growing tumor thereby enhancing tumor survival and growth. So it has evolved as a therapeutic target in case of cancer by inhibiting angiogenesis. In this study we investigated the cytotoxicity and angiogenic activity of CQDs.

Quantum dots (QDs) with size less than 10 nm are emerging star in the field of nanoscience. Among various dots, CQDs received remarkable attention because of less toxicity, high water solubility, surface modification flexibility and unique photoluminescence property.[3, 4] Hence CQDs would be a better choice in the field of biomedical, biosensing, catalysis and solar cell applications.[5-8] Recently CQDs could be produced from bulk graphite materials, active carbon, pyrolyzed polymers, or carbohydrates through various methods. [9-12] Several approaches including arc discharge, laser ablation, electrochemical synthesis and combustion/thermal/hydrothermal/acidic oxidation have been proposed to produce fluorescent CQDs.[3, 13-18] Herein, we present a facile method for synthesizing photoluminescent carbon quantum dots by NaOH passivation of styrene soot. The proposed method avoided strong acids and reduced the

preparation steps. To the best of our knowledge, this is the first report demonstrating the anti-angiogenic properties of CQDs. The anti-angiogenic properties of CQDs combined with nontoxicity to noncancerous cells will give a new potential to CQDs.

5.3 Preparation of CQDs

Carbon soot was collected by burning styrene in a limited supply of air. Thus collected soot was stirred at 900 rpm for 25 minutes along with NaOH of pH 7.4. Solution was then sonicated and filtered through whatman filter paper.

5.4 XTT cell viability assay

HEK 293 and A549 cells were seeded in a 96 well plate with a cell density of 4000 cells/well. The plates were incubated overnight at 37 °C in a humidified incubator with 5 % CO_2 for the cells to attach. CQDs at different concentrations were applied to the cells in triplicate wells and incubated for 24 h followed by XTT assay. Briefly, XTT assay was done by adding 25 μL of working solution of XTT prepared in DMEM with 5 mM PMS to each wells. After 4 h of incubation, absorbance was read at 630 nm and 450 nm. Percentage viability was calculated by considering the viability of untreated control as 100 %.[19]

5.5 Cell labelling studies of CQDs

Cell labelling studies were executed by fluorescence imaging of adherent cells, based on the intrinsic fluorescent property of CQDs. HEK-293 cells were seeded at a density of 10^5 cells/ well of 96 well plates. After attachment the cells were incubated with CQDs in DMEM for 1 h. Subsequently, the cells were washed thrice with PBS and subjected to imaging under fluorescence microscope.

5.6 Chick chorioallantoic membrane (CAM) assay for angiogenesis

CAM assay was performed on fertilized chick eggs, which were incubated for 4 days at 37 ^oC and at a relative humidity of 80 %. During this period, the eggs were positioned with pointed end down and were spun several times. After incubation, the

eggs were opened on the air sac side, shell was carefully removed with forceps and the sample soaked in filter discs were applied on to the CAM. The cavity was covered with parafilm, and the eggs were incubated at 37 ^{o}C at a relative humidity of 80 % for 8 days. At the end of the incubation period, the CAMs were photographed and level of hemoglobin in the CAM was estimated using Drabkin's reagent as a measure of vessel density. For this the CAMs were homogenized in Drabkin's reagent, centrifuged and the absorbance of the clear supernatant was recorded at 546 nm. CAMs treated with filter discs soaked in PBS served as the vehicle control.[20, 21] The levels of hemoglobin in the CAMs were normalized to total protein content of CAMs.

5.7 Quantitative real-time PCR

Total RNA was extracted from Chick (*Gallus gallus*) chorioallantoic membrane with TRIzol reagent (Invitrogen) according to the manufacturer's protocol. cDNA was synthesized from 1 μg of RNA using high capacity cDNA Reverse Transcription kit (Applied Bio systems) and Quantitativereal time-PCR was performed in Light Cycler 480 machine. Actin served as the internal control. Nucleotide sequence of primer pairs used to determine the levels of chick VEGF, VEGFR2 and FGF mRNA were as follows:

ACTIN Forward primer 5'- GCT CTG ACT GAC CGC GTT A-3'

Reverse primer5'- ACG AGC GCA GCA ATA TCA T -3'

VEGF Forward primer 5'-GGA GTT GTC GAA GGC TGC T-3'

Reverse primer5'-TTG ATA ACT TCG TTG GGC TTC-3'

FGF Forward primer 5'-TTC TTC CTG CGC ATC AAC-3'

Reverse primer 5'-CGA TAG CTC GTCCAG-3'

VEGFR2 Forward primer 5'GGG GAAGAT GTA CTC GGT GA-3'

Reverse primer 5' CAT CC A TGT TCA AAC ATC ACA A-3'

5.8 Characterization of prepared CQDs

Dynamic light scattering (DLS) was carried out to analyze the aggregation tendency of prepared CQDs in solution. The DLS data (Figure 5.1a) revealed that CQDs possessed a particle size of 3 nm and it was also observed that CQDs do not exist in big aggregated form in the aqueous solution. The particle size of CQDs was further confirmed to be 3 nm from TEM analysis (Figure 5.1b).

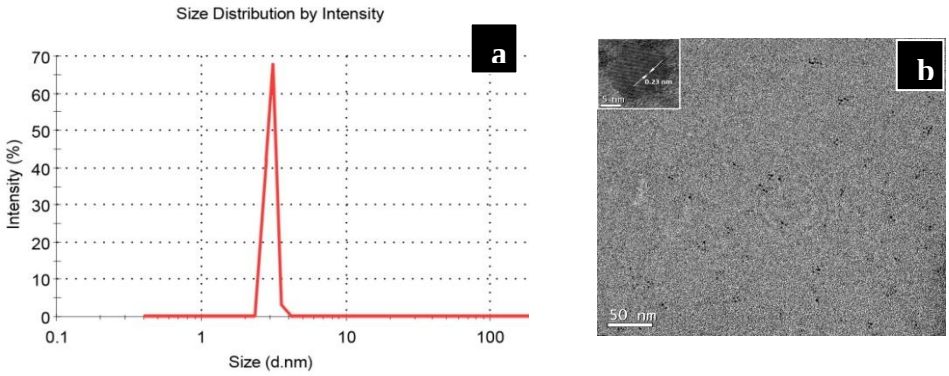

Figure 5.1: ***(a)*** *DLS* ***(b)*** *TEM and* ***(inset)*** *HRTEM images of CQDs*

UV-Visible spectra showed two characteristic peaks; one at 290 nm due to n -π* transition of C=O and another at 210 nm due to π-π* transition of C=C (Figure 5.2a). From PL spectra (Figure 5.2b) an emission peak at 480 nm was observed under 360 nm excitation. Moreover no bathochromic shift was observed under different excitation conditions (from 360 to 490 nm). FTIR analysis was carried out for identifying the functional groups present on CQDs. A feeble absorption at 3452 cm^{-1} was due to O-H stretching vibration of hydroxyl group. Two bands at 2920 and 2880 cm^{-1} were because of the stretching vibration of C-H in the CH_2 group. A peak corresponding to C=O group at 1687 cm^{-1} and another peak corresponding to aromatic C=C (ring stretching) at 1628 cm^{-1} was depicted clearly by Figure 5.3a. A peak at 1032 cm^{-1} was also observed due to C-O stretching of alcoholic OH group. From Raman spectra (Figure 5.3b) two major peaks at 1578 cm^{-1} and 1331 cm^{-1} corresponding to G-band and D-band was observed.

This confirmed the formation of sp^2 nature of carbon quantum dots. Along with these two peaks an additional peak at 2654 cm^{-1} due to 2D band was also observed.

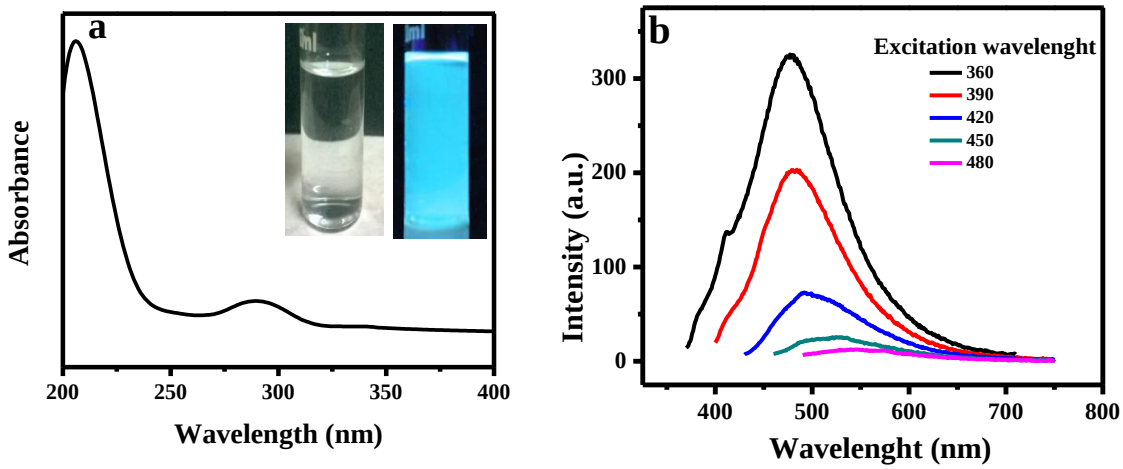

Figure 5.2: ***(a)*** *UV-Vis absorption spectra and inset shows appearance of CQDs in absence and presence of UV light and* ***(b)*** *PL spectra of the CQDs at different excitation wavelength*

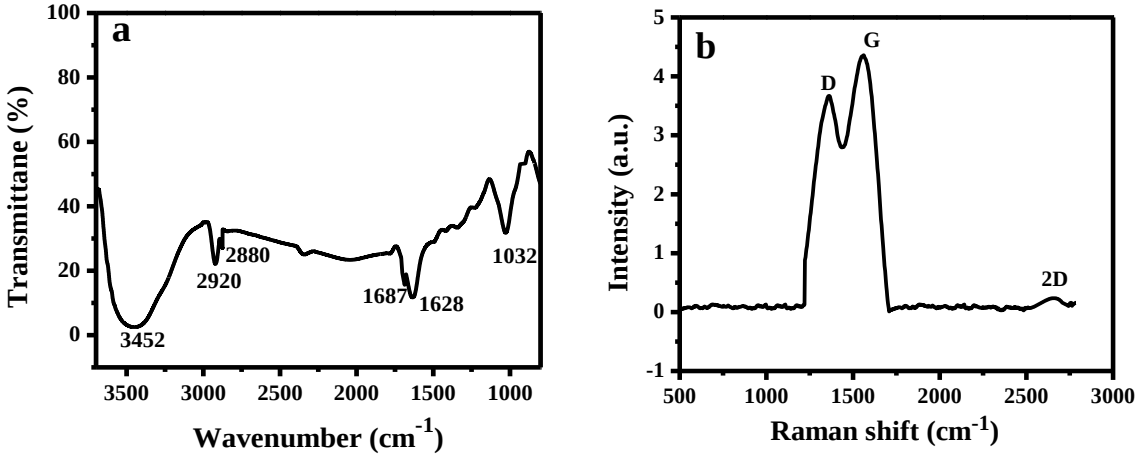

Figure 5.3: ***(a)*** *FTIR and* ***(b)*** *Raman spectra of the CQDs*

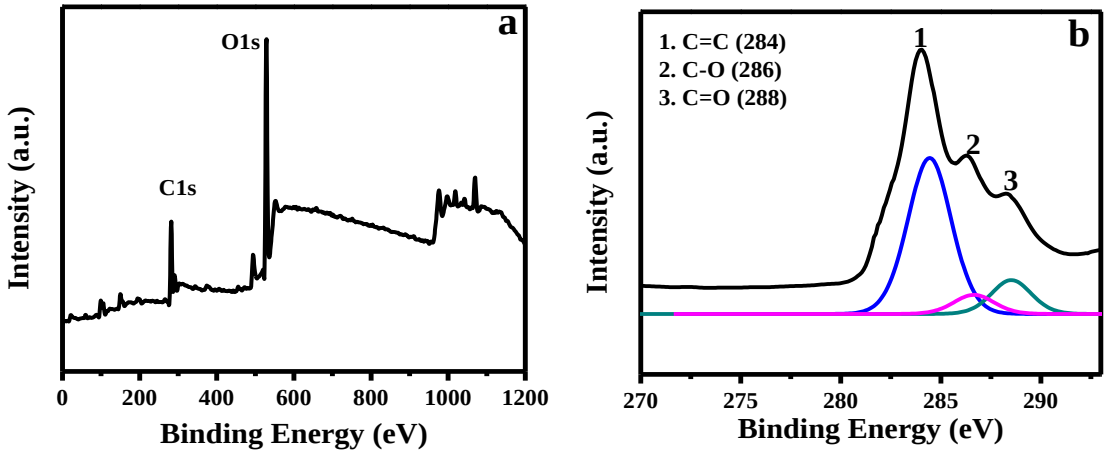

Figure 5.4: ***(a)*** *XPS wide spectra and* ***(b)*** *C 1s spectra of CQDs*

XPS measurement (Figure 5.4a) showed that the CQDs contained mainly carbon (55 wt %) and oxygen (44 wt %). The C 1s spectra (Figure 5.4b) revealed the presence of different types of carbon atoms such as C=C, C-O and C=O at 284, 286 and 288 eV respectively.

5.9 Cell viability assay

CQDs were tested for their cytotoxic effects in cancer and non-cancer cell lines. Results from XTT assay showed that CQDs at concentrations (250,125, 65, 31.25, 15.62 μg/ml) did not reduce the viability of HEK293 (non cancer cell line) beyond 20 % (Figure 5.5a). However, in case of lung cancer cell line, 15.625 μg/ml was sufficient for reducing cell viability beyond 50 % (Figure 5.5b). Further, viability of cancerous cells decreased beyond 80 % with 250 μg/ml of CQDs (16 times higher than that required for non cancerous cells).

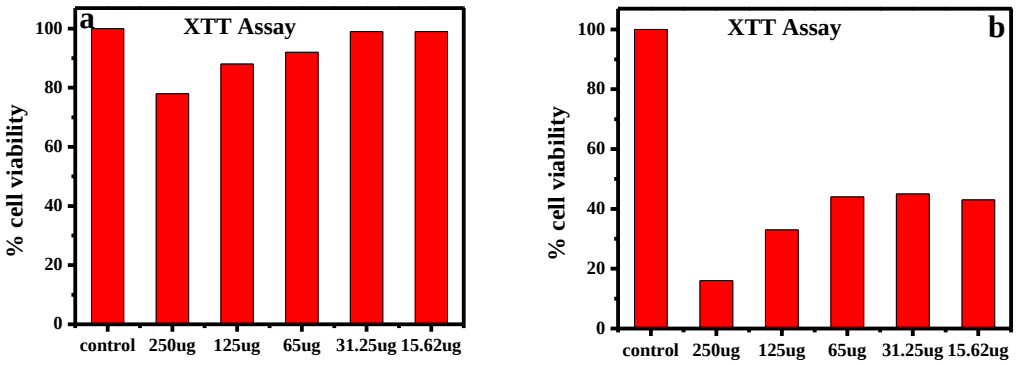

Figure 5.5: *Percentage cell viability assay performed with XTT reagent. CQDs with serially decreasing concentrations (250,125, 65, 31.25, 15.62 μg/ml) were tested on **(a)** normal (HEK 293) and **(b)** lung cancer cell line (A549)*

5.10 Cell labelling studies of CQDs by fluorescence imaging

Figure 5.6a & 5.6b showed the transmitted light image and fluorescent image of HEK-293 cells after incubation with green CQDs for 1 h. HEK-293 cells were seeded in 96 well plates to study the cell labelling activity of fluorescent CQDs. After 1 h incubation with dots, cells were washed with PBS and visualized the fluorescence inside

the cells under fluorescence microscope. Cell viability was found to be unaffected after incubation of cells with CQDs.

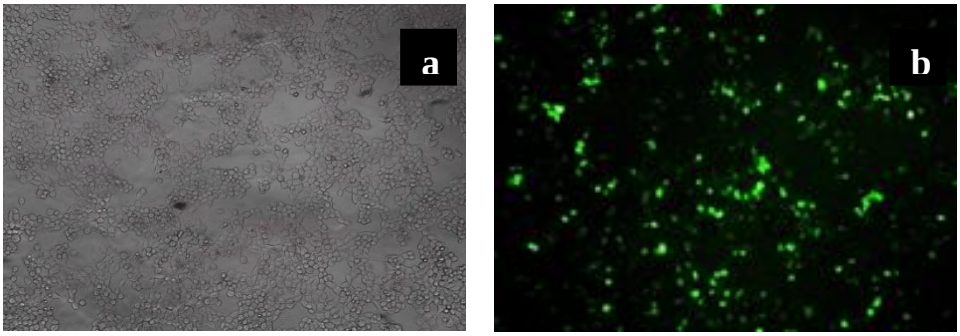

Figure 5.6: ***(a)*** *Transmitted light image and* ***(b)*** *fluorescent image of HEK 293 cell lines after incubation with green CQDs for 1 h*

5.11 Anti-angiogenic effects of CQDs

Fertilized chick embryo was selected as the in vivo model system to study angiogenic effect of CQDs. 100 μg of CQDs solution was applied on to the CAM of 4-day-old chick embryo. The vascular densities in the CAMs were photographed on the 12th day followed by estimation of hemoglobin as a measure of vascular density and angiogenesis. The results were as presented in Figure 5.7c.

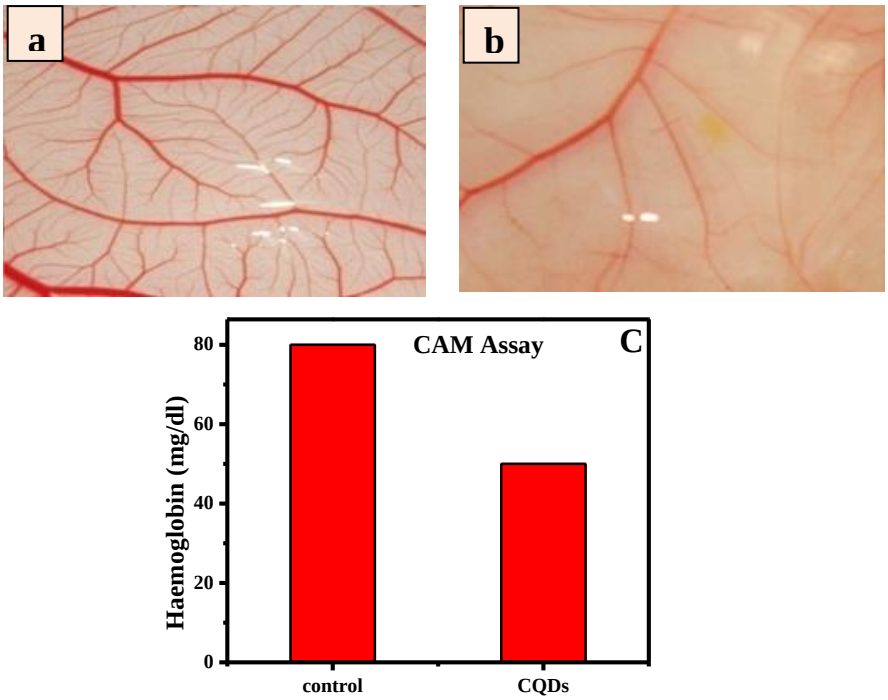

Figure 5.7: *Angiogenic activity of CQDs. Photographs of chick embryo CAMs treated with* ***(a)*** *PBS and* ***(b)*** *CQDs* ***(c)*** *Graphical representation of Hemoglobin levels in control and treated CAMs*

Photo micrographic analysis revealed that, compared to the control (PBS) (Figure 5.7a), CAMs treated with CQDs exhibited significantly lower blood vessel density (Figure 5.7b). Hemoglobin levels also suggested the anti-angiogenic nature of the CQDs.

5.12 Relative expression level of angiogenic markers

Further, to confirm the anti-angiogenic potential of CQDs, the expression levels of major angiogenic cytokines (VEGF (Figure 5.8a) and FGF (Figure 5.8b)) and markers (VEGFR2 (Figure 5.8c)) were studied. The results suggested that the expression levels of VEGF, FGF and VEGFR2 were significantly lower in CAMs treated with CQDs when compared to the untreated controls.

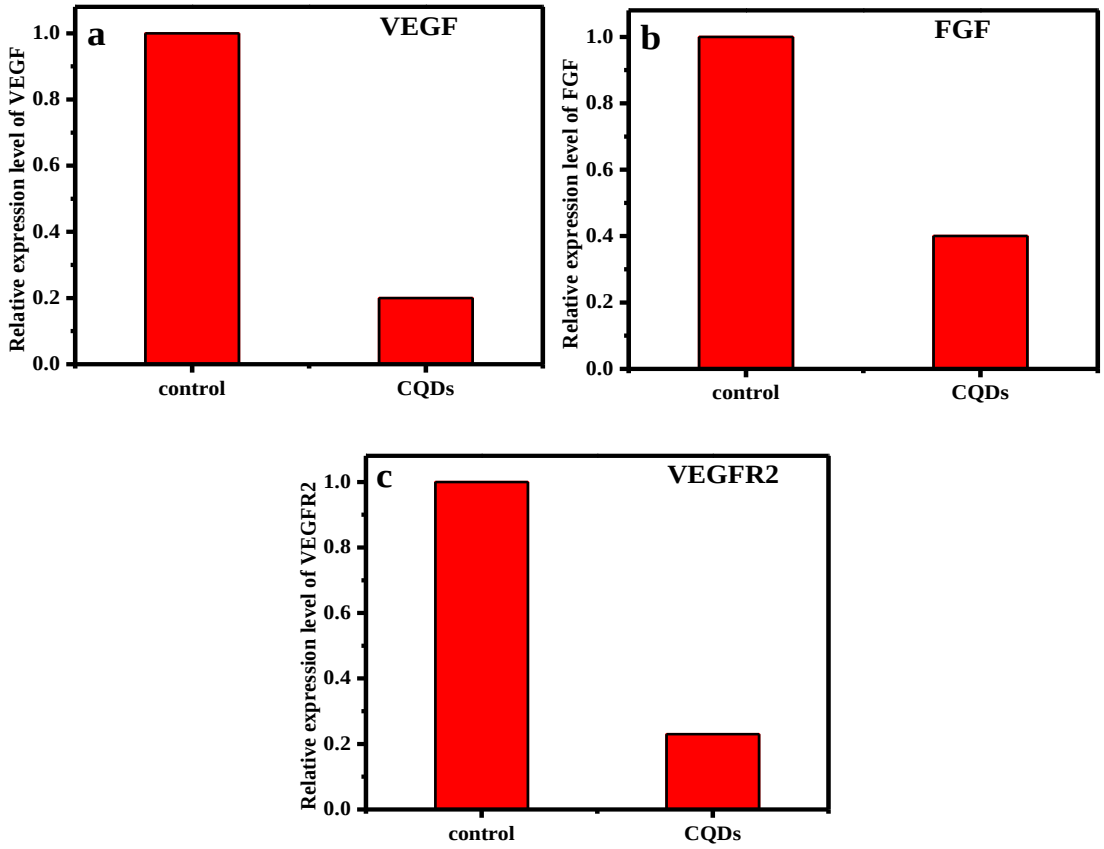

Figure 5.8: *Expression levels of angiogenic markers. Total RNA was isolated and the expression levels VEGF* ***(b)*** *FGF and* ***(c)*** *VEGFR2 were analyzed by Real Time PCR. Relative expression levels of above genes were down regulated*

5.13 Experimental

5.13.1 Reagents and Chemicals

Styrene, Drabkins Reagent and XTT Reagent were purchased from sigma-aldrich, Milwauke, WI, USA, Dulbecco's Modified Eagles Medium (DMEM) was purchased from Himedia, TRizol was purchased from Invitrogen, PMS from SRL, Fast Start Essential Master Mix was purchased from Roche, and High Capacity CDNA Reverse Transcription kit was purchased from Applied Biosystems.

5.13.2 Apparatus

The size and morphology were studied through high-resolution transmission electron microscopy (HRTEM) on a FEI, TECNAI 30G2 S-TWIN microscope with an accelerating voltage of 300 kV. XPS experiments were performed on x-ray photoelectron spectroscopy (XPS) (model ESCALAB220IXL) equipped with an Axis Ultra, Kratos (1486.7 eV) monochromatic source for excitation. XPS spectra over a binding energy (BE) range of 0–1200 eV were obtained using analyzer pass energy of 117.4 eV. UV-Visible spectra were recorded with a Shimadzu computer controlled double beam UV-Vis spectrophotometer UV-2401PC (Shimadzu, Kyoto, Japan), The photoluminescence (PL) spectrum of the CQDs was recorded on a Spex-Fluorolog FL22 spectrofuorimeter equipped with a double grating 0.22 m Spex 1680 monochromator and a 450 W Xe lamp as the excitation source. The IR spectra were recorded as KBr pellets on a Perkin-Elmer Spectrum One FT-IR spectrometer operating between 4500 and 400 cm^{-1}. Raman spectra were recorded with a confocal Raman microscope WITec alpha 300R (WITec GmbH, Ulm, Germany). A laser beam with 633 nm from air cooled argon was used for excitation. Inverted Fluorescent Microscope (Leica) was used for cell labelling studies; Real time-PCR was carried out on Light Cycler 480 (Roche) machine.

5.14 Conclusions

Green luminescent CQDs with an average size of 3 nm were prepared and their anti-angiogenic property was tested. In vitro cell culture showed that these CQDs could be useful in cell imaging application by virtue of their fluorescent properties. The cell proliferation assay of lung cancer cell line confirmed that CQDs have anticancer activity with almost no effect on normal cells. Angiogenesis is the formation of blood vessels from preexisting vasculature. In the case of tumors the new vessels formed by angiogenesis process supply nutrients and oxygen to the growing tumor. Therefore inhibition of angiogenesis is a critical therapeutic target for restricting growth and metabolism of tumors. In the present study, CQDs were shown to inhibit the blood vessel formation by targeting VEGF, FGF, and VEGFR2, major angiogenic signaling pathway.

5.15 References

1) Folkman, J. What the Evidence that Tumours are Angiogenesis Dependent? *J. Nat. Cancer Inst.* **1990,** *82*, 4-6.
2) Carmeliet, P.; Collen, D. Vascular Development and Disorders: Molecular Analysis and Pathogenic Insights. *Kidney Int.* **1998,** *53*, 1519–1549.
3) Xu, X. Y.; Ray, R.; Gu, Y. L.; Ploehn, H. J.; Gearheart, L.; Rakerand, K.; Scrivens, W. A. Electrophoretic Analysis and Purification of Fluorescent Single-Walled Carbon Nanotube Fragments. *J. Am. Chem. Soc*. **2004,** *126*, 12736-12737.
4) Shen, J. H.; Zhu, Y. H.; Yang, X. L.; Li, C. Z. Graphene Quantum Dots: Emergent Nanolights for Bioimaging, Sensors, Catalysis and Photovoltaic Devices. *Chem. Commun.* **2012,** *48*, 3686- 3699.
5) Yang, S. T.; Cao, L.; Luo, P. G.; Lu, F. S.; Wang, X.; Wang, H. F.; Meziani, M. J.; Liu, Y. F.; Qi, G.; Sun, Y. P. Carbon Dots for Optical Imaging In Vivo. *J. Am. Chem. Soc*. **2009,** *131*, 11308-11309.
6) Yang, S. T.; Wang, X.; Wang, H. F.; Lu, F. S.; Luo, P. J. G.; Cao, L.; Meziani, M. J.; Liu, J. H.; Liu, Y. F.; Chen, M.; Huang, Y. P.; Sun, Y. P. Carbon Dots as Nontoxic and High-Performance Fluorescence Imaging Agents. *J. Phys. Chem. C* **2009,** *113*, 18110-1114.
7) Li, Q.; Ohulchanskyy, T. Y.; Liu, R. L.; Koynov, K.; Wu, D. Q.; Best, A.; Kumar, R.; Bonoiu, A.; Prasad, P. N. Photoluminescent Carbon Dots as Biocompatible Nanoprobes for Targeting Cancer Cells In Vitro. *J. Phys. Chem. C* **2010,** *114*, 12062-12068.
8) Pan, D. Y.; Guo, L.; Zhang, J. C.; Xi, C.; Xue, Q.; Huang, H.; Li, J. H.; Zhang, Z. W.; Yu, W. J.; Chen, Z. W.; Li, Z.; Wu, M. H. Cutting sp^2 Clusters in Graphene Sheets into Colloidal Graphene Quantum Dots with Strong Green Fluorescence. *J. Mater. Chem.* **2012**, *22*, 3314-3318.

9) Zhai, X. Y.; Zhang, P.; Liu, C. J.; Bai, T.; Li, W. C.; Dai, L. M.; Liu, W. G. Highly Luminescent Carbon Nanodots by Microwave-Assisted Pyrolysis. *Chem. Commun.* **2012,** *48*, 7955– 7957.

10) Liu, H. P.; Ye, T.; Mao, C. D. Fluorescent Carbon Nanoparticles Derived from Candle Soot. *Angew. Chem. Int. Ed.* **2007,** *46*, 6473 – 6475.

11) Li, H. T.; He, X. D.; Liu, Y.; Huang, H.; Lian, S. Y.; Lee, S. T.; Kang, Z. H. One-Step Ultrasonic Synthesis of Water-Soluble Carbon Nanoparticles with Excellent Photoluminescent Properties. *Carbon* **2011,** *49*, 605– 609.

12) Zheng, M.; Xie, Z. G.; Qu, D.; Li, D.; Du, P.; Jing, X. B.; Sun, Z. C. On–Off–On Fluorescent Carbon Dot Nanosensor for Recognition of Chromium (VI) and Ascorbic Acid Based on the Filter Effect. *ACS Appl. Mater. Interfaces* **2013,** *5*, 13242 – 13247.

13) Cao, L.; Wang, X.; Meziani, M. J.; Lu, F.; Wang, H.; Luo, P. G.; Lin, Y.; Harruff, B. A.; Veca, L. M.; Murray, D.; Xie, S. Y.; Sun, Y. P. Carbon Dots for Multiphoton Bioimaging. *J. Am. Chem. Soc.* **2007,** *129*, 11318-11319.

14) Lu, J.; Yang, J. X.; Wang, J.; Lim. A.; Wang, S.; Loh, K. P. One-Pot Synthesis of Fluorescent Carbon Nanoribbons, Nanoparticles, and Graphene by the Exfoliation of Graphite in Ionic Liquids. *ACS Nano* **2009,** *3*, 2367-2375.

15) Bourlinos, A. B.; Stassinopoulos, A.; Anglos, D.; Zboril, R.; Georgakilas, V.; Giannelis, E. P. Photoluminescent Carbogenic Dots. *Chem. Mater.* **2008,** *20*, 4539-4541.

16) Tian, L.; Ghosh, D.; Chen, W.; Pradhan, S.; Chang, X.; Chen, S. Nanosized Carbon Particles from Natural Gas Soot. *Chem. Mater.* **2009,** *21*, 2803-2809.

17) Pan, D.; Zhang, J.; Li, Z.; Wu, M. Hydrothermal Route for Cutting Grapheme Sheets into Blue-Luminescent Graphene Quantum Dots. *Adv. Mater.* **2010,** *22*, 734-738.

18) Pan, D. Y.; Zhang, J. C.; Li, Z.; Wu, C.; Yan, X. M.; Wu, M. H. Observation of pH-, Solvent-, Spin-, and Excitation-Dependent Blue Photoluminescence from Carbon Nanoparticles. *Chem.Commun.* **2010,** *46*, 3681-3683.

19) Longo-Sorbello, G. S. A.; Saydam, G.; Banerjee, D.; Bertino, J. R. *Cell Biology a Laboratory Handbook*; Elsevier Academic Press: London, 2005, p 315.

20) Kumar, V. B. S.; Viji, R. I.; Kiran, M. S.; Sudhakaran, P. R. Endothelial Cell Response to Lactate; Implication of Par Modification of Vegf. *J. Cell. Physiol.* **2007,** *211*, 477-485.

21) Ribatti, D.; Gualandris, A.; Bastaki, M.; Vacca, A.; Luraro, A.; Roncalli, L.; Presta, M. New Model for the Study of Angiogenesis- Antiangiogenesis in the Chick Embryo Chorioallantoic Membrane: The Gelatin Sponge/ Chorioallantoic Membrane Assay. *J. Vasc. Res.* **1997,** *34*, 55-463.

Summary of the Thesis

Biological analysis is a potential key application for chemical sensors owing to their inherent ability to detect analytes on –line and in real time in distributed system. There has been a pressing societal need for the development of electrochemical sensors for the detection of various analytes in solution and in biological condition, which are less expensive, highly reproducible and able to use for very low concentrations. Most of the compounds are electrochemically active and could be detected by means of electrochemical techniques. Mostly metal electrodes failed to detect them in lower concentration; they are often modified with some modifiers. Metal nano particles is the one of the most efficient modifier that offer lower detection limit and reduces the signal to noise ratio considerable.

The introductory chapter envisages the need for the development of electrochemical sensors and the advantages of electrochemical methods especially potentiomeric techniques over other methods have been highlighted. A small introduction for the methods, material used, chemistry behind the electrochemical process and characterization techniques has also been highlighted. Requirement of new electrochemical sensors have been brought out culminating with the scope of present work to use CQDs and metal nano particles in the fabrication of electrochemical sensors and the biological applications of CQDs.

Chapter 2 deals with the design and development of CeO_2-MWCNTs on GCE. The electrochemical behaviors of fabricated electrode towards the acetaldehyde molecule in different conditions have been explained. The study revealed that the fabricated electrode processes better sensing performance towards the electrochemical detection of acetaldehyde. Moreover a lower detection limit was also achieved with the modified

electrode. The developed electrode has shown higher selectivity over the analogous compounds and also shows higher reproducibility and reusability. It has been applied for the analysis of synthetic fruit juice sample with quantitative recoveries.

In chapter 3 Synthesis of bimetallic AuPt alloy nanoparticles on the GCE has been discussed. Conformations of the formation of AuPt alloy nanoparticles by various techniques have been explained. The prepared electrode has shown ability to detect phenol in the lower concentration range. The well characterized electrode was further used for the detection of phenol. From the optimization studies, 0.1 M CH_3COONa+0.05 M KCl electrolyte of pH 6.8 was selected as the better condition for the nano molar level detection of phenol. A sensitivity and selectivity study of the sensor towards various coexisting analytes has also explained in this chapter. The sensor has shown excellent detection and quantification of environmental samples.

Chapter 4 deals with the method of synthesis of CQDs and its characterizations. A thorough analytical evaluation of the CQDs modified CPE confirmed that the modified electrode has a better electrocatalytic activity towards the oxidation of dopamine. Here the sensor has shown capacity to detect the dopamine individually and in the presence of compounds like ascorbic acid and uric acid. The developed sensor has been successfully used for analyzing real sample analysis. The applicability of prepared CQDs towards biomarking has also been demonstrated.

Chapter 5 gives a brief overview of the angiogenesis and CQDs. A discussion of the preparation of CQDs from styrene has been provided. The scope of CQDs towards angiogenesis has been brought out. The cytotoxicity of CQDs towards normal and cancer cell line have also been discussed. Angiogenic activity of CQDs by using CAM assay has been emphasized.

List of Publications

List of Publications from the Ph. D thesis

1. **Shereema, R. M.;** Shankar, S. S.; Nambiar, S. R.; Rao, T. P. CeO_2–MWCNT Nanocomposite Based Electrochemical Sensor for Acetaldehyde. *Anal. Methods* **2015**, *7*, 4912-4918.
2. **Shereema, R. M.;** Shankar, S. S.; Sankar, V.; Raghu, K. G.; Rao, T. P. One Step Green Synthesis of Carbon Quantum Dots and its Application Towards the Bioelectroanalytical and Biolabelling Studies. *Electrochim. Acta* **2015,** *182*, 588–595**.**
3. **Shereema, R. M.;** Shankar, S. S.; Sruthi, T. V.; Sameer Kumar, V. B.; Rao, T. P. Angiogenic Profiling of Synthesized Carbon Quantum Dots. *Biochemistry* **2015,** *4*, 6352–6356.
4. **Shereema, R. M.;** Shankar S. S.; Rao, T. P. Bimetallic $Au_{90}Pt_{10}$ Alloy Nanoparticles on Glassy Carbon Electrode for the Nanomolar Detection of Phenol. (communicated to J. Hazard. Mater.).

Publications not related to the thesis

1. Shankar, S. S.; **Shereema, R. M.;** Prabhu, G. R. D.; Rao T. P.; Kumara Swamy, B. E. Electrochemical Detection of Dopamine in Presence of Serotonin and Ascorbic Acid at Tetraoctyl Ammonium Bromide Modified Carbon Paste Electrode: A Voltammetric Study. *J. Biosens. Bioelectron*. **2015,** *6*, 1-7.
2. Manu, K. M. S.; Sreeraj, K.; Rajan, T. P. D.; **Shereema, R. M.;** Pai, B. C.; Arun, B. Structure and Properties of Modified Compocast Microsilica Reinforced Aluminum Matrix Composite. *Mater. Des.* **2015,** *88*, 294–301.

3. **Shereema**, **R. M.;** Prabhu, G. R. D.; Rao, T. P.; Shankar, S. S. Carbon Quantum Dots Modified Carbon Paste Electrode Based Sensor for Selective and Sensitive Determination of Adrenaline. (communicated to Sens. Actuator B- Chem.).

Contributions to academic conferences

1. "CeO_2–MWCNT nanocomposite based electrochemical sensor for acetaldehyde" **R. M. Shereema,** S. R. Nambiar, K. V. Radhakrishnan and T. P. Rao, presented a poster in **2nd International Conference on Advanced Functional Materials (ICAFM-2014)** held at NIIST-CSIR, Trivandrum on 19-21th February 2014.
2. "Electrochemical synthesis of bimetallic AuPt alloy nanoparticles and its application towards the nanomolar detection of phenol" **R. M. Shereema,** S. S. Shankar and T. P. Rao, presented a poster in **International Symposium on Clusters, Cluster-Assemblies and Nanomaterials** (**ISCAN-2016)** held at IISER, Trivandrum on 9-12th March 2016.